Aus dem Institut für Humangenetik

(Prof. Dr. med. B. Wollnick)

der Medizinischen Fakultät der Universität Göttingen

In vitro analyses of CD4-protein function in dedifferentiated keratinocyte cell lines

INAUGURAL-DISSERTATION

zur Erlangung des Doktorgrades

der Medizinischen Fakultät der

Georg-August-Universität zu Göttingen

vorgelegt von

Slavica Hristomanova Mitkovska

aus

Skopje

Göttingen 2022

Dekan:	Prof. Dr. med. W. Brück

Betreuungsausschuss

Betreuerin:	PD Dr. rer. nat. A. Uhmann
Ko-Betreuer:	Prof. Dr. M. P. Schön

Prüfungskommission

Referentin:	PD Dr. rer. nat. A. Uhmann
Ko-Referent:	Prof. Dr. M. P. Schön
Drittreferent:	Prof. Dr. R. Dressel

Datum der mündlichen Prüfung: 12.09.2023

Hiermit erkläre ich, die Dissertation mit dem Titel „*In vitro* analyses of CD4-protein function in dedifferentiated keratinocyte cell lines“ eigenständig angefertigt und keine anderen als die von mir angegebenen Quellen und Hilfsmittel verwendet zu haben.

Göttingen, den …… ……

(Unterschrift)

Table of Contents

List of Figures IV
List of Tables VI
Abbreviations VII
1. Introduction 1
1.1. The structure of the integumentary system 1
1.2. The epidermis 2
1.2.1. The development of the epidermis 2
1.2.2. Structure and markers of the adult epidermis 3
1.2.3. Epidermal homeostasis and wound healing 5
1.2.4. Epidermal stem cells 8
1.3. $CD4^+$ stem cell-like epidermal cells 11
1.3.1. Structure and function of CD4 in immune cells 12
1.3.2. Putative function of CD4 on epidermal keratinocytes 14
1.4. Aims of the work 16
2. Materials and Methods 17
2.1. Technical equipment 17
2.2. Consumable materials 18
2.3. Reagents and chemicals 19
2.4. Buffers and solutions 20
2.5. Kits and ready-to-use reaction systems 21
2.6. Enzymes 21
2.7. Plasmids 22
2.8. Antibodies 22
2.8.1. Antibodies for immunocytochemistry 22
2.8.2. Antibodies for flow cytometry 23
2.9. Synthetic DNA-oligonucleotides 23
2.9.1. DNA-oligonucleotides for polymerase chain reaction (PCR) 23
2.9.2. DNA-oligonucleotides for quantitative real-time PCR 24
2.9.3. DNA-oligonucleotides for Sanger sequencing 25
2.10. Cell cultivation media and reagents 25
2.10.1. Media and reagents for the cultivation of prokaryotic cells 25
2.10.2. Media and reagents for cultivation of eukaryotic cells 25

2.11. Biological materials 26
2.11.1. Bacterial strains 26
2.11.2. Eukaryotic cell lines 26
2.11.3. Mouse strains 27
2.11.4. Patient (human) samples 27
2.12. Software and databases 27
2.13. Cell biology methods 27
2.13.1. Cultivation of eukaryotic cell lines 28
2.13.2. Passaging of eukaryotic cell lines 28
2.13.3. Cryopreservation and thawing of eukaryotic cells 28
2.13.4. Cell counting 28
2.13.5. Cell proliferation assay 29
2.13.6. Transfection 30
2.13.7. Passaging of transfected cells 31
2.13.8. Determination of cAMP levels in cells 31
2.13.9. Inactivation of the cell proliferation by mitomycin C treatment 32
2.13.10. Chemotaxis 32
2.13.11. Isolation of $CD4^+$ T cells from mouse spleen 34
2.14. Molecular biology methods 34
2.14.1. Restriction enzyme hydrolysis 34
2.14.2. Plasmid ligation 34
2.14.3. Cloning of the *pCR3.1-hCD4* expression plasmid and the *pTRE-Dual2-hCD4* plasmid for generating a Tet-On® Advanced Inducible Gene Expression System 35
2.14.4. Transformation of *E.coli* with plasmid DNA 37
2.14.5. Polymerase chain reaction (PCR) 37
2.14.6. Reverse transcription of RNA 38
2.14.7. Quantitative real time PCR 38
2.14.8. Agarose gel electrophoresis with ethidium bromide 39
2.14.9. Sanger sequencing 39
2.15. Isolation and purification of nucleic acids 40
2.15.1. Medium-scale isolation of plasmid DNA and purification 40
2.15.2. Small-scale isolation of plasmid DNA and purification 41
2.15.3. Isolation of DNA fragments from agarose gel 41

2.15.4. RNA Isolation from cell culture 42
2.15.5. RNA isolation from fibrous tissue 42
2.15.6. Photometric quantification of nucleic acids 43
2.16. Immunohistochemical stainings 43
2.16.1. Immunocytochemistry 43
2.16.2. Flow cytometry 44
3. Results 45
3.1. Development of basal cell-like keratinocyte cell lines 45
3.1.1. Generation of a human and a murine basal cell-like, dedifferentiated keratinocyte cell line 45
3.1.2. Characterization of the basal cell-like, dedifferentiated keratinocyte cell lines 49
3.2. Generation of an *in vitro* system for inducible expression of human *CD4* 60
3.2.1. Generating of HaCaT cells with stable expression of Tet-ON Advanced protein 63
3.2.2. Isolation and establishment of a homogeneous HaCaT cell line with stable expression of Tet-ON Advanced protein 64
3.3. Analyzing the function of CD4 in ddHaCaT cells 66
3.3.1. MHCII treatment decreases cAMP levels of CD4-expressing ddHaCaT cells 66
3.3.2. MHCII treatment decreases the proliferation rate of CD4-expressing ddHaCaT cells 68
3.3.3. The influence of IL-1α and TNFα on basal cell-like keratinocytes *in vitro* 69
4. Discussion 78
4.1. Generation of dedifferentiated, stable keratinocyte cell lines 78
4.2. Generation of an inducible *in vitro CD4*-expression system 82
4.3. Analyses of the putative function of CD4 in ddHaCaT cells 83
4.3.1. MHCII treatment decreases cAMP levels and the proliferation rate of CD4-expressing ddHaCaT cells 83
4.3.2. The influence of IL-1α and TNFα on basal cell-like keratinocytes *in vitro* 86
5. Summary 89
6. References 91

List of Figures

Figure 1: Schematic representation of the human skin structure. 1
Figure 2: Schematic representation of human epidermal differentiation and its key molecular markers.....5
Figure 3: Stem cell hypotheses. 11
Figure 4: CD4 involvement in T cell activation and hypothetical CD4 function in stem cell-like keratinocytes. 14
Figure 5: Schematic representation of the hypothetical role of cytokines in regulating $CD4^+$ epidermal stem cells in wounded skin. 15
Figure 6: Chemotaxis assay chamber. 33
Figure 7: Plasmids for generating a Tet-On® Advanced Inducible Gene Expression System. 36
Figure 8: Flow cytometric analysis of $CD4^+$ splenocytes isolated using EasySep™ Mouse $CD4^+$ T Cell Isolation Kit. 44
Figure 9: Experimental setup for the generation of basal cell-like dedifferentiated human HaCaT and murine C5N cells. 45
Figure 10: Morphological changes in HaCaT cells upon culture in low [Ca^{2+}] concentration medium. 47
Figure 11: Morphological changes in C5N cells upon culture in medium with low [Ca^{2+}] concentrations. 48
Figure 12: Low [Ca^{2+}] concentrations increase expression of the basal marker K5 and decrease the expression of differentiation marker K10 but does not impact proliferative activity of HaCaT cells. 50
Figure 13: Culture of C5N cells in medium containing low [Ca^{2+}] concentrations induce the expression of the basal cell marker K5. 50
Figure 14: Phenotype switch of ddHaCaT cells upon culture in high [Ca^{2+}] concentration medium. 52
Figure 15: Culture of ddHaCaT cells in medium containing high [Ca^{2+}] concentrations induce a phenotype switch from a basal cell-like to a more differentiated expression profile. 54
Figure 16: Culture of ddC5N cells in medium containing high [Ca^{2+}] concentrations induce a phenotype switch from a basal cell-like to a more differentiated expression profile. 55
Figure 17: Panoramic pictures of immunofluorescent anti-K5/anti-K10 antibody stained HaCaT and ddHaCaT cells. 56
Figure 18: Image analysis workflow for the quantification of the K5 and K10 protein expression level analysis. 56
Figure 19: Culture of ddHaCaT cells in medium containing high [Ca^{2+}] concentrations induce a phenotype switch from a basal cell-like to a more differentiated protein expression profile. 57
Figure 20: The p63 expression pattern of ddHaCaT cells is not influenced by culture in high [Ca^{2+}] level medium. 58

Figure 21: The proliferation rate of ddHaCaT and ddC5N cells is reduced compared to HaCaT and C5N CTRL cells and decreases further upon culture in high [Ca^{2+}]-containing medium. 59
Figure 22: Inducible expression of a gene of interest (GOI) using the Tet-On Advanced System from Clontech. 60
Figure 23: Schematic representation of the generation of a cell line harboring the Tet-On® Advanced Inducible Gene Expression System. 61
Figure 24: Generation of TetON-Advanced protein-expressing HaCaT cells. 64
Figure 25: cAMP levels of CD4-expressing ddHaCaT cells decrease 180 minutes after MHCII stimulation. 67
Figure 26: MHCII-treatment decreases the proliferation rate of CD4-expressing ddHaCaT cells. 69
Figure 27: IL-1α-treatment does not impact the proliferation rate of ddHaCaT and HaCaT cells. 70
Figure 28: IL-1α reduces *CD4*-expression in ddHaCaT cells. 71
Figure 29: Co-transfection of ddHaCaT cells with *pCR3.1-hCD4* and *pEGFP-N1*. 72
Figure 30: Immunofluorescence analysis of *CD4*-expression in *pCR3.1-hCD4*-transfected ddHaCaT cells within the time schedule of the migration experiment. 73
Figure 31: CD4-expressing ddHaCaT cells migrate towards a TNFα gradient. 75

List of Tables

Table 1. Technical equipment. 17
Table 2. Consumable materials. 18
Table 3. Reagents and chemicals. 19
Table 4. Buffers and solutions. 20
Table 5. Kits and ready-to-use reaction systems. 21
Table 6. Enzymes. 21
Table 7. Commercially available and *de novo*-generated plasmids. 22
Table 8. Primary and secondary antibodies. 23
Table 9. Antibodies and dyes used for flow cytometry. 23
Table 10. PCR Primers. 24
Table 11. qRT-PCR Primers. 24
Table 12. Primers used for Sanger sequencing. 25
Table 13. Media and reagents required for eukaryotic cell cultivation. 25
Table 14. Eukaryotic cell lines. 26
Table 15. Software and databases. 27
Table 16. Number of cells seeded for different in vitro assays. 29
Table 17. Cell type and number, plasmid amount and electroporation conditions. 30
Table 18. PCR cycling conditions 37
Table 19. PCR conditions for amplifying hCD4 37
Table 20. qRT-PCR cycling conditions. 38
Table 21. Genes of interest and standards for qRT-PCR. 39
Table 22. Sanger sequencing reaction components. 40
Table 23. Cycling conditions for DNA amplification for Sanger sequencing. 40
Table 24. Antibiotic concentrations for selection and maintenance of ddHaCaT and HaCaT cells after transfection with linear selection markers for hygromycin or puromycin resistance. 63

Abbreviations

3H-TdR	Tritiated thymidine
Ab	Antibody
AC	Adenylyl cyclase
AmpR	Ampicillin resistance
APCs	Antigen-presenting cells
ATP	Adenosine triphosphate
BCC	Basal cell carcinoma
bp	Base pairs
BrdU	5-bromo-2'-deoxyuridine
BSA	Bovine serum albumin fraction V
Ca^{2+}	Calcium ions
$CaCl_2$	Calcium chloride dihydrate
cAMP	Cyclic adenosine 3′, 5′-monophosphate
CD	Cluster of differentiation
cDNA	Complementary DNA
cFCS	Chelexed fetal calf serum
CMV	*Cytomegalovirus*
CRAC	Calcium release-activated channels
CT	Cycle threshold
CTLs	Cytolytic T cells
CTRL	Control
Cy3	Cyanine dye 3
Cy7	Cyanine dye 7
DAPI	4′,6-diamidino-2-phenylindole
DC	Dendritic cell
ddC5N	Dedifferentiated C5N cells
ddH_2O	Double-distilled H_2O
ddHaCaT	Dedifferentiated HaCaT cells
DMBA	7,12-dimethylbenzo [α]-anthracene
DMEM	Dulbecco's modified eagle medium
DMSO	Dimethyl sulfoxide
DNA	Deoxyribonucleic acid
dNTPs	Deoxyribonucleotide triphosphates
DTT	Dithiothreitol
E. coli	*Escherichia coli*
EDTA	Ethylenediamine tetraacetic acid disodium salt dihydrate
EGF	Epidermal growth factor
EGFP	Enhanced green fluorescent protein
ELISA	Enzyme-linked immunosorbent assay
EtBr	Ethidium bromide
EtOH	Ethanol
F	Forward
FCS	Fetal calf serum

FGF	Fibroblast growth factor
FITC	Fluorescein isothiocyanate
GOI	Gene of interest
h	Human
HBSS	Hanks' balanced salt solution
HEPES	4-(2-hydroxyethyl)-1-piperazineethanesulfonic acid
Hh	Hedgehog
Hh / Ptch	Hedgehog-patched
hiFCS	Heat-inactivated fetal calf serum
HIV	Human immunodeficiency virus
HRP	Horseradish peroxidase
ICC	Iimmunocytochemistry
IL	Interleukin
IL-1α	Interleukin – 1 alpha
IVL	Involucrin
K	Keratin
kb	Kilobase
LB	Lysogeny broth
Lrig1	Leucine rich repeats and immunoglobulin like domains 1
mAb	Monoclonal antibody
MATra	Magnet assisted transfection
MHCII	Major histocompatibility complex class II
MolTaq	Taq-polymerase (named after *Thermus aquatius*)
OD	Optical density
P/S	Penicillin (10.000 U/ml) / Streptomycin (10 mg/ml)
pAb	Polyclonal antibody
PBS	Phosphate buffered saline
PCR	Polymerase chain reaction
PDEs	Phosphodiesterases
PDGF	Platelet derived growth factor
pDNA	Plasmid DNA
PFA	Paraformaldehyde
PKA	Protein kinase A
PMCA	Plasma membrane Ca^{2+} ATPase
PMSF	Phenylmethylsulfonyl fluoride
qRT-PCR	Quantitative real-time polymerase chain reaction
R	Reverse
RLU	Relative light intensity unit
RNA	Ribonucleic acid
rpm	Rounds per minute
RPMI	Roswell Park Memorial Institute
rRNA	Ribosomal RNA

RT	Room temperature
rTetR	Reverse tetracycline repressor protein
S.O.C.	Super optimal broth with catabolite repression
Sca-1	Stem cell antigen-1
TA	Transit-amplifying cells
TBE	Tris-boric acid-EDTA solution
TBS	Tris buffered saline
TCR	T cell receptor
TetR	Tetracycline repressor protein
Th	T helper cell
TNFα	Tumor necrosis factor - alpha
TPA	12-O-tetra decanoylphorbol-13-acetate
TRE	Tetracycline response element
Treg	Regulatory T cell
TRE_{mod}	Modified tetracycline response element
U	Enzymatic unit
UV	Ultraviolet
v/v	Volume/volume
VEGF	Vascular endothelial growth factor
w/v	Weight/volume
WT	Wild type

1. Introduction

1.1. The structure of the integumentary system

The integumentary system is the largest organ of the human body, consisting of the skin and its appendages, including the sebaceous, apocrine and eccrine (sweat) glands, the nails and hair follicles. The integument or the skin is in a state of continuous change and accounts for 1.5 to 2 m^2 of the adult human surface area and up to 16 % of the human body weight (Zaidi and Lanigan 2010). It lines the body with mucous membranes to ultimately form a physical barrier that regulates the in- and outward water and electrolyte passage and acts as a defensive barrier for various microorganisms, ultraviolet radiation, toxic agents and mechanical insults (Kolarsick et al. 2011). Moreover, the skin is also responsible for the production, organization, management and metabolism of different proteins and essential biomolecules. Altogether, the skin is a significant part of the immune, nervous and endocrine systems, with multiple patterns of intracutaneous cross-talk established between them (Chuong et al. 2002). This plethora of functions arises from the complex and sophisticated skin structure, which is organized in three layers: the epidermis, dermis and the hypodermis (Figure 1A).

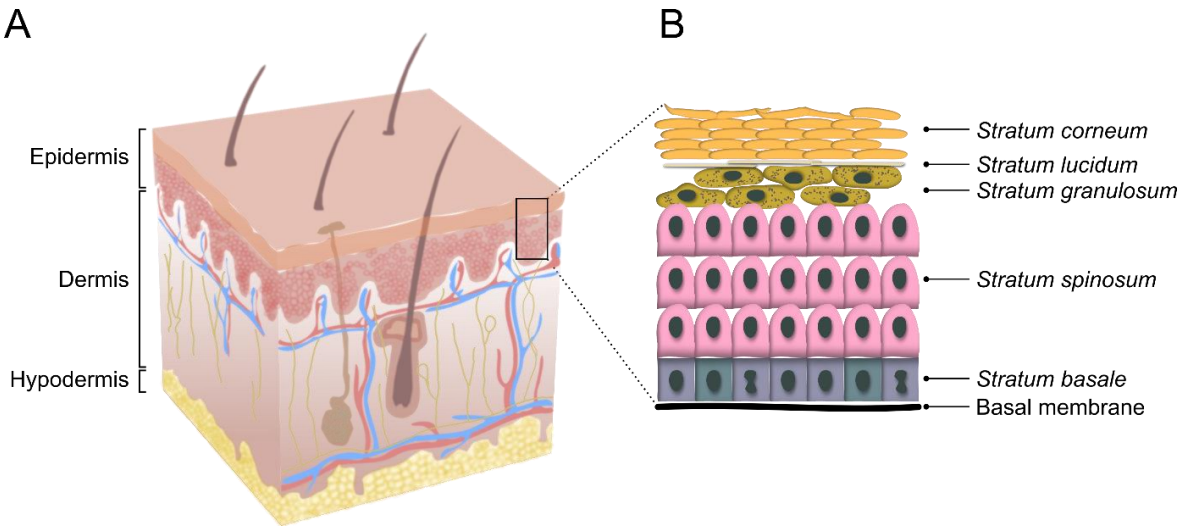

Figure 1: Schematic representation of the human skin structure. (A) The hypodermis, dermis and the epidermis are the main skin layers. **(B)** Anatomy of the epidermis. Structure of the outermost skin layer: cornified (*stratum corneum*), clear or translucent layer (*stratum lucidum*), granular (*stratum granulosum*), spinous (*stratum spinosum*) and basal layer (*stratum basale*). Adapted from Smeden (2013).

The external skin layer is the epidermis, a stratified epithelial layer also referred to as the interfollicular epidermis (Blanpain and Fuchs 2009), which is further divided into several, morphologically distinct sublayers (Figure 1B). The outermost epithelial layer is the *stratum corneum* (cornified or horny cell layer) acting as a significant physical barrier, followed by the *stratum lucidum*, which is only found on the palms and soles. Then follow the *stratum granulosum* (granular layer), the *stratum spinosum* (squamous cell layer) and the *stratum basale* (basal cell layer) (Figure 1B). Keratinocytes make up 95 % of all epidermal cells, with the remaining cells including melanocytes, Langerhans and Merkel cells. No blood vessels are present in the

epidermis. However, diffusion through dermo-epidermal junctions of the dermis allow contact with the circulatory system (Zaidi and Lanigan 2010).
The dermis or *corium* is a collagen and elastin rich connective tissue located beneath the epidermis. It contains fibroblasts, macrophages, mast cells and dermal adipocytes, as well as blood and lymph vessels, sweat and sebaceous glands, nerve endings and hair follicles. It is divided into two parts, the upper (papillary) and the lower (reticular) dermis, without having an exact border (Zaidi and Lanigan 2010). The dermis protects the body from injuries, produces sweat, regulates the body's temperature, is responsible for the skin turgor and plays a role in sensory stimuli (Khavkin and Ellis 2011).
The subcutaneous tissue or hypodermis, a layer located beneath the dermis, represents a fatty tissue consisting mainly of adipocytes, which attach the dermis to the underlying tissues (Driskell et al. 2014). The subcutaneous tissue plays a role in body temperature regulation (thermoregulation), protection of the body against trauma and in nutritional energy storage (Kanitakis 2002). Anatomically and histologically, there is a clear separation between the dermis and the hypodermis. However, they are functionally and structurally integrated with nerves and blood vessels (Chu 2008).

1.2. The epidermis

1.2.1. The development of the epidermis

The human epidermis consists of different layers, which guard the body against infection, mechanical injuries and wounding by a fine-tuned homeostatic process of constant renewal (Stark et al. 2006). This mechanism is initiated during embryonic development in a particular sequence of specification, commitment, stratification and terminal differentiation in direct dependency on the dermal development (Koster and Roop 2007). Only a single sheet of epithelial cells surrounds the embryo during the blastula stage of early embryonic development. During gastrulation, cells from the ectoderm invaginate from the surface into the embryo resulting in the formation of meso- and endodermal germ layers (McGrath et al. 2004). Subsequently, the nervous system and skin epithelium are formed from the newly developed neuroectodermal layer. At this embryonal stage, the epithelium consists of only one sheet of multipotent epithelial cells that are protected by the periderm layer comprised of low cuboidal cells connected with junctional complexes (Benitah and Frye 2012). The mesoderm gives rise to the dermis which is separated from the epidermis via the basal membrane, an extracellular matrix that is produced by epidermal keratinocytes and dermal fibroblasts (McMillan et al. 2003). The basal cells are connected to the basal membrane through hemidesmosomes and focal adhesions characterized by their expression of α6β4 and α3β1 integrins, respectively (Fuchs 2007). Some of the basal cells leave the basal layer with the onset of skin differentiation and stratification between 4 and 9 weeks in human and from day 13 to 16 in murine embryos (Hertle et al. 1991) by changing the orientation of their mitotic spindle and thereby generating the intermediate (suprabasal) layer (Lechler and Fuchs 2005). This latter layer only exists in embryonic skin and later differentiates into the *stratum*

spinosum (Smart 1970). Afterwards, the cells from the *stratum spinosum* proliferate and differentiate to further generate the granular and cornified layers mainly driven by increased extracellular calcium concentrations and the resulting intracellular sensing (Koster and Roop 2007). The mature epidermis is fully formed at week 24 in human and at day 17 in murine embryonic development (Hertle et al. 1991).

1.2.2. Structure and markers of the adult epidermis

In adult humans, keratinocytes comprise approximately 95 % of all epidermal cells, which maintain the epidermis as a structure or barrier. During skin homeostasis, the basal layer epithelial stem cells continually undergo a terminal differentiation program that moves them into the upper epidermal layers (see Figure 2), where they are ultimately shed from the skin surface (Fuchs 2007). The process of differentiation and the cell movement from the basal to the cornified layer followed by desquamation lasts 40 to 56 days in humans and 7 to 10 days in murine skin (Halprin 1972; Potten et al. 1987).

Keratinocytes exhibit morphological and protein expression changes during differentiation and the process of stratification. A hallmark of these processes is the production of keratin. These intermediate filaments are major structural proteins of keratinocytes, rendering the cytoskeletal network more resilient and providing great structural integrity of the cells. Each epidermal layer expresses different keratin types (Fuchs 1995) and thus the expression of specific keratins is a reliable indicator of terminal cell differentiation at the basal membrane (Figure 2).

The innermost basal layer of the epidermis is composed of a single layer of cuboidal to columnar basal cells including the epidermal stem cell subpopulation (Yousef et al. 2021) as well as melanocytes, Langerhans and Merkel cells (Zaidi and Lanigan 2010). Melanocytes, which make up less than 10 % of the basal layer cells, are involved in protecting the skin from ultraviolet radiation through the production of melanin (Tsatmali et al. 2002). Langerhans cells, members of the dendritic cell (DC) / macrophage family, represent the first line of immunological defense of the skin (Clayton K et al. 2017). The Merkel cells function as transducers of fine touch (Abraham and Mathew 2019). Basal cells which are mitotically active and constantly produce keratinocytes are characterized by expression of the keratin 5 (K5) and K14 variants (Byrne et al. 1994; Fuchs 2007), as well as the expression of the stem cell marker integrin α6, also known as cluster of differentiation (CD) 49f (Krebsbach and Villa-Diaz 2017). K15 is a keratin co-expressed in minor amounts along with K5 and K14 in human basal keratinocytes (Bose et al. 2013; Lloyd et al. 1995). Human and mice basal cell layers additionally express p63, a protein that plays a significant role in epidermal stem cell self-renewal (Senoo et al. 2007), in epithelial stratification and differentiation (Truong et al. 2006) and is necessary for the proliferation of the epithelial stem cells (Koster 2010; Yang et al. 1999). The basal cells begin the terminal differentiation process by leaving the basal cell layer and moving upward into the spinous layer. The spinous layer is composed of 8 to 10 layers of keratinocytes with many desmosomes attaching the cells to each other. Spinous cells have a polyhe-

dral shape with a centrally placed, oval nucleus in the lower layers. During development, they move upward toward the granular layer, where they become more flattened (Zaidi and Lanigan 2010). The initiated differentiation process in spinous cells leads to substitution of the K5/K14 by K1/K10 expression (Fuchs and Green 1980). The K1 expression in spinous cells is induced by Notch signaling, which directs the cells to continue with the differentiation (Blanpain et al. 2006). Moreover, it was demonstrated that K10 expression also promotes the differentiation process by suppressing cell proliferation (Paramio et al. 1999) and inhibiting the cell cycle progression (Chen et al. 2006). However, the human and murine spinous cells are still transcriptionally active (Fukuyama and Epstein 1968; Fukuyama et al. 1965). As spinous cells, they continue to differentiate and move into the next upper, granular layer of flattened, diamond shaped cells containing keratohyalin and lamellar granules (Freeman and Sonthalia 2021). The major component of the keratohyalin granules is profilaggrin, a precursor of filaggrin (Fleckman et al. 1985). As the cells transition from the spinous into the granular layer, their K1 and K10 expression is downregulated by protein kinase C, which also induces the expression of transglutaminase and loricrin (Dlugosz and Yuspa 1993; 1994) that are expressed in the superficial parts of the granular layer (Hohl et al. 1991b). As the process of terminal differentiation proceeds, the granular layer cells undergo a de-gradation phase in which the cytoplasmic organelles are removed (Lavker and Matoltsy 1970). The outermost, cornified layer of the human epidermis consists of enucleated, dead keratinocytes organized in about 15 to 20 sublayers (Roop 1995) and keratins which are surrounded by a cross-linked protein envelope (Elias et al. 2014). Involucrin was the first identified component of the cell envelope (Rice and Green 1979), while loricrin is the most abundant protein expressed in the cornified layer (Hohl et al. 1991b), with 65 to 70 % abundance in humans and up to 85 % in mice (Steven and Steinert 1994). A family of S100, small calcium-binding proteins, is also expressed in the cornified cell envelope (Eckert et al. 2004). Moreover, a fillagrin, which represents dephosphorylated profilaggrin (Markova et al. 1993), is also expressed in this layer. Filaggrin, lipids and other proteins from the cornified layer regulate water-loss from the skin and it's pH (Kezic and Jakasa 2016; Sandilands et al. 2009). Dead cells of this layer are constantly lost from the skin surface and are renewed by the maintenance of epidermal homeostasis, which depends on basal layer cells.

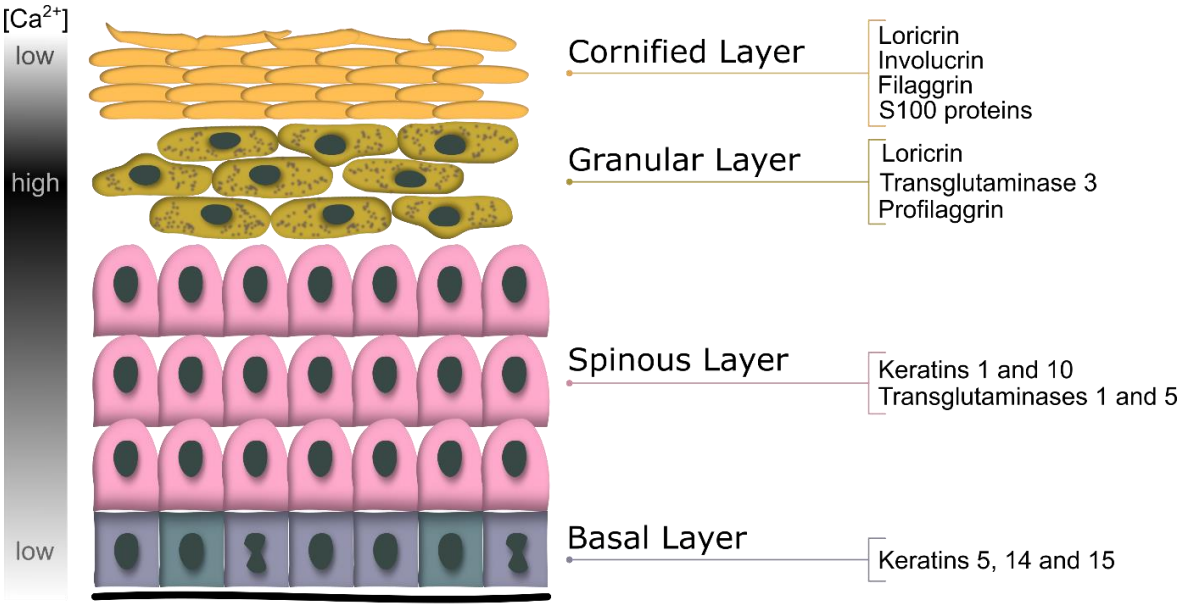

Figure 2: Schematic representation of human epidermal differentiation and its key molecular markers. Keratinocytes from the basal layer proliferate and move upward through different epidermal layers (spinous and granular layer) reaching the cornified layer. They undergo a programmed series of differentiation during which keratinocytes enucleate, enlarge, flatten, and ultimately are shed from the skin surface. Specific gene expression during differentiation and calcium concentrations are associated with each epidermal layer. The key molecular markers of each epidermal layer are shown on the right side. Adapted from Sandilands et al. (2009).

1.2.3. Epidermal homeostasis and wound healing

The epidermal turnover rate, one of the highest in the body (Iizuka 1994), is accomplished through an epidermal homeostasis that balances cell proliferation and cell loss through terminal differentiation and apoptosis (Stark et al. 2006). However, the skin, as the body's outermost defense organ, is particularly susceptible to injury and tissue damage during which the epidermal homeostasis is disrupted (Rosińczuk et al. 2016). Restoring of the barrier function implies closure and regeneration of the damaged skin, which involves interaction between many different cell types (Reinke and Sorg 2012). Moreover, the process of wound healing is precisely arranged, regulated at multiple levels and is divided in sequential, overlapping phases such as hemostasis, inflammation, proliferation and remodeling (Landén et al. 2016). Furthermore, wound healing involves a re-establishment of the epidermal homeostasis.

1.2.3.1. Calcium-dependent epidermal keratinocyte differentiation

Calcium is one of the most important factors regulating keratinocyte differentiation and skin barrier maintenance. Early studies of murine keratinocytes demonstrated that in the presence of 0.09 mM calcium most of the keratinocytes initiated proliferation, while higher calcium concentrations (1.2 mM) led to cell differentiation (Hennings H. et al. 1980). The remarkable influence of the extracellular calcium levels on proliferation and differentiation was also confirmed later in human keratino-

cytes. Human keratinocytes isolated from newborn foreskins were placed in low calcium-containing medium (0.1 mM), which resulted in a higher cell proliferation rate than keratinocytes kept in medium with normal (1.2 mM) and high calcium concentrations (1.8 mM) that showed the highest level of differentiation (Pillai et al. 1988). Overall, these studies demonstrated that high calcium concentrations initiate keratinocyte differentiation, in contrast to low calcium concentrations, which only trigger proliferation. The mechanisms for calcium-induced keratinocyte differentiation involve genomic and non-genomic pathways (Bikle et al. 2012). One of the earliest recognized calcium-induced, non-genomic pathways in keratinocytes is the formation of desmosomes and cell-cell contacts as a precondition for the onset of cell differentiation. The asymmetric desmosome formation between neighboring cells starts already after a five-minute exposure to higher calcium concentrations and results in functional, symmetric desmosomes two hours later (Hennings Henry and Holbrook 1983; Hennings H. et al. 1980). As a result, the intracellular calcium concentrations are regulated by desmosomes and cell-cell junctions through a signaling complex, which additionally facilitates keratinocyte differentiation (Niessen 2007; Pillai et al. 1990).

The calcium-induced genomic pathway in keratinocytes involves the expression of differentiation markers and requires a longer effector time. As described above, basal layer keratinocytes express K5 and K14 and the differentiation process is characterized by the sequential expression of K1 and K10 in the spinous layer, loricrin and transglutaminase 3 in the granular layer and by loricrin, involucrin and filagrin expression in the cornified layer (Figure 2) (Pillai et al. 1990; Yuspa et al. 1989). Interestingly, some of the genes encoding for these differentiation markers contain calcium responsive promoters, e.g. the human K1 (Huff et al. 1993; Rothnagel et al. 1993) and involucrin genes (Bikle et al. 2001; Deucher et al. 2002; Ng et al. 1996) contain activator 1 sites (Eckert et al. 1997a). In addition, also the transcription of the human loricrin gene is induced by high calcium concentrations (Hohl et al. 1991a). Moreover, a study investigating genes involved in the process of keratinocyte terminal differentiation showed that 290 of 840 analyzed genes were related to the process of keratinocyte differentiation and were up-regulated by calcium treatment in primary cultured human keratinocytes (Seo et al. 2005).

In vivo, calcium is gradually distributed in the epidermis and forms a vertical concentration gradient. Thus, the extracellular calcium levels are the lowest in the proliferating basal and the highest in the differentiated granular layer (Figure 2). In the outermost layer of the skin, the cornified layer, the calcium levels decrease again (Elias et al. 2002; Menon and Eliam 1985). The main storage of the intracellular calcium are the Golgi apparatus and the endoplasmic reticulum (Behne et al. 2011; Celli et al. 2010). However the maintenance of the calcium gradient depends also on the integrity of the epidermal barrier (Menon et al. 1994) and is formed not only by calcium uptake, release and influx from the keratinocytes (Feingold et al. 2007), but also depends on the epidermal tight junctions of the granular layer (Kurasawa et al. 2011). In the intact epidermis the calcium gradient represents a crucial regulator of keratinocyte proliferation and differentiation (Yuspa et al. 1989). Calcium

influx is furthermore responsible for directed keratinocyte migration following skin wounding and plays a major role in the associated healing process (Trollinger et al. 2002). Thus, wounding induces calcium release from the endoplasmic reticulum, which corresponds with a transient rise in extracellular calcium (Celli et al. 2016). Furthermore, it was also shown that upon wounding, calcium controls the desmosome formation, as well as the activation of protein kinase C (Garrod and Chidgey 2008; Hobbs et al. 2011).

1.2.3.2. The role of cAMP in epidermal homoeostasis, wound healing and diseased skin

Within cell migration during epidermal wound healing and tissue regeneration calcium influx crosstalk with the cyclic adenosine 3′, 5′-monophosphate (cAMP) - dependent protein kinase (PKA) (Berridge 1975; Borodinsky and Spitzer 2006; Bugrim 1999). This interaction results from the calcium-mediated regulation of the adenylyl cyclase (AC) activity and its associated cAMP production. cAMP, an intracellular second signaling messenger, is participating in the regulation of diverse biological events including cell proliferation and differentiation (Stork and Schmitt 2002). However, the cAMP effect on cell proliferation is cell-type dependent (Graves and Lawrence 1996). It induces proliferation in some cell types (Frödin et al. 1994; Withers DJ et al. 1995), while inhibiting it in others (Burgering et al. 1993; Cook and McCormick 1993). In keratinocytes at least four independent, cAMP producing systems have been identified (Adacehi et al. 1982), but while high cAMP levels activate keratinocyte differentiation (Mammone et al. 1998), the studies analyzing the effect of cAMP on keratinocyte proliferation are inconsistent. Some *in vitro* studies reported decreased keratinocyte proliferation upon high cAMP levels (Delescluse et al. 1974; Yamanishi et al. 1989), whereas others demonstrated the opposite effect (Green 1978; Kuroki et al. 1982). However, different cell densities may explain these effects since cAMP enhances keratinocyte proliferation under subconfluent culture conditions, while inhibiting it at confluent conditions (Okada et al. 1982; Takahashi et al. 2004). Additionally, there are numerous reports of altered cAMP activity in skin diseases like psoriasis, an inflammatory disease with unbalanced differentiation and proliferation processes (Brion et al. 1986; Delescluse et al. 1974; Halprin et al. 1975). Furthermore, cAMP plays an important role in inflammatory skin processes mediated through T and other immune cells. Thus, elevated intracellular cAMP levels in these cells suppress the production of various pro-inflammatory mediators (Serezani et al. 2008) confirming its immunosuppressive and anti-inflammatory actions. Moreover, it has also been revealed that cAMP is involved in the permeability barrier homeostasis of murine skin, where the barrier recovery rate depends on intracellular cAMP levels, which increased immediately after barrier disruption (Denda et al. 2004).

1.2.3.3. The role of cytokines in epidermal homoeostasis, wound healing and diseased skin

The complex process of barrier recovery or wound healing involves inflammation, proliferation and remodeling phases (Robson et al. 2001). During this process, in which both immune and non-immune cells are involved, multiple cytokines and growth factors are produced (Barrientos et al. 2008). Among the variety of cytokines, the tumor necrosis factor - alpha (TNFα) was found to play a significant role in the early process of wound healing. TNFα is released immediately by keratinocytes and fibroblasts after injury and promotes and supports inflammatory leukocyte movement towards the wounded tissue (Mast and Schultz 1996). Moreover, additional TNFα is released from the recruited neutrophils and macrophages which causes an extension of the inflammatory response (Eming et al. 2007). Furthermore, TNFα has an important role in the epidermal repair phase by increasing the keratinocyte motility and attachment, as well as affecting the keratinocytes fate through regulation of the cell-cycle and apoptosis-associated genes (Banno et al. 2004).

Another important cytokine whose synthesis is triggered by other cytokines such as TNFα and in skin injury is interleukin – 1 (IL-1) (Partridge et al. 1991). It is a major epidermal cytokine synthesized by keratinocytes, Langerhans cells and dermal fibroblasts (Kumar et al. 1992; Sauder et al. 1984), mostly cell-associated and lost by desquamation (Blanton et al. 1989; Kupper et al. 1986). IL-1, which is essentially expressed in the epidermis, also plays an important part in skin homoeostasis. Moreover, dysregulated expression and activation of IL-1 was related to several skin diseases. In particular, high IL-1 levels are associated with elevated psoriasis, atopic dermatitis, melanoma and squamous cell carcinoma incidence (Abramovits et al. 2013; Cai et al. 2019; Gelfo et al. 2020; León et al. 2015). In skin injury, this proinflammatory cytokine initiates a rapid immune response (Kupper et al. 1988). It was shown in *in vivo* experiments that IL-1 stimulates keratinocyte proliferation in inflammatory diseases (Ristow 1987), as well as the growth of cultured primary keratinocytes (Sauder et al. 1988). These effects are thought to be IL-1 concentration dependent, but could not be confirmed in other studies (Partridge et al. 1991). However, Eller *et al.* (1995) suggested that IL-1 plays also a role in initiation of the keratinocytes differentiation process by regulating the expression of keratinocyte differentiation-associated genes.

1.2.4. Epidermal stem cells

Homeostasis and skin repair after injury are physiological processes that rely on stem cells. These cells are defined by their self-renew potential and the capability to give rise to different cell lineages that form mature tissues. Thus the progeny of stem cells replaces keratinocyte loss in the normal process of differentiation or cell death after injury (Blanpain et al. 2007; Weissman et al. 2001). The stem cells of the epidermis are slow-cycling cells *in vivo* capable of proliferation after skin injury. *In vitro*, they can imitate tissue proliferation and regeneration upon changed culturing conditions (Potten and Hendry 1973; Potten and Morris 1988; Watt 1998). Currently, three major skin stem cell compartments are known: the hair follicle bulge region,

the interfollicular epidermis and in the sebaceous gland (Sotiropoulou and Blanpain 2012; Watt et al. 2006).

1.2.4.1. Murine epidermal stem cells

First recognition of the existence of epidermal stem cells is traced back to research conducted in the 1970s. These approaches showed, that after severe irradiation of murine skin radioresistant epidermal cells form cellular clones that repopulate the skin (Potten and Hendry 1973; Withers HR 1967). Several studies conducted during the 1980 to 1990 period exploited the possibility to label murine stem cells during neonatal development with tritiated thymidine (^{3}H-TdR), which enabled their later detection with autoradiography and immunohistology. The results showed that both, the epidermis and the hair follicle bulge region contain epidermal stem cells (Cotsarelis et al. 1990; Mackenzie IC and Bickenbach 1985; Morris et al. 1985). Moreover, two different populations of proliferating stem cell-like keratinocytes were identified in the murine epidermal basal layer: stem cells, that proliferate and can generate other stem cells, and transit-amplifying (TA) cells, that undergo terminal differentiation (Potten and Morris 1988). Further investigations in the 1990s postulated that four progenitor cell types originate from the hair follicle bulge epithelial stem cells, one of which is located in the epidermis, while the remaining three are located at the hair follicle itself (Kamimura et al. 1997). However other studies showed that 8 % of the basal cells represent stem cells characterized by their high α6 integrin (α6) expression level and low or undetectable expression of the transferrin receptor CD71 ($\alpha6^{bri}CD71^{dim}$). In contrast, TA cells comprise 60 % of the basal cells and express high levels of α6 and CD71 ($\alpha6^{bri}CD71^{bri}$). Besides $\alpha6^{bri}CD71^{dim}$ and $\alpha6^{bri}CD71^{bri}$ cells of the basal layer, additionally $CD71^{dim}$ cells were found in the hair follicle bulge region (Tani et al. 2000). Additionally, proliferating cells characterized as $CD49f^{+}CD34^{neg}$ expressing hematopoietic stem cell marker stem cell antigen-1 (Sca-1) were recognized in the basal layer of the interfollicular epidermis (Triel et al. 2004). Finally, lineage tracing experiments identified the three distinguishable skin stem cell compartments: the interfollicular epidermis, the hair follicle bulge and the sebaceous gland (Braun et al. 2003; Ghazizadeh and Taichman 2001). However, it has not been clearly demonstrated so far whether long-term repopulating cells of the interfollicular epidermis represent a separate stem cell population responsible for epidermal homeostasis (Garcin and Ansell 2017; Ito et al. 2005; Levy et al. 2005). In contrast, stem cells of the murine hair follicle bulge region and their progeny populate the entire hair follicle and the sebaceous glands in normal homeostasis, but also participate in regeneration processes of the epidermis after injury (Oshima et al. 2001; Taylor et al. 2000).

1.2.4.2. Human epidermal stem cells

In 1989, a fully structured and functional human epidermis, though without hair follicles or sweat glands, was generated from cultured epithelial autografts and implanted on burn-injured skin (Compton et al. 1989). Together with the fact that the

human skin consists of a large interfollicular epidermis with less hair follicles compared to the murine skin, Compton *et al.* (1989) suggested that in humans the epidermal stem cells are located in the basal layer rather than in the hair follicle. Indeed - similar to the murine skin - also in humans the existence of two types of proliferating keratinocytes in the basal layer were confirmed: stem cells, characterized by low CD71 and high α2β1, α3β1 and α6β4 integrin expression (Li A et al. 1998) and TA cells (Carter et al. 1990), which undergo the process of terminal differentiation (Jones et al. 1995) by detaching from the basal membrane and inactivating of β1 cell surface integrin receptors (Hotchin et al. 1993). On a morphological level, basal stem cells were identified at the epidermal rete ridges, expressing high levels of β1 integrin and low levels of desmoglein 3 (Wan et al. 2003). Additionally, $K15^{+}\alpha6^{high}$ stem cells were described to be located at the edge of the rete ridges (Kaur 2006). Finally, epidermal growth factor (EGF) receptor antagonist leucine-rich repeats and immunoglobulin-like domains 1 (Lrig1) were identified as a human stem cell marker in basal cells (Jensen KB and Watt 2006; Jensen KB et al. 2009).

1.2.4.3. Stem cell hypotheses

A balancing mechanism within the epidermis that regulates the rate of cell division and cell loss is maintained throughout the lifetime of the organism and is essential for the epithelial homeostasis (Potten 1981). This balance is maintained by regulation of the epidermal basal layer cell proliferation, which detach from the basal lamina, move upward, while undergoing the process of terminal differentiation to ultimately be shed from the skin surface (Fuchs and Raghavan 2002). This epidermal maintenance further depends on the proliferation and differentiation of the interfollicular epidermal stem cells. Currently, multiple model theories (Figure 3) exist that describe the epidermal regeneration process (Blanpain and Fuchs 2009; Hsu et al. 2014; Senoo 2013). The first proposed model is the hierarchical model, with epidermal proliferative units being composed of centrally placed stem cells that give rise to TA cells that undergo the process of terminal differentiation (Allen and Potten 1974; Potten and Morris 1988). These TA cells go through several cell divisions before leaving the basal cell layer and committing to their differentiation program (Barrandon and Green 1987). On the other hand, in the stochastic model, daughter cells of a single type of progenitor stem cell of the epidermal basal layer randomly differentiate or remain as a progenitor cell (Clayton E et al. 2007; Doupé et al. 2010). Finally, Mascré *et al.* (2012) proposed a mechanism whereby slowly dividing stem cells generate self-renewing stem cells of limited lifetimes or committed progenitors, which maintain the epidermal repair and regeneration and play a short-term role during wound healing. A mathematical modeling approach conducted by Li X et al. (2013) favored the latter model, as it did not result in major stem cell depletion over a three year period.

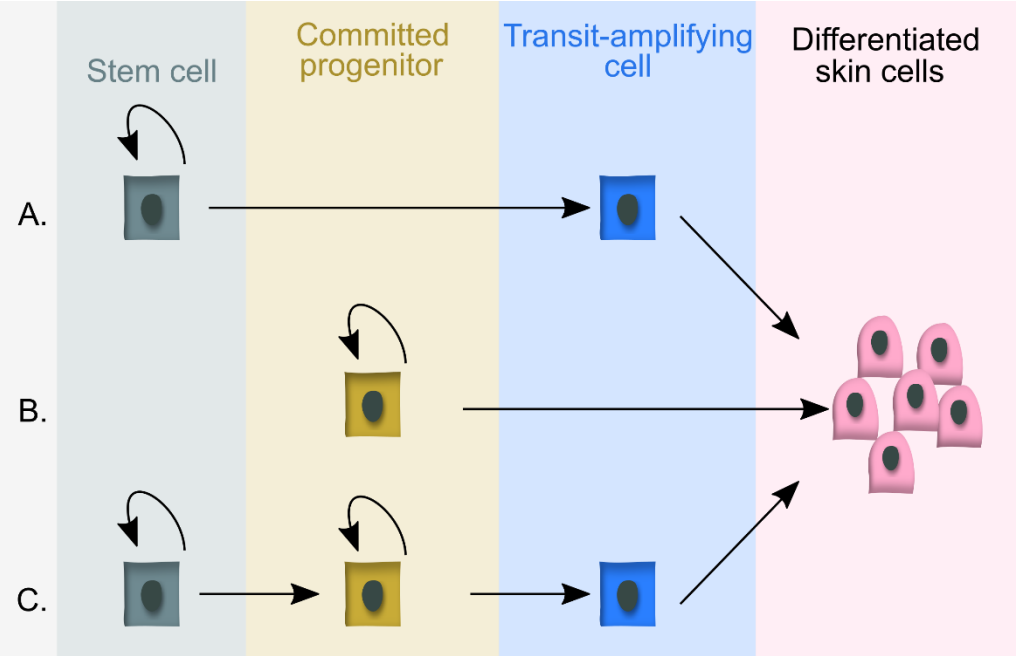

Figure 3: Stem cell hypotheses. Three current theories describing the epidermal regeneration process are shown. **(A)** The hierarchical model according to which the epidermal proliferative units play the central role in the regeneration process. These units are composed of centrally placed stem cells that give rise to TA cells that undergo the process of terminal differentiation. **(B)** The stochastic model, whereby committed progenitor cells exist that directly give rise to differentiated skin cells. **(C)** The newest model combines both of these two theories, according to which the stem cells give rise to committed progenitors, which further generate TA cells and differentiated skin cells.

1.3. CD4^{+} stem cell-like epidermal cells

The Hedgehog (Hh) signaling pathway is involved in regulation of embryonic differentiation processes and in the maintenance of adult tissue homeostasis and regeneration (Briscoe and Therond 2013; Yao and Chuang 2015). Deregulation of this pathway (e.g. by activating mutations) plays a key role in uncontrolled proliferation and differentiation and can lead to tumorigenesis or tumor growth acceleration in a wide variety of tissues (Skoda et al. 2018). Functional studies to enlighten the impact of a deregulated Hedgehog-Patched (Hh / Ptch) signaling pathway in the adult organism have been conducted in a mouse model for conditional Hh signaling pathway overactivation (*Ptch*$^{flox/flox}$ mice). These approaches showed that the ubiquitous, biallelic loss of *Ptch* (which is an Hh signaling inhibitor) in adult mice results in hyperproliferation of various tissues and in severe immune defects (Uhmann A. et al. 2011; Uhmann A. et al. 2007). Subsequent analyses of *Ptch*$^{flox/flox}$*CD4Cre*$^{+/-}$ mice in which *Ptch* is depleted in CD4-expressing cells showed that the overactivation of the Hh signaling pathway in T cells did not impair their immunological function (Michel et al. 2013; Uhmann A. et al. 2011). However, to investigate the function of *Ptch*-deficient T cells in cancer the development of skin tumors was induced in *Ptch*-$^{flox/flox}$*CD4Cre*$^{+/-}$ mice by a chemical carcinogenesis protocol using 7,12-dimethylbenzo [α]-anthracene / 12-*O*-tetra decanoylphorbol-13-acetate (DMBA/TPA) (Uhmann Anja et al. 2014). Usually the DMBA/TPA protocol induces the formation

of papilloma and squamous cell carcinoma (DiGiovanni 1992). Unexpectedly and in contrast to wild type skin (Indra et al. 2007), DMBA/TPA-treated *Ptch*$^{flox/flox}$*CD4Cre*$^{+/-}$ skin harbors papilloma and squamous cell carcinoma but also basal cell carcinoma (BCC) (Uhmann Anja et al. 2014). Subsequent lineage tracing experiments and bone marrow transplantations excluded a hematopoietic origin of the BCC and rather suggested a CD4$^+$ stem cell-like population of the basal layer as the origin of DMBA/TPA-induced BCC. Following flow cytometric analyses verified the existence of CD4$^+$ cells in the murine skin expressing the keratinocyte marker CD49f, as well as the stem cell markers CD34 and Sca-1, which differentiate these cells from CD49f^{high} CD34$^+$Sca-1$^-$ stem cells of the hair follicle and from CD49f^{low}CD34$^-$Sca-1$^+$ basal cells (Uhmann Anja et al. 2014). Beyond that, the progeny of CD4$^+$ epidermal cells have been shown to grow permanently and increasingly with age and upon wound healing in adult mice in all epidermal layers and as multipotent hair follicle stem cells (Brandes 2021). Finally, the existence of CD4$^+$ epidermal cells in human skin was also confirmed. In contrast to the murine skin CD4$^+$ epidermal cells of the human skin are characterized by the expression of the keratinocyte marker CD49f and the epidermal stem cell markers CD29 and K15. Since they furthermore lack the expression of immune cell markers such as CD3 (T-cells, Langerhans cells), CD14 (interfollicular dendritic cells, Langerhans cells, monocytes, macrophages, granulocytes) or CD1a (T-cells, B-cells, monocytes, macrophages, Langerhans cells, dendritic cells) (Scheile 2020) human CD4$^+$ epidermal cells are proven of a non-hematopoietic origin. Taken together, CD4-expressing epidermal cells exhibit tumorigenic potential and stem cell-like characteristics (Brandes et al. 2020).

1.3.1. Structure and function of CD4 in immune cells

The existence of an epidermal keratinocyte population expressing the T cell marker CD4 was highly unexpected. Initially the CD4 receptor was identified in rat, where it was of specific interest, as it represented the first known marker of T helper (Th) lymphocytes (White et al. 1978; Williams et al. 1977). CD4 is a membrane-spanning glycoprotein (55 kDa) with an extracellular region composed of four extracellular immunoglobulin-like domains (D1 – D4), a transmembrane region of 22 hydrophobic amino acids and a short cytoplasmic tail of 40 amino acids (Brady and Barclay 1996; Littman 1987). The four extracellular immunoglobulin-like domains represent different functional binding sites (Wu H et al. 1997). In T cells, the D1 domain of the CD4 protein binds to the major histocompatibility complex class II (MHCII) protein thus forming a complex with the T cell receptor (TCR) and CD3. Beyond that, the CD4 receptor is an entry point for the human immunodeficiency virus (HIV), whose gp120 domain also interacts with the D1 domain (Kwong et al. 1998). The CD4 D4 domain is crucial for protein dimerization and serves as a binding site for interleukin 16 (IL-16) (Liu et al. 1999; Richmond et al. 2014). Besides its expression in a subset of T cells, like Th cells, regulatory T (Treg) cells (Corthay 2009) and natural killer T cells (Krijgsman et al. 2018), CD4 is also expressed in monocytes, macrophages and natural killer cells (Bernstein et al. 2006), dendritic cells (Lee B et al. 1999), Langerhans cells (Lynch et al. 2003), neutrophils (Biswas et al. 2003), basophils and mast

cells (Li Y et al. 2001), eosinophils (Lucey et al. 1989), megakaryocytes (Kouri et al. 1993) and in some neuronal cells of the central nervous system (Omri et al. 1994). In the thymus, CD4 plays a role in the positive thymic selection and $CD4^+$ T cells development (Killeen et al. 1993; Rahemtulla et al. 1991). However, its best-known function is its involvement in T cell activation, as CD4 regulates T cell adhesion, signaling and increases antigen sensitivity. Thus, CD4 is essential for recognition of most antigens *in vivo.* In T cells, the CD4 protein acts as a co-receptor of the TCR/CD3 complex, by strengthening the contact between the TCR and MHCII molecule on the antigen-presenting cells (APCs) (Janeway 1989; Kinch et al. 1993). Beyond that, CD4 enhances the MHCII T cell activation and thus increases sensitivity to antigen stimulation (Irvine et al. 2002). After binding to MHCII, CD4 molecules dimerize and form a complex with the TCR/CD3 molecules. The subsequent phosphorylation of Fyn and the tyrosine kinase $p56^{lck}$ (Wu H et al. 1997) then initiate a tyrosine phosphorylation cascade leading to an intracellular mobilization of calcium ions (Ca^{2+}) (Berridge 1993; Corado et al. 1990). Since the temporary rise in cytosolic Ca^{2+} triggers acute reactions, including motility decline, improved spreading, and degradation of the target cells by cytolytic T cells (CTLs), Ca^{2+} mobilization is essential for Th cell activation (Wülfing et al. 1997) (see Figure 4A).
Together with cytoskeleton-dependent mechanisms, Ca^{2+} mobilization leads to translocation of mitochondria to the calcium release-activated channels (CRAC) and plasma membrane Ca^{2+} ATPase (PMCA), providing support to sustain the established extensive Ca^{2+} elevation necessary for generalized activation of T lymphocytes in terms of differentiation, cytokine production and proliferation (Feske 2007; Lewis 2001). Ca^{2+} mobilization in T cells furthermore activates the AC. This enzyme along with nucleotide phosphodiesterases (PDEs) regulates the level of second intracellular messenger cAMP, which is a potent negative regulator of T cell immune function through the cAMP/PKA signaling pathway (Laxminarayana and Kammer 1996) by inhibiting the antigen-induced T cell activation and cytokine production (Bjørgo et al. 2011; Vang T et al. 2001). While AC catalyzes the conversion of adenosine triphosphate (ATP) into cAMP (Khannpnavar et al. 2020), PDEs degrade cAMP to AMP (Bender and Beavo 2006). From the eleven known PDE families (PDE_1 – PDE_{11}), which are categorized according to their primary sequences, protein domains and enzymatic characteristics (Omori and Kotera 2007) families 1, 2, 3, 4, 5, 7 and 8 have been found in T cells (Essayan 2001). However the activity of each PDE family is triggered and controlled by different mechanisms, e.g. PDE1 is stimulated by calmodulin binding in the presence of Ca^{2+} (Charbonneau et al. 1991; Loughney et al. 1996), while PDE4 is known as the main enzyme responsible for cAMP degradation in inflammatory cells (Ahmad et al. 1999; Francis et al. 2011; MacKenzie SJ et al. 1998). Together, Ca^{2+} mobilization, regulation of AC and PDE activity as well as the cAMP/PKA signaling pathway play a central role in balancing the maintenance of T cell homeostasis (Wehbi and Taskén 2016) and T cell activation (Krummel et al. 2000) (see Figure 4A).

1.3.2. Putative function of CD4 on epidermal keratinocytes

As already described, T cells and TCR and/or CD3 negative immune cells, express CD4 (e.g. monocytes, macrophages and natural killer cells, dendritic cells, Langerhans cells, neutrophils, basophils and mast cells, eosinophils, megakaryocytes, neuronal cells). This fact points towards a TCR/CD3-independent CD4 function in these cells. Indeed, TCR-independent dimerization of CD4 molecules or binding of CD4 with MHCII molecules in T cells cause increased intracellular Ca^{2+} and decreased intracellular cAMP levels via inhibition of the AC and induction of the PDE1 and 4 (Zhou and König 2003) (Figure 4A). In addition, CD4-MHCII ligation in TCR/CD3^{neg} monocytes induces their differentiation to macrophages (Zhen et al. 2014) demonstrating that a TCR/CD3-independent CD4 signaling is possible. Unfortunately, so far, the exact mechanisms of a TCR/CD3-independent CD4 signaling is not well understood. However, the fact that CD4$^+$ epidermal cells neither express CD3 nor other immune cell markers (see above) suggests that CD4 signaling in these cells most likely also occurs in a TCR/CD3-independent manner. Thus, hypothetically MHCII ligation to CD4 molecules may be also involved in Ca^{2+} mobilization and/or cAMP generation in CD4-expressing keratinocytes (Figure 4B) and lead to an increased proliferation or differentiation rate, as it is the case with CD4$^+$ monocytes.

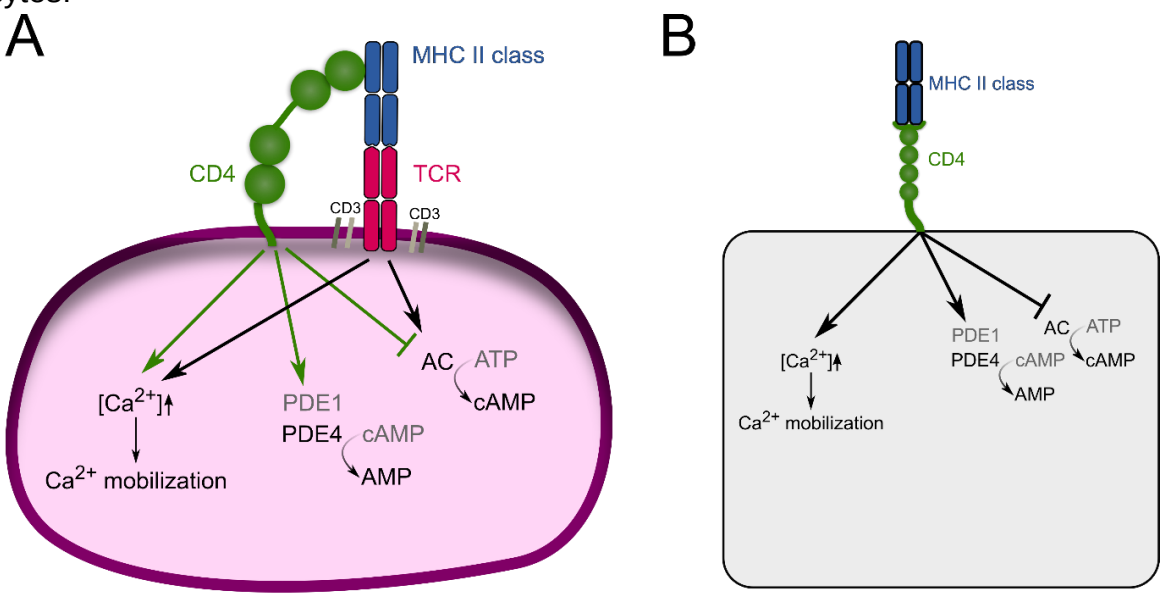

Figure 4: CD4 involvement in T cell activation and hypothetical CD4 function in stem cell-like keratinocytes. A). In T cells CD4 participates in the antigen/MHCII binding to the TCR/CD3 complex which results in cytosolic Ca^{2+} mobilization from intracellular Ca^{2+} stores ([Ca^{2+}]) and in increased intracellular cAMP levels via activation of AC (black arrows). However, TCR/CD3-independent CD4 dimerization (not shown) or ligation of CD4 to MHCII molecules inhibits AC but induces PDE1 and 4 activity resulting in decreased intracellular cAMP levels (green arrows/lines). Adapted from König and Zhou (2004). **B)** In stem cell-like keratinocytes CD4 binding to MHCII molecules hypothetically may cause intracellular [Ca^{2+}] increase and [cAMP] decrease. The latter is achieved through inhibition of the AC and activation of the PDE1 and PDE4 families. Abbreviations: MHC II - major histocompatibility complex class II, TCR - T cell receptor, PDE – phosphodiesterase, cAMP - cyclic adenosine 3′, 5′-monophosphate, AMP - adenosine monophosphate, AC - adenylyl cyclase, ATP - adenosine triphosphate. Adapted from König and Zhou (2004).

The activation of $CD4^+$ T cells leads to their differentiation into Th1, Th2 or Th17 cells (Zhu J and Paul 2010). Within this process, the pro-inflammatory cytokine IL-1 plays a central role, since it regulates lymphocyte differentiation, activation and homeostasis (Ben-Sasson et al. 2009; Santarlasci et al. 2013). However, IL-1 is also secreted by epidermal keratinocytes upon skin injury (Feldmeyer et al. 2010; Murphy et al. 2000) and stimulates fibroblast and keratinocyte growth (Chedid et al. 1994), collagen synthesis of fibroblasts (Postlethwaite et al. 1988), chemotaxis of keratinocytes (Raja et al. 2007) and together with the other pro-inflammatory cytokines plays a role in wound healing (Behm et al. 2012) (see also chapter 1.2.3.3). Beyond that, IL-1 induces *CD4*-expression in microglial cells (Yu et al. 1998). Thus, it can be assumed that IL-1 may be involved in *CD4*-expression in epidermal keratinocytes too (see Figure 5). Similarly also TNFα plays an important role in epidermal wound healing, stimulation of hair follicle stem cells upon wound-induced hair regrowth and mesenchymal stem cell migration during osteoarthritis (Wang X et al. 2017; Wang Y et al. 2017) (see also chapter 1.2.3.3). Thus, TNFα may also be involved in the migration of $CD4^+$ stem cell-like keratinocytes (Figure 5).

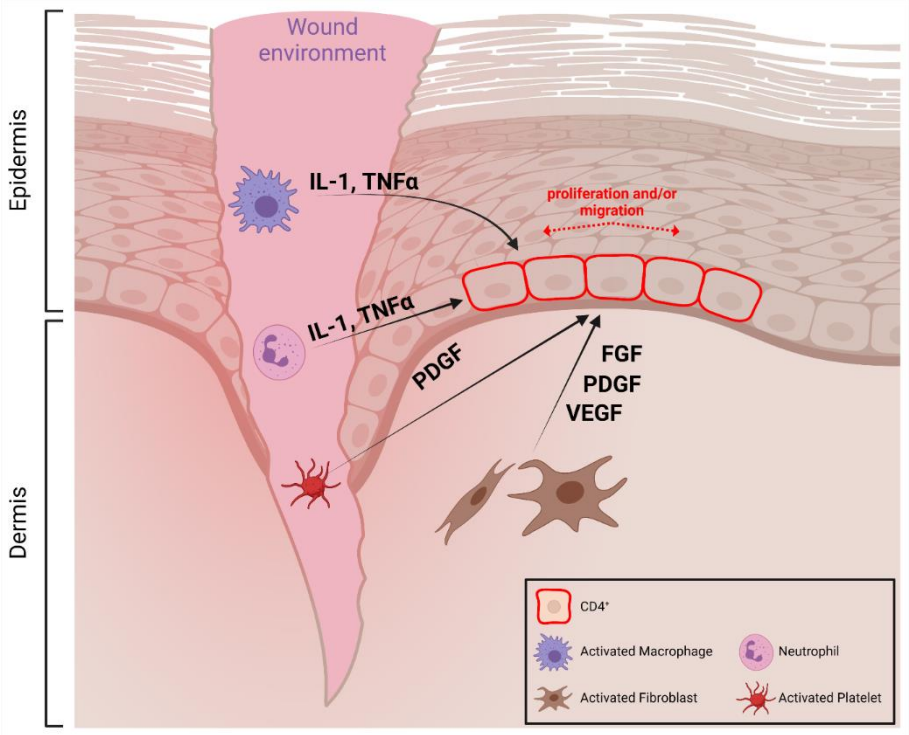

Figure 5: Schematic representation of the hypothetical role of cytokines in regulating $CD4^+$ epidermal stem cells in wounded skin. TNFα released immediately after injury from keratinocytes and fibroblasts supports inflammatory leukocyte recruitment, platelets and fibroblasts and triggers IL-1 synthesis. The infiltrating cells in the wound environment produce various growth factors (PDGF, FGF, VEGF) and cytokines (TNFα and IL-1) and participate in wound healing, which hypothetically induce proliferation and/or migration in $CD4^+$ epidermal keratinocytes, and/or increased *CD4*-expression. Abbreviations: PDGF - platelet derived growth factor, FGF- fibroblast growth factor, VEGF - vascular endothelial growth factor. (Created with BioRender.com).

1.4. Aims of the work

The function of the CD4 protein in stem cell-like keratinocytes is currently unknown although a TCR/CD3-independent CD4 signaling may be conceivable. However, the knowledge about the functionality of CD4 in stem cell-like keratinocytes may have a critical impact on the understanding of skin homoeostasis, wound healing and cancer development. Thus, the main aim of this dissertation was to analyze the CD4 protein function in stem cell-like keratinocytes. For this purpose, first dedifferentiated, stem cell-like, stable murine and human keratinocyte cell lines for analyzing the CD4-protein function *in vitro* should be developed. Subsequently these cells should be used to generate an inducible *CD4*-expression system for future studies, as well as to investigate whether MHCII, IL-1 and/or TNFα play a role in TCR/CD3-independent CD4-mediated signaling (e.g. MHCII, TNFα) or as *CD4*-expression stimuli (e.g. IL-1). For the latter approaches, transiently *CD4*-overexpressing, dedifferentiated, stem cell-like keratinocyte cell lines should be analyzed for their proliferation rate, differentiation status and intracellular cAMP levels or for their cellular migration upon MHCII or TNFα treatment, respectively. Additionally, it should be analyzed whether IL-1 treatment induces endogenous *CD4*-expression in dedifferentiated, stem cell-like keratinocyte cell lines, as it has been previously described for microglia.

2. Materials and Methods

2.1. Technical equipment

Technical equipment utilized in this dissertation is shown in Table 1.

Table 1. Technical equipment.

Technical Equipment	Supplier
3500xL Genetic Analyzer	Thermo Fisher Scientific Inc., Waltham, MA, USA
7900 HT Fast Real-Time PCR System	Applied Biosystems, Waltham, MA, USA
Agarose gel electrophoresis chamber	Peqlab Biotechnology GmbH, Erlangen, Germany
Autoclave (9216E)	Fedegari Autoclavi SpA, Albuzzano, Italy
Autoclave (Systec DX-150)	Systec GmbH & Co. KG, Linden, Germany
Centrifuge (1-15K)	Sigma Laborzentrifugen GmbH, Osterode, Germany
Centrifuge (5427 R, 5415 R)	Eppendorf AG, Hamburg, Germany
Centrifuges (Biofuge pico, fresco, primo, Multifuge 3LR)	Heraeus Holding GmbH, Hanau, Germany
CO_2-Incubator (6000, BBD, 6220)	Thermo Fisher Scientific Inc., Waltham, MA, USA
CO_2-Incubator (CB220-230V-G)	Binder GmbH, Tuttlingen, Germany
Digital monochrome thermal video printer (P91D)	Mitsubishi Electric Co., Tokyo, Japan
Dispersing tool for homogenizer (DS-8/P)	Miccra GmBH, Heitersheim, Germany
Dissection tools	Karl Hammacher GmbH, Solingen, Germany
EasySep™ Magnet	Stemcell Technologies, Germany GmbH, Cologne, Germany
Flow cytometer BD™ LSR II	BD Biosciences, San Jose, CA, USA
Freezer (-20°C)	Liebherr GmbH, Bulle, Switzerland
Freezer (-80°C)	Sanyo Electric Co., Ltd., Osaka, Japan
Freezing container (Mr. Frosty™)	Thermo Fisher Scientific Inc., Waltham, MA, USA
Fridge (4°C)	Robert Bosch GmbH, Stuttgart, Germany
Gas burner	Campingaz, Hattersheim, Germany
Heating block shaker (ThermoMixer©)	Eppendorf AG, Hamburg, Germany
High-precision scales (Sartorius Basic plus 2100)	Sartorius AG, Göttingen, Germany
HiSeq4000	Illumina, San Diego, CA, USA
Homogenizer (Miccra D-1)	Miccra GmBH, Heitersheim, Germany
Inverted fluorescence microscope (Axiovert 25)	Carl Zeiss GmbH, Jena, Germany
Inverted research microscope (IX71)	Olympus Optical Co., Ltd., Tokyo, Japan
Liquid nitrogen tank	L'air liquide S.A., Paris, France
Magnetic stirrer (MR3000/3001)	Heidolph Instruments GmbH & Co. KG, Schwabach, Germany
Microplate reader (SynergyMx)	BioTek Instruments GmbH, Bad Friedrichshall, Germany
Microscope (FV3000)	Olympus Optical Co., Ltd., Tokyo, Japan
Microscope (Olympus BX 60)	Olympus Optical Co., Ltd., Tokyo, Japan
Microwave oven (Dimension 4)	Panasonic Corp., Kadoma, Japan
Mini Centrifuge ROTILABO ®	Carl Roth GmbH & Co. KG, Karlsruhe, Germany
Neon™ Transfection system	Thermo Fisher Scientific Inc., Waltham, MA, USA
Neubauer counting chamber	Brand GmbH & Co KG, Wertheim, Germany
Nikon Eclipse Ti spinning disk confocal microscope equipped with a Yokogawa W1 spinning disk and an Andor iXon 888 EMCCD camera	Nikon GmbH, Düsseldorf, Germany

Technical Equipment	Supplier
Nikon Eclipse Ti2 widefield fluorescence microscope equipped with a Photometrics Prime 95b 25mm sCMOS camera and Okolabincubation chamber	Nikon GmbH, Düsseldorf, Germany
PCR Thermocycler (Labcycler Basic, Labcycler Gradient)	SensoQuest GmbH, Göttingen, Germany
PCR Thermocycler (Mastercycler®)	Eppendorf AG, Hamburg, Germany
pH-meter (inoLab, pH Level 1) and electrode (SenTix 91)	WTW, Weilheim, Germany
Pipette controller (accu-jet® pro)	Brand GmbH & Co. KG, Wertheim, Germany
Pipettes (Multi- and single-channel pipettes)	Eppendorf AG, Hamburg, Germany
Platform shaker (Unimax1010)	Heidolph Instruments GmbH & Co. KG, Schwabach, Germany
Power supply for agarose gel electrophoresis	Peqlab Biotechnology GmbH, Erlangen, Germany
Precision weighing balance (ALC-210.4)	Sartorius AG, Göttingen, Germany
Spectrophotometer (NanoDrop 8000)	Thermo Fisher Scientific Inc., Waltham, MA, USA
Sterile workbench (Euroflow EF/A 5)	Clean Air Techniek, Woerden, Netherlands
Ultraviolet (UV) light -Transilluminator	Intas Science Imaging Instruments GmbH, Göttingen, Germany
Vacuum pump (EcoVac)	Schuett-biotec GmbH, Göttingen, Germany
Vortex mixer (Vortex-Genie2®)	Scientific Industries Inc, Bohemia, NY, USA
Water purification system (Arium® 611 VF)	Sartorius AG, Göttingen, Germany

2.2. Consumable materials

Consumable materials used are shown in Table 2.

Table 2. Consumable materials.

Consumable Materials	Supplier
6-well cell culture plate	Sarstedt AG & Co., Nümbrecht, Germany
12-well cell culture plate	Sarstedt AG & Co., Nümbrecht, Germany
24-well cell culture plate	Corning Incorporated, New York City, NY, USA
384-well plate black & adhesive seal sheet	4titude® Ltd., Surrey, UK
Cell scraper	Sarstedt AG & Co., Nümbrecht, Germany
Cell Strainer 40 µm	Sigma-Aldrich Co., St. Louis, MO, USA
Centrifuge tubes (15 ml, 50 ml)	Greiner Bio-One International GmbH, Kremsmünster, Austria
Combitips advanced® (0.2 ml, 0.5 ml, 2.5 ml, 5 ml, 10 ml)	Eppendorf AG, Hamburg, Germany
Coverslips	Thermo Fisher Scientific Inc., Waltham, MA, USA
Coverslips (round) for cultivation	TH. Geyer GmbH & Co. KG, Renningen, Germany
CryoPure tubes	Sarstedt AG & Co., Nümbrecht, Germany
Delicate task wipes	Kimberly-Clark Europe Ltd., Surrey, UK
Disposable needles (Sterican Ø 0.45 x 12 mm or Ø 0.30 x 12 mm)	B.Braun AG, Melsungen, Germany
Disposable syringes (BD DiscarditTM II 1, 2, 10, 20, 50 ml)	BD Biosciences, San Jose, CA, USA
Falcon® 4-well Culture Slide	Corning Incorporated, New York City, NY, USA
Filter tips (Biosphere® 20 µl, 100 µl, 200 µl, 1000 µl)	Sarstedt AG & Co., Nümbrecht, Germany
Flow Cytometry Tubes (5 ml, sterile)	Sarstedt AG & Co., Nümbrecht, Germany
Fluted filters	Sartorius AG, Göttingen , Germany

Consumable Materials	Supplier
Folded filters	Sartorius AG, Göttingen, Germany
Glassware	Schott AG, Mainz, Germany
Microscope slides & Superfrost® plus microscope slides	Thermo Fisher Scientific Inc., Waltham, MA, USA
Nunclon™ disposables for cell culture (10 cm cell culture dish, 96-well plate)	Thermo Fisher Scientific Inc., Waltham, MA, USA
Parafilm® laboratory film	Bemis Company, Inc., Neenah, WI, USA
Pasteur pipettes	TH. Geyer GmbH & Co. KG, Renningen, Germany
PCR tear-a-way plates & cap strips	4titude® Ltd., Surrey, UK
Petri dishes	Ochs GmbH, Bovenden / Lenglern, Germany
Pipette tips (20 µl, 200 µl, 1000 µl)	Sarstedt AG & Co., Nümbrecht, Germany
Reaction tubes (1.5 ml, 2 ml, 5 ml)	Sarstedt AG & Co., Nümbrecht, Germany
Safeseal microtubes (1.5 ml, 2 ml)	Sarstedt AG & Co., Nümbrecht, Germany
Serological pipettes (2 ml, 5 ml, 10 ml, 25 ml)	Sarstedt AG & Co., Nümbrecht, Germany
Softa-Man® hand disinfectant	B.Braun AG, Melsungen, Germany
Sterile filters (0.2 µm)	Sartorius AG, Göttingen, Germany
Sterile filter (Filtropur - 0.2 µm)	Sarstedt AG & Co., Nümbrecht, Germany
Surgical blades	Aesculap AG, Tuttlingen, Germany
Weighing paper	Macherey-Nagel GmbH & Co. KG, Düren, Germany
Whatman® Blotting paper (GB 33 B003)	Heinemann Labortechnik GmbH, Duderstadt, Germany
µ-Slide Chemotaxis	Ibidi GmbH, Gräfelfing, Germany

2.3. Reagents and chemicals

Reagents and chemicals used are shown in Table 3.

Table 3. Reagents and chemicals.

Reagents and chemicals	Supplier
Agarose	VWR International GmbH, Erlangen, Germany
Agarose, low melting	Carl Roth GmbH & Co. KG, Karlsruhe, Germany
Ampicillin sodium salt	Carl Roth GmbH & Co. KG, Karlsruhe, Germany
Ampuwa H_2O	Fresnius Kabi Deutschland GmbH, Gemany
Bovine serum albumin fraction V (BSA), protease free	Carl Roth GmbH & Co. KG, Karlsruhe, Germany
Calcium chloride dihydrate ($CaCl_2$)	Sigma-Aldrich Co., St. Louis, MO, USA
Chloroform	Carl Roth GmbH & Co. KG, Karlsruhe, Germany
Deoxyribonucleotide triphosphates (dNTPs)	Roche Diagnostics GmbH, Mannheim, Germany
Dimethyl sulfoxide (DMSO)	Thermo Fisher Scientific Inc., Waltham, MA, USA
Dispase	Corning Incorporated, New York City, NY, USA
Dithiothreitol (DTT)	Thermo Fisher Scientific Inc., Waltham, MA, USA
DNase/RNase-free distilled H_2O (ultrapure H_2O)	Invitrogen, Carlsbad, CA, USA
Ethanol (EtOH) 99 %	J.T. Baker B.V., Deventer, Netherlands
Ethanol 99 %, denatured	TH. Geyer GmbH & Co. KG, Renningen, Germany
Ethidium bromide (EtBr) 0.07 %	Inno-Train Diagnostik GmbH, Kronberg im Taunus, Germany
Ethylenediamine tetraacetic acid (EDTA) disodium salt dihydrate	Carl Roth GmbH & Co. KG, Karlsruhe, Germany
Forskolin	Sigma-Aldrich Co., St. Louis, MO, USA

Reagents and chemicals	Supplier
GeneRuler DNA ladder (50 base pairs (bp), 100 bp plus, 1 kilobase (kb))	Thermo Fisher Scientific Inc., Waltham, MA, USA
Hanks' Balanced Salt Solution (HBSS), no calcium, no magnesium	Thermo Fisher Scientific Inc., Waltham, MA, USA
HEPES buffer solution (1M in H_2O)	Sigma-Aldrich Co., St. Louis, MO, USA
Hygromycin B (100 mg/ml)	InvivoGen, Toulouse, France
Hydrochloric acid (37 %)	Carl Roth GmbH & Co. KG, Karlsruhe, Germany
Interleukin-1α, human recombinant, expressed in *E. coli*	Sigma-Aldrich Co., St. Louis, MO, USA
Isopropyl alcohol	Carl Roth GmbH & Co. KG, Karlsruhe, Germany
Kanamycin A	Sigma-Aldrich Co., St. Louis, MO, USA
Loading dye solution for DNA (6x)	Thermo Fisher Scientific Inc., Waltham, MA, USA
Mitomycin C from *Streptomyces caespitosus*	Sigma-Aldrich Co., St. Louis, MO, USA
MHC Tetramer Class II	NIH Tetramer Core Facility, Atlanta, USA
Paraformaldehyde (PFA)	Carl Roth GmbH & Co. KG, Karlsruhe, Germany
Phenylmethylsulfonyl fluoride (PMSF)	Sigma-Aldrich Co., St. Louis, MO, USA
Phosphate buffered saline (PBS) Tab.ts	Invitrogen, Carlsbad, CA, USA
Primer “random” p(dN)6 Hexamer-oligonucleotides	Roche Diagnostics GmbH, Mannheim, Germany
ProLong Gold antifade mountant with 4′,6-diamidino-2-phenylindole (DAPI)	Thermo Fisher Scientific Inc., Waltham, MA, USA
Puromycin dihydrochloride (10 mg/ml)	Sigma-Aldrich Chemistry GmbH, Steinheim
RNase-free H_2O	Invitrogen, Carlsbad, CA, USA
RNaseZAP	Sigma-Aldrich Co., St. Louis, MO, USA
S.O.C. (Super optimal broth with catabolite repression) medium	Invitrogen, Carlsbad, CA, USA
Sodium hydroxide	Carl Roth GmbH & Co. KG, Karlsruhe, Germany
Triton™ X-100	Sigma-Aldrich Co., St. Louis, MO, USA
Tumor Necrosis Factor-α, human, recombinant (TNFα)	Sigma-Aldrich Co., St. Louis, MO, USA
Versene solution	Thermo Fisher Scientific Inc., Waltham, MA, USA
ß-Mercaptoethanol	Sigma-Aldrich, Chemie GmbH, Steinheim

2.4. Buffers and solutions

Buffers and solutions used are shown in Table 4.

Table 4. Buffers and solutions.

Buffer / Solution	Composition
Casein (0.2 %)	0.2 % (w/v) I-Block Dissolved in Tris-buffered saline (TBS)
Cresol	0.1 % (w/v) Cresol red Dissolved in saturated sucrose-solution
dNTP-Mix	10 mM dATP 10 mM dCTP 10 mM dGTP 10 mM dTTP
Lysogeny broth medium (LB medium)	1 % (w/v) Bacto-tryptone 1 % (w/v) NaCl (pH7.0) 0.5 % (w/v) Yeast extract
Lysogeny broth agar (LB agar)	1.5 % (w/v) Agar Dissolved in LB medium
Paraformaldehyde 4 %	4 % (w/v) Paraformaldehyde Dissolved in PBS

Buffer / Solution	Composition
10 x PBS; pH 7.4	1.4 M NaCl 65 mM Na_2HPO_4 27 mM KCl 15 mM KH_2PO_4
TBS-Triton X-100	0.1 % (v/v) Triton X-100 Dissolved in TBS
10 x Tris-boric acid-EDTA solution (TBE); pH 8.0	890 mM Tris/HCl, pH 8.0 730 mM boric acid 12.5 mM EDTA
10 x TBS; pH 7.4	150 mM NaCl 10 mM Tris/HCl, pH 8.0
Trypan blue staining solution; pH 7.2 - 7.3	0.4 % (w/v) Trypan blue Dissolved in PBS

2.5. Kits and ready-to-use reaction systems

All kits and ready-to-use systems are shown in Table 5.

Table 5. Kits and ready-to-use reaction systems.

Reactions system	Supplier
BigDyeTM Terminator v3.1 Cycle Sequencing Kit	Thermo Fisher Scientific Inc., Waltham, MA, USA
Cell proliferation Enzyme-linked immunosorbent assay (ELISA), BrdU chemiluminescent	Roche Diagnostics GmbH, Mannheim, Germany
Cyclic AMP XP ® Chemiluminescent Assay Kit	Cell Signaling Technology, Danvers, MA, USA
EasySep™ Mouse CD4+ T Cell Isolation Kit	STEMCELL Technologies, Germany GmbH, Cologne, Germany
MATra Starter Set (Universal Magnet Plate, 8x13 cm and MATra-A Reagent)	IBA GmbH, Göttingen, Germany
NEON Transfection kit	Thermo Fisher Scientific Inc., Waltham, MA, USA
NucleoSpin Gel and PCR Clean-up, Mini kit for gel extraction and PCR clean up	Macherey-Nagel, Düren, Germany
Platinum™ SYBR™ Green qPCR SuperMix-UDG w/ROX	Invitrogen, Carlsbad, CA, USA
PureLink®HiPure Plasmid Midiprep Kit	Invitrogen, Carlsbad, CA, USA
RNeasy Fibrous Tissue Mini Kit	Qiagen GmbH, Hilden, Germany
Tet-On® Advanced Inducible Gene Expression System	Clontech Laboratories, Inc. A Takara Bio Company, Mountain View, CA, USA
TRIzol® Reagent	Life Technologies Co., Camarillo, CA, USA

2.6. Enzymes

Table 6 summarizes all enzymes used in the dissertation. The enzymes were stored at -20˚C and the reactions were performed according to manufacturer's instructions.

Table 6. Enzymes.

Enzymes	Supplier
*Ase*I	New England Biolabs, Ipswich, MA, USA
*EcoR*I	New England Biolabs, Ipswich, MA, USA
*EcoR*V	New England Biolabs, Ipswich, MA, USA
*Kpn*I	New England Biolabs, Ipswich, MA, USA
*Mfe*I	New England Biolabs, Ipswich, MA, USA
Q5 DNA Polymerase	New England Biolabs, Ipswich, MA, USA
RNase A	Carl Roth GmbH & Co. KG, Karlsruhe, Germany

Enzymes	Supplier
*Sal*I	New England Biolabs, Ipswich, MA, USA
*Ssp*I	New England Biolabs, Ipswich, MA, USA
SuperScript™ II Reverse Transcriptase	Thermo Fisher Scientific Inc., Waltham, MA, USA
T4 DNA Ligase	Invitrogen, Carlsbad, CA, USA
Taq - Polymerase (MolTaq)	Molzym GmbH & Co. KG, Bremen, Germany
*Xba*I	New England Biolabs, Ipswich, MA, USA

2.7. Plasmids

Commercially available plasmids, as well as plasmids created for this dissertation are listed in Table 7.

Table 7. Commercially available and *de novo*-generated plasmids.

Plasmid	Application	Selection Antibiotic	Supplier
pBluescript II SK (+)	High copy plasmid, that enables blue/white screening of bacterial colonies	Ampicillin	Stratagene, San Diego, CA, USA
pCR3.1	Vector for transient transfection, contains a CMV-promoter for high expression of downstream-cloned genes in mammalian cells	Ampicillin	Invitrogen, Carlsbad, CA, USA
pCR3.1-CD4	Transient transfection of this plasmid enables the transient expression of human CD4 in mammalian cells	Ampicillin	Generated in this work
pEGFP-N1	Transient transfection of this plasmid enables the transient expression of EGFP in mammalian cells, used as transfection control and in co-transfection experiments	Kanamycin	BD Bioscience Clontech, Heidelberg, Germany
pTET-DualON	Co-transfected with linear selection marker (Hygromycin or Puromycin) for selecting the cells and creating a stable pTet-ON advanced cell line	Hygromycin or Puromycin	Clontech Laboratories, Inc. A Takara Bio Company, Mountain View, CA, USA
pTre-Dual2-hCD4	Co-transfected with linear selection marker (Hygromycin or Puromycin) for selecting the cells from the stable pTet-ON advanced cell line and stably transfected cells that express high levels of CD4 in response to Doxycycline treatment	Hygromycin or Puromycin	Clontech Laboratories, Inc. A Takara Bio Company, Mountain View, CA, USA

2.8. Antibodies

2.8.1. Antibodies for immunocytochemistry

Table 8 lists all primary and secondary antibodies used for immunocytochemistry.

Table 8. Primary and secondary antibodies.

Primary Antibodies		
Antibody	**Dilu-tion**	**Supplier/Clone**
pAb rabbit – anti K1	1:1000	Covance Inc., Princeton, New Jersey, United States / Poly19056
pAb rabbit – anti (human/mouse) K5	1:500	BioLegend, San Diego, CA, United States / Poly19055
pAb rabbit – anti (human) K10	1:500	BioLegend, San Diego, CA, United States/Poly19054
pAb mouse – anti K10	1:100	Abcam plc, Cambridge, UK / DE-K10
mAb mouse – anti (human/mouse) K15	1:500	Thermo Fisher Scientific Inc., Waltham, MA, USA / LHK15
mAb mouse – anti (human) Ki67	1:50	BD Pharmigen, Heidelberg, Germany / B56
mAb mouse – anti p63	1:100	Santa Cruz Biotechnology, Santa Cruz, USA / D-9
mAb rabbit – anti CD4	1:50	DCS Innovative Diagnostik-Systeme, Hamburg, Germany / SP35
mAb mouse – anti CD29	1:35	Antikörper-online.de; / ABIN119209
Secondary Antibodies		
Antibody	**Dilu-tion**	**Supllier**
pAb goat anti – mouse IgG Alexa Fluor 488	1:200	Invitrogen, Carlsbad, CA, USA
pAb donkey anti – rabbit IgG Cy™3	1:400	Jackson ImmunoResearch Europe Ltd., Cambridgeshire, Dianova, UK
pAb donkey anti – mouse IgG Alexa Fluor 488	1:200	Jackson ImmunoResearch Europe Ltd., Cambridgeshire, Dianova, UK

mAb/pAb: monoclonal/polyclonal antibody; **ICC:** immunocytochemistry; **Cy3**: Cyanine Dye 3

2.8.2. Antibodies for flow cytometry

Fluorescent dye-labelled antibodies used for flow cytometry are listed in Table 9.

Table 9. Antibodies and dyes used for flow cytometry.

Name	Fluorescent dye-labeling	Method	Supplier / Clone
Rat anti – mCD4	FITC	Flowcytometry	BD Pharmigen, Heidelberg, Germany/RM4-5
Rat anti – mCD3	PE-Cy™7	Flowcytometry	BD Pharmigen, Heidelberg, Germany/17A2

FITC: Fluorescein isothiocyanate; **Cy7:** Cyanin Dye 7.

2.9. Synthetic DNA-oligonucleotides

DNA-oligonucleotides were purchased from Eurofins Scientific SE (Luxemburg, Luxembourg) and were kept at -80°C as 100 µM stock solutions dissolved in ultrapure H_2O.

2.9.1. DNA-oligonucleotides for polymerase chain reaction (PCR)

The deoxyribonucleic acid (DNA) oligonucleotides used in polymerase chain reactions (PCR) were designed using the Ensembl genome browser (https://www.ensembl.org). Primer concentrations, reaction components and PCR conditions are described in section 2.14.5. Used primers are listed in Table 10.

Table 10. PCR Primers.

Primer Name	Sequence (5→3' orientation)	Amplicon size
hCD4cloningF	ATGAACCGGGGAGTCCCTTTTAGGCAC	1377 bp
hCD4cloningR	TCAAATGGGGCTACATGTCTTCTGAAAC	

2.9.2. DNA-oligonucleotides for quantitative real-time PCR

DNA-oligonucleotides used for quantitative real-time polymerase chain reaction (qRT-PCR) are listed in

Table 11. 10 µM working solutions were applied in qRT-PCR. Primer concentrations and qRT-PCR cycling conditions are described in the respective 2.14.7 section.

Table 11. qRT-PCR Primers.

Transcript	Name	DNA-oligonuceotide sequence (5'→3' orientation)	Location	Amplicon size
Primers for human sequences				
KRT1	hsKRT1F.2	GCAGACATGGGGATAGTGTGAGAA	Exon 6	170 bp
	hsKRT1R.2	CTTGGCATCCTTGAGGGCAT	Exon 7	
KRT10	hsKRT10F.2	AGCCTCCTTGGCAGAAACAGA	Exon 6	214 bp
	hsKRT10R.2	GCCTCCGGAACTTCCCTCT	Exon 6/7	
KRT15	hKRT15-F	GATGTCGAGGCCTGGTTCTTC	Exon 6	114 bp
	hKRT15-R	CATCGTGCGTCTCAGGTCTGT	Exon 7	
IVL	hsIVOF.2	CTGCCTCAGCCTTACTGTGAGTCT	Exon 1	192 bp
	hsIVOR.2	CGACAGGCACCTTCTGGCAT	Exon 2	
CD4	hCD4 qRT-F1	GCAGCCACTCAGGGAAAGAAAG	Exon 3	186 bp
	hCD4 qRT-R1	TGAGTCAGCGCGATCATTCAG	Exon 4	
KRT6	hKRT6F	GAGATCGACCACGTCAAGAAGC	Exon 8	123 bp
	hKRT6R	TGACTTGTCCAACGCCTTCG	Exon 9	
S100A7	hS100A7F	TGCTGACGATGATGAAGGAG	Exon 2	82 bp
	hS100A7R	AAGACATCGGCGAGGTAATTT	Exon 3	
Primers for murine sequences				
Krt1	mK1-F	TCAACGTTGAGGTTGACCCTC	Exon 1	232 bp
	mK1-R	ACCTTCCTTCTGAGGATGCTG	Exon 2	
Krt10	mK10-F2	GTCACAGTGCTGGAAGTGG	Exon 7	106 bp
	mK10-R2	GTGTCACCTCCTCAATAATCG	Exon 8	
Krt15	mKrt15-F	GTAGAGGCCTGGTTCTTC	Exon 4	114 bp
	mKrt15-R	CTGCAGGGTCCGTCTCA	Exon 5	
Lor	Lor-F1	CACTCATCTTCCCTGGTGCTTC	Exon 1	103 bp
	Lor-R1	GTCTTTCCACAACCCACAGGAG	Exon 2	
Ivl	Ivl-1-F2	GACTCTGCTGGAAGCCTCTGCC	Exon 1	154 bp
	Ivl-1-R2	TGCTGGATATGATCTGGAGAAC	Exon 2	
Primers for human and murine sequences				
***KRT5* human, *Krt5* murine**	h+m KRT5-F	CATGAAGATGTTCTTTGATGCG	Exon 4	126 bp
	h+m KRT5-R	GCCTTGACCTCAGCGATG	Exon 5	
human and murine *18S*	18S-fwd	CGCAAATTACCCACTCCCG	Exon 1	81 bp

The forward (F) and reverse (R) primers used in qRT-PCR reactions were designed using the Ensembl genome browser and none of the primer sequences showed genomic cross reactivity with other genes in a Primer-BLAST search analysis. The web addresses of these online software tools are shown in section 2.12.

2.9.3. DNA-oligonucleotides for Sanger sequencing

DNA oligonucleotides used for Sanger sequencing (Table 12) were purchased from Addgene (Watertown, Massachusetts, United States). 10 µM working solutions were applied in Sanger sequencing reactions. Primer concentrations, reaction components and cycling conditions are described in section 2.14.9.

Table 12. Primers used for Sanger sequencing.

DNA-Oligonucleotide	Sequence (5'→3' orientation)
T3	GCAATTAACCCTCACTAAAGG
T7	TAATACGACTCACTATAGGG

2.10. Cell cultivation media and reagents

2.10.1. Media and reagents for the cultivation of prokaryotic cells

Bacterial cells were cultured either in lysogeny broth (LB) medium or on LB agar plates. After preparing the LB medium (Table 4) in double-distilled H_2O (ddH_2O), it was autoclaved and stored at 4°C until use. Transformed cells were selected through addition of the suitable antibiotic (100 µg/ml ampicillin or 50 µg/ml kanamycin) to the LB medium.

To generate LB agar plates, 1.5 % (w/v) agar was dissolved in LB medium and the solution was autoclaved and allowed to cool to 55ºC. At this point, the suitable selection antibiotic (100 µg/ml ampicillin or 50 µg/ml kanamycin) was added and the LB agar was poured into 10 cm Petri dishes. After the agar had solidified, the plates were placed in sterile plastic bags and stored at 4°C until use.

2.10.2. Media and reagents for cultivation of eukaryotic cells

All media and reagents used to cultivate eukaryotic cells are listed in Table 13.

Table 13. Media and reagents required for eukaryotic cell cultivation.

Media / Reagent	Supplier
$CaCl_2$	Sigma-Aldrich Co., St. Louis, MO, USA
Chelex - 100 Resin	Bio-Rad Laboratories, Inc., Hercules,California, USA
DMSO	Sigma-Aldrich Co., St. Louis, MO, USA
Dulbecco's Modified Eagle Medium supplemented with 4500 mg/L Glucose, without L-Glutamine, Sodium Pyruvate, Calcium (DMEM---)	Life Technologies, Europe, BV, Bleiswijk, Netherlands
Dulbecco's Modified Eagle Medium supplemented with 4500 mg/L Glucose, L-Glutamine, Sodium Pyruvate (DMEM+++)	Life Technologies, Europe, BV, Bleiswijk, Netherlands
Fetal calf serum (FCS)	Invitrogen, Carlsbad, CA, USA
L-Glutamine (200 mM)	Life Technologies, Europe, BV, Bleiswijk, Netherlands

Media / Reagent	Supplier
PBS Tab.ts for cell culture (1 Tab.t dissolved in 500 ml ddH_2O, autoclaved before use)	Invitrogen, Carlsbad, CA, USA
Penicillin (10.000 U/ml) and Streptomycin (10 mg/ml) (P/S)	Thermo Fisher Scientific Inc., Waltham, MA, USA
RPMI 1640 Medium, GlutaMAX™ Supplement	Thermo Fisher Scientific Inc., Waltham, MA, USA
Sodium Pyruvate (100 mM)	Life Technologies, Europe, BV, Bleiswijk, Nether-lands
TrypLE Express	Life Technologies, Europe, BV, Bleiswijk, Nether-lands

Some of the eukaryotic cells were grown in medium containing heat-inactivated, chelexed fetal calf serum (cFCS). Briefly, 500 ml fetal calf serum (FCS) was heat-inactivated for 30 min at 56°C (hiFCS). Free Ca^{2+} ions of hiFCS were removed by incubation with a chelating agent. In particular, 100 g of Chelex - 100 resin was slurred with 450 ml ddH_2O and the pH was adjusted to 7.4 with 1 M NaOH while stirring. The solution was filtered through a Whatman filter and the remaining resin was added to 500 ml hiFCS, which was then stirred overnight at 4 °C. Next the chelated hiFCS was filtered through a Whatman filter, the resin was discarded, the chelated hiFCS was sterile-filtered with a Filtropur filter (0.2 µm pore size), aliquoted and stored at -20°C until use.
Media with a defined calcium concentration were generated by adding specific amounts of $CaCl_2$. In particular, $CaCl_2$ was added to ddH_2O and stirred until dissolved and then filter-sterilized through a 0.2 µm sterile filter to prepare a 0.1 M stock solution.

2.11. Biological materials

2.11.1. Bacterial strains

The chemically competent *Escherichia coli* (*E. coli*) strain DH5α (Invitrogen GmbH, Karlsruhe) was used for plasmid DNA (pDNA) transformation and amplification. The bacteria were stored in 50 µl aliquots at -80°C until use.

2.11.2. Eukaryotic cell lines

Eukaryotic cell lines used in this thesis are summarized in Table 14. The cells were cultured in appropriate cell culture media under constant conditions (37°C, 5 % CO_2, humidified atmosphere) in a CO_2-incubator.

Table 14. Eukaryotic cell lines.

Cell Line	Species	Description	Reference and/or Supllier (ATCC Number)
C5N	Murine	Non-tumorigenic murine keratinocyte cell line	Zoumpourlis et al. (2003)
HaCaT	Human	Stable human keratinocyte cell line isolated from histologically normal skin	Boukamp et al. (1988)
HL-60	Human	Acute promyelocytic leukemia cell line	ATCC® CCL-240™

2.11.3. Mouse strains

For some experiments, splenic cells from wildtype 129/SV WT (breeding in the animal house of the Institute for Human Genetics, University of Göttingen) and C57BL/6N (B6N) (Charles River Laboratories, Inc., Wilmington, USA) were used.

2.11.4. Patient (human) samples

The use of human skin samples was approved by the Ethical Committee of the Medical University in Göttingen, Germany on 29.01.2016. The Application Number is 3/19/4 and the study title is “Characterization of human $CD4^+$ stem cell like epidermal cells and their role in tumorigenesis and HIV-infection” (Brandes 2021).

2.12. Software and databases

A summary of all proprietary and open-source software and databases used in this thesis is shown in Table 15.

Table 15. Software and databases.

Software	Developer
Adobe Photoshop CS5	Adobe Systems Incorporated, San Jose, USA (https://www.adobe.com/de)
BioRender	BioRender, Toronto, Canada (https://biorender.com/)
Chemotaxis and Migration Tool	Ibidi GmbH, Gräfelfing, Germany (https://ibidi.com/chemotaxis-analysis/171-chemotaxis-and-migration-tool.html)
CellProfiler	McQuin et al. (2018) (https://cellprofiler.org/)
Endnote X5	Thomson ISI ResearchSoft, Carlsbad, CA, USA (https://endnote.com)
FIJI V2.1.0/1.53c	Open-source software for biological image analysis (Schindelin et al. 2012) (https://fiji.sc)
GraphPad Prism 6	GraphPad Software, Inc., La Jolla, CA, USA (https://www.graphpad.com/scientific-software/prism)
Inkscape V1.1.2	Inkscape Community (https://inkscape.org/)
Microsoft Office 2016	Microsoft Co., Redmond, WA, USA (https://www.microsoft.com)
NanoDrop 800 V2.3	Thermo Fisher Scientific Inc., Waltham, MA, USA
INTAS GDS 3.39 software	INTAS Science Imaging Instruments GmbH, Göttingen, Germany
SDS 2.2 software	Applied Biosystems, Waltham, MA, USA
SnapGene Viewer	GSL Biotech LLC, San Diego, USA (https://www.snapgene.com/snapgene-viewer/)
TrackMate	Tinevez et al. (2017) (https://imagej.net/TrackMate)
Databases	**Web site/ Source/ Internet Link**
Basic Local Alignment Search Tool (BLAST)	https://blast.ncbi.nlm.nih.gov/Blast.cgi
Ensembl genome browser	https://www.ensembl.org/index.html
Online Mendelian Inheritance in Man (OMIM)	https://www.omim.org/
Primer-BLAST	https://www.ncbi.nlm.nih.gov/tools/primer-blast/

2.13. Cell biology methods

The entire cell culture work was conducted in a laminar flow hood ensuring aseptic conditions, while using the appropriate sterile equipment. Cell morphology (shape

and appearance), confluency and adhesion, as well as possible cell contamination were monitored with regular microscopic observations.

2.13.1. Cultivation of eukaryotic cell lines

Eukaryotic cell lines (Table 14) were seeded in 10 cm-diameter culture plates in their respective media and grown in an incubator at 37°C, 5 % CO_2 and 95 % atmospheric humidity. The cell culture medium was exchanged every third day and the cells were passaged at 60 - 70 % confluence.

2.13.2. Passaging of eukaryotic cell lines

To passage cells, the cell culture medium was discarded and 5 ml TrypLE™ Express, a recombinant enzyme used for dissociation of wide range of adherent cells, were added and allowed to incubate for 5 - 10 min inside the cell culture incubator. The cells were observed under a microscope to confirm their detachment from the culture plate. The resulting cell suspension was collected, transferred into tubes (15 or 50 ml), which were then centrifuged at 4 °C, at 300 x *g* for 5 min. The supernatant was aspirated and the cell pellet resuspended in the respective, fresh growth medium. A sample of this suspension was used to establish the cell concentration (section 2.13.4), after which the cell suspension was diluted to seeding density and plated onto new culture dishes containing the appropriate media and supplements.

2.13.3. Cryopreservation and thawing of eukaryotic cells

Cells were frozen in liquid nitrogen for long-term storage and preservation. First, the cells were detached and centrifuged (section 2.13.2) and the resulting cell pellet resuspended in the corresponding cell culture medium containing 5 % (v/v) DMSO. 1 ml cell suspension was aliquoted into CryoPure tubes and placed into a *Mr. Frosty* freezing container (filled with 100 % isopropyl alcohol) ensuring a slow, gradual (1°C/min), overnight freezing process down to -80°C, after which they were placed into a liquid nitrogen tank.

Cells were thawed by retrieving the frozen cell aliquots from the liquid nitrogen storage tank and quickly warming them up to room temperature (RT). After diluting the thawed cells in their respective cell culture medium and subsequent centrifugation at 4°C at 300 x *g* for 5 min, the DMSO-containing supernatants were discarded and the resulting pellets resuspended in fresh, appropriate cell culture medium. The cells were seeded in culture plates and placed in the incubator. The medium was refreshed the next day to further ensure removal of any potentially remaining DMSO.

2.13.4. Cell counting

To determine the number of viable cells we used a Neubauer counting chamber. First, the chamber and coverslip were cleaned with 70 % ethanol and allowed to dry and affix to each other. Proper coverslip adhesion was verified by the appearance of Newton's refraction rings at the coverslip-chamber interface. After cell detachment (section 2.13.2), a small sample from the prepared single-cell suspension was mixed with 0.04 % trypan blue (in 1x PBS) in a ratio of 1:1. As trypan blue is unable to penetrate through the cell membrane of live, intact cells, it is used to quantify

viable cells by labeling dead cells exclusively. Next, 10 µl trypan blue-treated cell suspension were applied slowly under the coverslip. Afterwards, the chamber was positioned on an inverted microscope above a 10x objective, equipped with phase contrast optics and the cells were counted manually using a hand tally counter. Only live, unstained cells were counted in the 4 largest quadrants of the Neubauer chamber. The number of the counted cells in one set of 16 small squares is equivalent to the number of cells *x* 10^4 /ml. The total cell number was calculated according to Equation 1:

$$\frac{\text{Total Cells} * 10^4}{ml} = \text{Total Cells Counted} * \left(\frac{\text{Dilution Factor}}{\text{Number of Squares Counted}}\right)$$

Equation 1. Neubauer chamber-based total cell number calculation.

After counting, the appropriate number of cells for the respective experiment were seeded (Table 16).

Table 16. Number of cells seeded for different in vitro assays.

Experimental setup	Cultivation vessel (Plate format)	Seeding density	Total volume of medium
Chemotaxis assay	µ-slide	2,5 × 10^3 cells / chamber	6 µl in observation area
Immunocytochemistry	4-chambers per slide / or cover slips in 24 well cell plate	2 x 10^4 cells / chamber	500 µl / chamber or well
Magnet Assisted Transfection	6-well plate	2 x 10^5 cells / well	2 ml / well
Proliferation assay (BrdU assay)	96 well plate black	5 × 10^3 cells/well	100 µl / well
RNA isolation	6-well plate	2 x 10^5 cells / well	2 ml / well
Transfection with electroporation	6-well plate	2 x 10^5 cells / well	2 ml / well

2.13.5. Cell proliferation assay

The cell proliferation was quantified with a ready-to-use ELISA kit (Table 5), which is based on the detection of 5-bromo-2´-deoxyuridine (BrdU) incorporated into the genomic DNA of proliferating cells. Shortly, 5 *x* 10^3 cells were seeded in 96-well culture microplates in the respective medium. After cell attachment (24h), the culture medium was replaced with 100 µl culture medium containing 10 µM BrdU. As a negative control, cells without BrdU labeling were used. Following variable incubation time (for specification of the respective incubation time please see the respective experiments), the BrdU-containing medium was removed and the cells were fixed while simultaneously denaturing their DNA by adding 200 µl / well FixDenat Solution for 30 min at RT. After FixDenat removal, 100 µl of an anti-BrdU-POD antibody solution (1:100) were added and incubated for 1h at RT, during which the anti-BrdU-POD antibody bound to the BrdU incorporated into the newly synthesized cellular DNA. The antibody solution was discarded and the cells were washed three times with the provided 1x washing buffer, followed by addition of a peroxidase sub-

strate solution and subsequent luminescence measurement of the immune complexes with a microplate reader (SynergyMx). Data were analyzed using Microsoft Excel and GraphPad Prism 6 software.

2.13.6. Transfection

2.13.6.1. *Electroporation*

pDNA was introduced into the cells by means of electroporation. The electrical pulse applied during this method generates temporary pores in the cell membrane through which pDNA present in the transfection solution may pass (Potter 2003). All cell types were transfected using the Neon Transfection System and Kit (Table 1, Table 5) according to manufacturer instructions. The cells were seeded (Table 16) and allowed to reach 70 % confluence 24 – 48 h prior to electroporation. On the day of the electroporation, the cells were detached and centrifuged (section 2.13.2), after which the resulting pellet was resuspended in DMEM--- (Table 13). After the cell concentration was determined (section 2.13.4), the corresponding cell suspension volume was transferred into 15 ml tubes and centrifuged at 4°C, 300 x *g* for 5 min. The pellet was resuspended in resuspension buffer R and supplemented with pDNA, resulting in a final volume of 110 µl. The Neon®Pipette containing the solution in the Neon® Tip was inserted into the Neon®Tube containing 3 ml electrolytic buffer and the electroporation was conducted. The amounts and cell types, plasmids, as well as the electroporation conditions used in the respective experiments are listed in Table 17. After electroporation, the cells were seeded in 6-well plates containing 2 ml of the respective medium. Prior to performing further experiments, all cells were allowed to attach for at least 24 – 26 h. Control electroporations were conducted with the *pEGFP-N1* plasmid or without pDNA.

Table 17. Cell type and number, plasmid amount and electroporation conditions.

Cell Type	Number of cells	Plasmid amount	Voltage (V)	Pulse length (ms)	Pulse width
HaCaT	1,000,000	1,000 ng	1,3	30	2
dd HaCaT	1,000,000	1,000 ng	1	30	2

ddHaCaT: dedifferentiated HaCaT cells

The transfection conditions for different experimental approaches were established by varying the *pEGFP-N1* amount, the electroporation conditions and cell number. Typically, transfection efficiency was monitored 24 – 48 h after transfection.

2.13.6.2. *Magnet-assisted transfection*

For some experiments pDNA was transferred into HaCaT cells with magnet assisted transfection (MATra), an efficient and gentle method to transfect adherent cells in culture. In particular, HaCaT cells were seeded (Table 16) and grown to 30 – 60 % confluency 24 – 26 h prior to transfection. On the day of the transfection, 2 µg pDNA were diluted in 200 µl DMEM---. Next, the nanoparticles provided by the manufacturer (MATra-A) were vortexed shortly, added to the medium containing pDNA in a 1:1 ratio (µlMATra-A : µgDNA) and the solution was incubated at RT for 20 min, during which the cell medium was refreshed. After the incubation, the pDNA-bound

nanoparticles were added directly to the cells, gently mixed and placed for 15 min on a strong magnet (MATra Starter Set, Table 5) inside a cell culture incubator. Next, the plate was gently removed from the magnet and placed back into the incubator for the next 48 h. 4 – 6 h after the transfection, the medium of the transfected cells was exchanged with fresh, nanoparticle-free cell culture medium. MATra conditions were established by varying pEGFP-*N1* concentration, cell number and nanoparticle concentration. Typically, transfection efficiency was monitored 48 h after transfection.

2.13.7. Passaging of transfected cells

Cell detachment during passaging was performed with dispase and HBSS (Table 3) to avoid cleavage of the expressed CD4 protein in transfected cells. 200 µl dispase and 1800 µl HBSS were added to every well of a 6-well plate containing the transfected cells. After 5 – 7 min incubation in a CO_2-incubator, the cells were collected and added to a Falcon tube containing additional 2 ml HBSS, centrifuged at 4˚C and 300 x *g* for 5 min. The supernatant was discarded, the pellet was resuspended into fresh medium and the cells were seeded for further experiments. The protocol for splitting and passaging of the transfected cells was established using different dissociation reagents (e.g. Versene solution) and the transfected cells were checked for CD4 presence using immunocytochemistry.

2.13.8. Determination of cAMP levels in cells

An enzyme-linked immunoassay ready-to-use kit (Table 5) was used to determine cellular cyclic adenosine monophosphate (cAMP) levels. In this assay, the cAMP of samples to be analyzed compete with a fixed amount of HRP (horseradish peroxidase)-linked cAMP for binding to an anti-cAMP rabbit mAb immobilized onto a 96-well plate. In particular, following the experimental treatment of the adherent cells, the respective medium was aspirated and the cells were washed with 1x PBS to remove residual medium. Next, 200 µl lysis buffer containing 1 mM PMSF were added to each well of the 6-well plate, which was then incubated on ice for 5 min. The cells were scraped off, transferred in 2 ml tubes and snap-frozen in liquid nitrogen. Subsequently, the samples were placed on ice for approximately 30 min and allowed to thaw completely. After a 10 min centrifugation at 14,000 x *g* and 4ºC, the supernatants were used for cAMP level measurement. Lysate preparation for the non-adherent cells was done as follows: after the experimental treatment, the cells were transferred into tubes and centrifuged at 300 x *g*, 4ºC for 4 min. The pellet was resuspended in 1x PBS and the cells were centrifuged once more with the same conditions. Next, 200 µl of 1x lysis buffer with 1 mM PMSF were added and the samples were incubated on ice for 10 min with intermittent, short vortexing. The samples were then snap frozen in liquid nitrogen and left on ice until thawed. Supernatants were collected for cAMP level measurement after a 10 min, 14000 x *g* centrifugation of the samples at 4ºC. Afterwards the respective sample lysate or the cAMP standard (cAMP concentrations 80, 26.7, 8.9, 3.0, 1.0, 0.3 and 0 nM) provided with the kit was added (15 µl/well) and mixed with an equal volume of the HRP-

linked cAMP solution, Then the covered plate was incubated at RT for 3 hours on a horizontal plate shaker. Next, the plate content was discarded and the wells were washed 4 times with 200 µl/well of 1x washing buffer. Subsequently, 50 µl/well of the Luminol/enhancer solution (Luminol/enhancer solution and stable peroxide buffer) were added. Within the next 10 min, the plate was read twice on a luminescence-detecting microplate reader (SynergyMx).
Underlying the quantitative cAMP measurement is the inverse proportional relationship between the ensuing relative light intensity units (RLUs) and the cAMP concentration. Thus, the absolute cAMP content in the samples of interest was calculated by utilizing measurements originating from the cAMP standards. Data were analyzed using Microsoft Excel and GraphPad Prism 6 software.

2.13.9. Inactivation of the cell proliferation by mitomycin C treatment

To exclude the influence of cell proliferation during the cell migration experiments we used mitomycin C treated cells. Mitomycin C is a cytostatic drug that prevents further cell proliferation by inducing DNA interstrand crosslinks that block the DNA unwinding.
Dedifferentiated HaCaT cells (ddHaCaT) were seeded in 10 cm plates in the respective medium and grown until approx. 70% confluence (2.13.1). After three washing steps, the cells with 5 ml 1x PBS the cells were treated with 10 µg/ml mitomycin C dissolved in the respective medium and incubated in a cell culture incubator for a period of 2.5 hours. Afterwards, the mitomycin C-containing medium was discarded, the cells were washed with 1x PBS and the inactivated cells were either further used for migration studies (section 2.13.10) or cryopreserved (section 2.13.3) for later usage. To confirm the mitotic inactivation, the mitomycin C treated cells were cultured at the same density and conditions as untreated cells for a period of 7 days. Afterwards, the cell numbers of treated and untreated cells on day 1 and on day 7 were compared.

2.13.10. Chemotaxis

Cell migration analyses were performed using 2D chemotaxis *µ-slides* (Ibidi GmbH, Germany), each of which contains three chambers for analyzing simultaneously performed assays that enable the performance of reproducible chemotaxis assays with a defined chemotactic gradient. A detailed view of the chamber, as well as its cross section are shown in Figure 6.

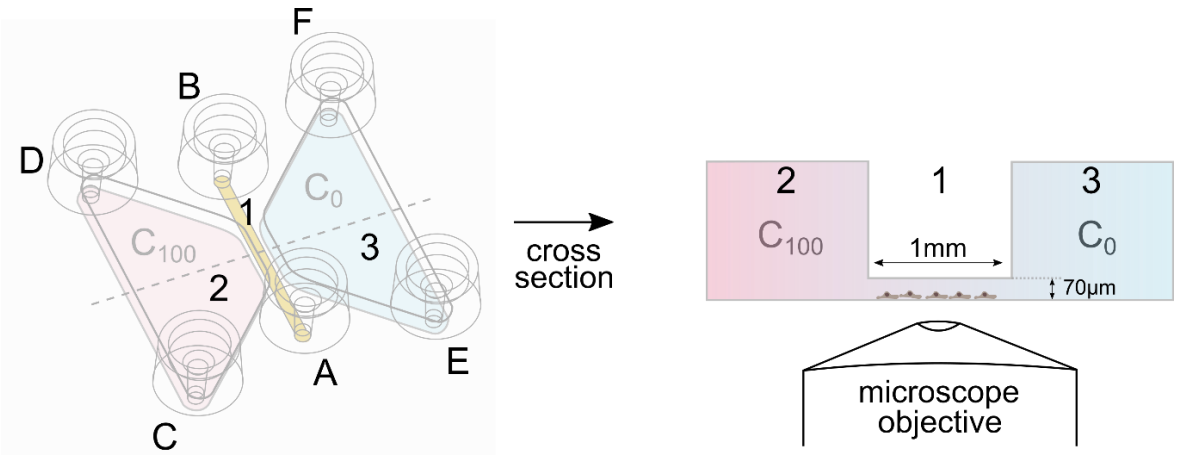

Figure 6: Chemotaxis assay chamber. The chemotaxis chamber is composed of two large reservoirs (2 and 3) connected by a small gap (1), which is the observation area for the microscope recording. Cells are placed into the observation area using the filling ports A and B. The large reservoirs are filled through filling ports E, F and C, D. If the large reservoirs contain different chemoattractant concentrations, then a linear concentration gradient (pink-blue gradient) is formed inside the observation area, which enable the monitoring of the cell movement. C_{100} is max. concentration in stable gradient equilibrium; C_0 is solution without chemoattractant. Modified from Ibidi GmbH.

One day prior to the experiment, cells were transfected (section 2.13.6.1), seeded on 10 cm plates in the respective media and incubated in a cell culture incubator for 26 h. In parallel, the respective culture medium, the *µ-slide* and the plugs were placed in the CO_2-incubator to allow them to achieve gas equilibrium, which ultimately prevented air bubble formation in the chemotaxis slide during the experiment. On the day of the experiment, the slide was placed in a 10 cm Petri dish surrounded by wet paper tissue to prevent evaporation. The transfected cells were detached (section 2.13.7) and a 6 µl suspension containing 25,000 cells (section 2.13.4) was applied into filling port A, while the remaining ports were closed off with plugs. The air was then gently aspirated through port B, thereby pulling the cells into the imaging channel in which they settled in a homogenous fashion. After removing the plugs, the slide was incubated for 6 h to allow cell attachment. The attachment process and cell morphology were controlled with regular observations under a microscope during the initial incubation process. After 6 h, the non-adherent, dead cells, as well as the seeding medium were removed with a washing procedure. In particular, all filling ports, except A and B, were again closed and a cell-free medium was filled through port A and gently aspirated through port B. The washing procedure was performed twice. Next, both reservoirs (2 and 3) were filled with 65 µl medium, respectively, while keeping all ports of the opposing reservoir and imaging channel closed. After filling the chambers, cell attachment and morphology were again monitored with a microscope. 30 µl of the chemoattractant were added to one side of the slide resulting in the establishment of a stable chemotactic gradient determined to be stable for 48 h. After applying the chemoattractant, multi-position time lapse imaging of the slides was conducted with a Nikon Eclipse Ti2 inverted microscope equipped with an Okolab incubation chamber for 24 h with a 10 minutes time-lapse interval. Cell movement was analyzed with a workflow based on the FIJI

(Schindelin et al. 2012), TrackMate (Tinevez et al. 2017) and the Chemotaxis and Migration Tool (Ibidi GmbH) software packages.

2.13.11. Isolation of CD4$^+$ T cells from mouse spleen

For isolation of splenic cells, the spleen of wild type 129sv or C57BL6/N mice was dissected and meshed through a cell strainer in a 10 cm plate filled with 10 ml 1x PBS. The cell suspension was passed several times through syringe equipped with a 30 G x ½'' single-use needle and centrifuged at 300 x *g*, 4°C for 4 min. The pellet was resuspended in 10 ml 1x PBS and the cells were counted as described (section 2.13.4). Then, 2 x 10^5 unselected cells were transferred into a new sterile reaction tube and preserved on ice for later use. The remaining cells were used for negative selection of CD4$^+$ cells using the EasySep™ Mouse CD4$^+$ T Cell Isolation Kit (Table 5). Briefly, the cells were centrifuged at 300 x *g*, 4°C for 4 min and the pellet was resuspended in 1x PBS containing 2 % FCS and 1 mM EDTA within the volume range of 0.25 to 2 ml (1 x 10^8 cells / ml final concentration). After adding 50 µl rat serum per ml sample, the cells were transferred into 5 ml polystyrene round-bottom tubes supplied with the kit, 50 µl isolation cocktail per ml sample were added and the suspension was incubated at RT for 10 min. Then 75 µl RapidSpheres™ per ml sample were added and the suspension was incubated at RT for 2.5 min. Subsequently, 1x PBS containing 2 % FCS and 1 mM EDTA was supplemented up to 2.5 ml, gently mixed by pipetting and the tube was placed into the EasySep™ Magnet and incubated for 5 min. The supernatant was transferred into a new tube and the ready-to-use isolated cells were labeled as CD4$^+$ cells, while the remaining cells from the tube in the magnet were resuspended with 1x PBS and labeled as CD4$^-$ cells. Further confirmation of the cell identity was performed by flow cytometry (section 2.16.2). The isolated CD4$^+$ T mouse splenocytes were cultured in RPMI 1640 Medium, containing GlutaMAX™ supplement with 1% P/S, for further experiments.

2.14. Molecular biology methods

2.14.1. Restriction enzyme hydrolysis

Restriction enzyme hydrolysis of pDNA was performed for plasmid analysis and verification, as well as for the generation of new plasmids. Based on the experiment, one or two restriction endonucleases were chosen according to the plasmid sequence. To verify the plasmid identity, restriction hydrolysis reaction was performed using 2-3 units of restriction enzyme per 1 µg of DNA, together with the optimal restriction buffer (supplied by the manufacturer) in a total volume of 10 µl. The restriction hydrolysis reaction was performed for 1 h at the optimal temperature for the respective enzyme. If needed, the enzymes were afterwards heat inactivated. At the end, the sample separation was performed with agarose gel electrophoresis (2.14.8).

2.14.2. Plasmid ligation

New pDNA plasmids were generated by ligating pDNA endonuclease restricted fragments with *T4* - ligase according to the manufacturer recommendations. For this

purpose, endonuclease restricted pDNA (50 – 200 ng) was mixed with T4 DNA ligase (400 U / 1 µl), 1x ligation buffer provided by the manufacturer and ultrapure H_2O in a total volume of 20 µl. The ligation reaction was performed overnight at 16°C and the resulting plasmid was used for *E. coli* transformation (section 2.14.4).

2.14.3. Cloning of the *pCR3.1-hCD4* expression plasmid and the *pTRE-Dual2-hCD4* plasmid for generating a Tet-On® Advanced Inducible Gene Expression System

For the transient overexpression of the human CD4 protein in keratinocytes the human *CD4* cDNA (complementary DNA) was cloned into a *pCR3.1* plasmid under the control of a *CMV* promoter for efficient expression in mammalian cells (*pCR3.1-hCD4*). For this purpose, the forward and reverse primers listed in Table 10 and a reversely transcribed volunteer's RNA (section 2.14.6) were used for the amplification of the human *CD4* cDNA. Subsequently, the 1377 bp *CD4* cDNA amplification product was verified by agarose gel electrophoresis (section 2.14.8) followed by extraction and purification from the agarose gel (section 2.15.3). Finally, it was ligated into an *EcoR*V-opened *pBluescript II SK (+)* plasmid (section 2.14.2). The resulting plasmid was named *pBluescript II SK (+)-hCD4* (see Figure 7A). Several restriction enzyme hydrolyses followed by agarose gel electrophoresis were performed to verify the identity of the *pBluescript II SK (+)-hCD4* plasmid. First, the plasmid was analyzed after *EcoR*I-hydrolysis, which revealed the expected total plasmid size of 4335 bp (2961 bp of the *pBluescript II SK (+)* and 1376 bp of the human *CD4* insert). Secondly, *Xba*I/*Sal*I- and *Xba*I/*Kpn*I-hydrolyses verified the identity of the plasmid by resulting in fragment sizes of 1434 bp and 2901 bp or 1451 bp and 2884 bp, respectively.

For generating the *pCR3.1-hCD4* plasmid the 1451 bp long *CD4* fragment of the *Xba*I/*Kpn*I-hydrolysed *pBluescript II SK (+)-hCD4* plasmid was ligated into a *Xba*I/*Kpn*I-opened *pCR3.1* vector (see Figure 7B).

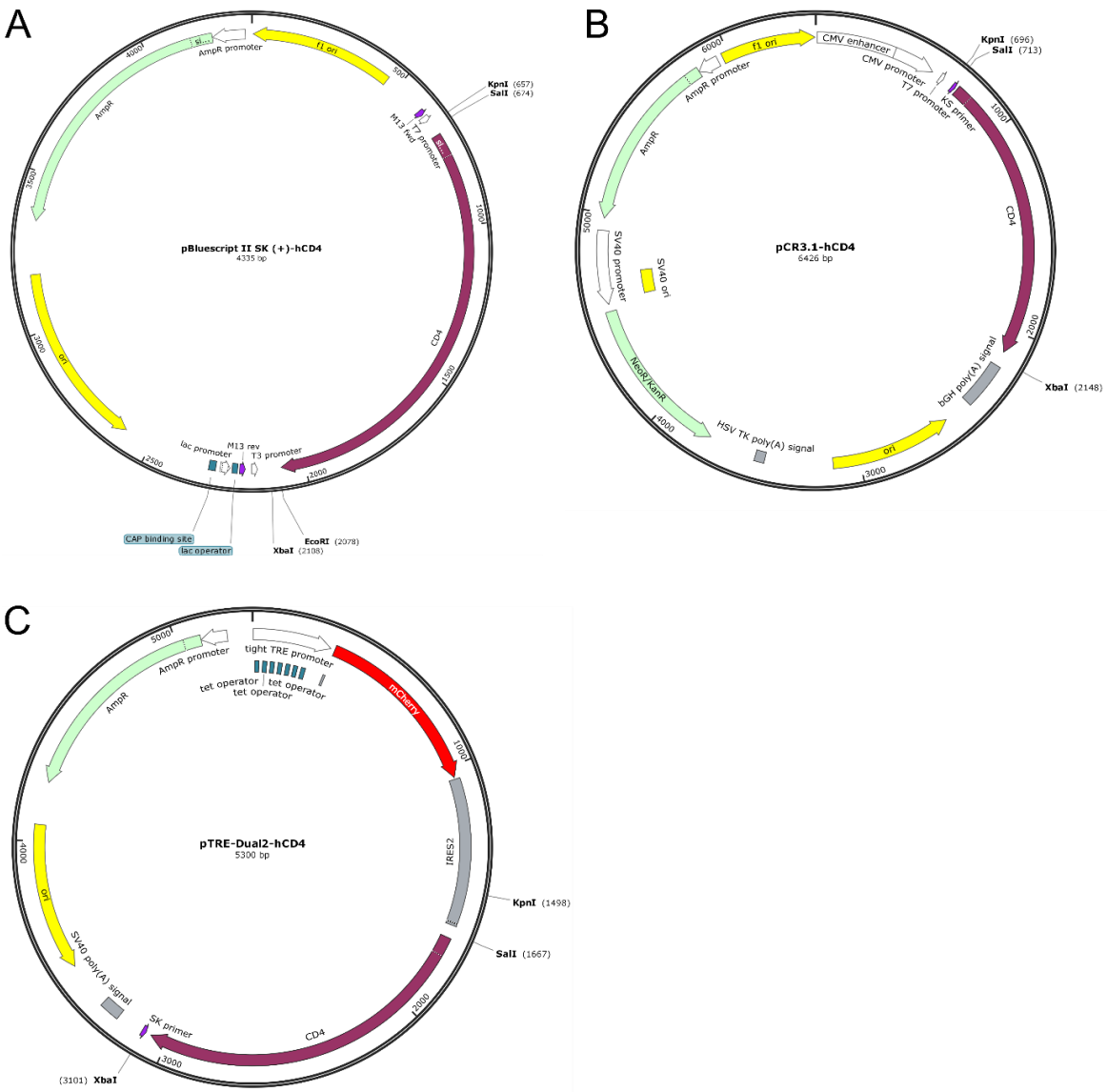

Figure 7: Plasmids for generating a Tet-On® Advanced Inducible Gene Expression System. (A) *pBluescript II SK (+)-hCD4* obtained by ligating human 1377 bp *CD4* cDNA amplification product into an *Eco*RV-opened *pBluescript II SK (+)* plasmid. **(B)** *pCR3.1-hCD4* created by ligating the 1451 bp long *CD4* fragment of the *Xba*I/*Kpn*I-hydrolysed *pBluescript II SK (+)-hCD4* plasmid into a *Xba*I/*Kpn*I-opened *pCR3.1* vector. **(C)** *pTRE-Dual2-hCD4* created by ligating the 1434 bp long *CD4* fragment of the *Xba*I/*Sal*I-hydrolysed *pBluescript II SK (+)-hCD4* plasmid into a *Xba*I/*Sal*I-opened *pTRE-Dual2* vector. For more details see the main text. The plasmid maps were created using the SnapGene Viewer (GSL Biotech LLC, San Diego, USA) software.

For generation of the *pTRE-Dual2-hCD4* plasmid that was used for establishing a cell line in which the expression of CD4 can be controlled by Tet-On® Advanced Inducible Gene Expression System the 1434 bp long *CD4* fragment of the *Xba*I/*Sal*I-hydrolysed *pBluescript II SK (+)-hCD4* plasmid was ligated into a *Xba*I/*Sal*I-opened *pTRE-Dual2* vector (see Figure 7C). The identity of the plasmids was verified by means of different restriction enzyme hydrolyses (data not shown).

2.14.4. Transformation of *E.coli* with plasmid DNA

The DH5α chemically competent *E. coli* strain was transformed with the respective pDNA (Table 7) or pDNA ligation mix (2.14.2). In particular, 50 µl of *E. coli* aliquots were thawed on ice and gently mixed with 1 µl of pDNA or 5 µl of a ligation reaction. The plasmid-bacteria mixture was incubated for 20 min on ice and afterwards exposed to a heat shock at 42°C for 45 sec. Next, the bacteria were cooled down on ice for 2 min and 500 µl of S.O.C. medium (Table 3) were added. Afterwards, the suspension was incubated on a shaker at 700 rpm at 37°C for 1 h. Subsequently, an appropriate volume of the mixture containing transformed bacteria (usually 20 to 200 µl) was plated onto LB agar plates containing the adequate selection antibiotic (section 2.10.1) and incubated overnight upside down in a 37°C incubator. The next day single colonies were chosen and inoculated into 100 ml LB medium containing suitable selection antibiotic and the bacteria were grown overnight on a shaker at 155 rpm, 37°C for subsequent pDNA isolation and amplification (sections 2.15.1 and 2.15.2). All utilized equipment was previously sterilized either in an autoclave or with a gas flame before use.

2.14.5. Polymerase chain reaction (PCR)

pDNA and cDNA were amplified with PCR in a total reaction volume of 10 µl containing 0.2 mM dNTPs, 1x polymerase buffer, 0.018 mM $MgCl_2$, 0.5 µM forward primer, 0.5 µM reverse primer, 10 % (v/v) cresol, 0.05 U/µl MolTaq polymerase, 1.25 ng / µl template DNA and filled with ultrapure H_2O to 10 µl. Samples were incubated in a PCR thermocycler under the cycling conditions summarized in Table 18.

Table 18. PCR cycling conditions

Step	Temperature	Time	Cycles
First denaturation	95°C	4 min	1x
Amplification	95°C	15 sec	40x
	60°C	30 sec	
	72°C	30 sec	
Final extension	72°C	5 min	1x

Table 19. PCR conditions for amplifying hCD4

Step	Temperature	Time	Cycles
First denaturation	98°C	30 sec	1x
Amplification	98°C	10 sec	35x
	55-65°C	30 sec	
	72°C	1 min 45 sec	
Final extension	72°C	2 min	1x

For the generation of a plasmid that utilizes an ectopic expression of CD4 in mammalian cells, the *CD4* cDNA sequence was amplified from human blood cDNA by using specific forward and reverse primer. The PCR reaction contained 0.2 mM dNTPs, 1x Q5 Reaction Buffer, 0.5 µM forward primer, 0.5 µM reverse primer, 20 U/ml Q5 High-Fidelity DNA Polymerase, 2 ng/µl template DNA and up to 25 µl ultrapure H_2O. The cycling conditions for human *CD4* amplification are shown in Table 19.

2.14.6. Reverse transcription of RNA

The SuperScript™ II Reverse Transcriptase kit was used for cDNA synthesis. The samples were kept on ice the entire time unless stated otherwise and all equipment and surfaces were kept RNAse-free with RNAseZap. First, 2 µg of previously isolated total RNA (section 2.15.4) were diluted in ultrapure H_2O in a total volume of 7 µl. Afterwards, 250 ng of random hexamer oligonucleotides (in 5 µl H_2O) were added to the RNA samples and incubated for 10 min at 70°C. After spinning the samples down, 7 µl from a mixture of 5x first strand buffer (4 µl), 0.1 M DTT (2 µl) and 10 mM dNTPs (1 µl) were added to the samples and incubated for 10 min at RT. The mixtures were then pre-warmed for 2 min at 42°C, and 1 µl of SuperScript II enzyme (200 U/µl) was added and the cDNA synthesis was performed at 42°C for 1 h. The synthesis was stopped by heat inactivation for 10 min at 70°C. The samples were spun down and stored at -20°C. Assuming a reaction efficiency of 50 %, the final cDNA concentration theoretically was 50 ng/µl.

2.14.7. Quantitative real time PCR

Gene expression levels were determined with qRT-PCR using the Platinum SYBR Green qPCR Super Mix (Invitrogen) with conditions shown in Table 20. For qRT-PCR reactions, 2 µl of diluted cDNA were mixed with 5 µl SYBR Green, 0.4 µM forward primer, 0.4µM reverse primer and 2.2 µl H_2O, in a total volume of 10 µl and pipetted in every well of a black 384 well plate in triplicates. The DNA-oligonucleotides used for qRT-PCR are summarized in Table 11. qRT-PCR was performed on the 7900 HT Fast Real-Time PCR System using the SDS software.

Table 20. qRT-PCR cycling conditions.

Invitrogen (SYBR Green)		
Temperature	**Duration**	**Cycles**
50 °C	2 min	1x
95 °C	2 min	1x
95 °C	30 sec	40 x
60 °C	2 min	
Dissociation stage		
95 °C:15 sec; 60 °C:15 sec; 95 °C:15 sec		

The standard curve method was used to calculate the gene expression values. As part of this workflow, 5-fold serial dilutions from tissue or cells known to express the target gene, starting with 20 ng/2µl cDNA (gene of interest) or with 250 pg/2µl (*18S rRNA*) were prepared and amplified by qRT-PCR. For each gene of interest, one standard curve with cDNA from a source that is known to express the gene of interest was generated. The standards used for each gene of interest are shown in Table 21. The standard curve was generated by plotting the logarithmic values of the calculated cDNA concentrations from the dilution series against the corresponding measured cycle threshold (CT) from the same sample. After that, regression analysis was applied to calculate the gene-specific cDNA concentration in the samples of

interest. These values were normalized to the corresponding values of the housekeeper gene (*18S rRNA*). If applicable, the obtained results were normalized to experimental control samples, e.g. solvent treated cells. The results were further analyzed using Microsoft Excel and GraphPad Prism 6 software.

Table 21. Genes of interest and standards for qRT-PCR.

Human genes		
Gene of interest	**Standard (cDNA from)**	**Sample dilution**
18S rRNA	E12.5	1:13.500
CD4	HL-60	1:10
KRT5	Human skin	1:10
KRT15	Human skin	1:10
KRT1	Human skin	1:10
KRT10	Human skin	1:10
IVL	HaCaT	1:20
S100A7	HaCaT	1:20
Mouse genes		
18S rRNA	E12.5	1:13.500
Krt5	Mouse tail	1:10
Ivl	C5N	1:10

2.14.8. Agarose gel electrophoresis with ethidium bromide

DNA fragments were separated by size with agarose gel electrophoresis. Depending on the expected size of the DNA fragment, agarose gels containing 0.5 to 2 % (w/v) agarose in 1 x TBE buffer (Table 4) were prepared by boiling for 1 – 2 min at 1000 W in a microwave in order to dissolve the agarose. After cooling down, a few droplets of ethidium bromide (0.07 %) were added to the solution, which was poured into trays and into which differently sized combs were placed to generate wells. After solidification and comb removal, the gels were placed in an electrophoresis chamber and covered with 1x TBE buffer. Prior to their loading, the samples were either diluted with 10 x Cresol or 6 x loading dye to obtain a final 1 x concentration. For the determination of the fragment size, a lane of the gel was reserved for the appropriate DNA ladder. After the samples and ladder were loaded, an electric field was applied (80– 120 V, 500 mA) for a time period from 30 min to 2.5 hours. The visualization of the fragments was accomplished with a UV transilluminator and documented using the INTAS GDS 3.39 software.

2.14.9. Sanger sequencing

Sanger sequencing was used to determine the DNA sequence with a ready-to-use kit (Table 5). The reactions were carried out in a total volume of 10 µl, whose components are shown in Table 22.

Table 22. Sanger sequencing reaction components.

Components	Volume / concentration
BigDye™ Terminator v1.1 & v3.1 5x Sequencing Buffer	2 µl of 1x
BigDye® Terminator v3.1 Ready Reaction Mix	1 µl
DNA oligonucleotide for Sanger sequencing (Table 11)	1 µl
DNase/RNase-free distilled H_2O (ultrapure H_2O)	1 µl
pDNA	5 µl of 50 ng/µl

Every reaction was afterwards incubated in a PCR thermocycler under conditions summarized in Table 23.

Table 23. Cycling conditions for DNA amplification for Sanger sequencing.

Temperature	Duration	Cycles
95°C	1 min	
95°C	30 sec	30x
60°C	2 min 20 sec	30x
60°C	5 min	

Next, 10 µl ultrapure H_2O were added to every reaction and the Sanger sequencing was analyzed on a 3500xL genetic analyzer at the Institute of Human Genetics, Göttingen, at the Molecular Diagnostics Laboratory. For data analysis, the SnapGene Viewer (GSL Biotech LLC, San Diego, USA) software was used.

2.15. Isolation and purification of nucleic acids

2.15.1. Medium-scale isolation of plasmid DNA and purification

Medium-scale, pDNA isolation was performed using the PureLink ® HiPure Plasmid Midiprep kit according to the manufacturer's instructions. Shortly, the HiPure Midi Column was washed with 10 ml Equilibration Buffer and allowed to drain by gravity flow. The bacterial overnight culture grown in 100 ml LB medium supplemented with a selection antibiotic (section 2.14.4) was transferred into 50 ml tubes and centrifuged at 10,000 x *g* for 10 min at 4°C. The resulting bacterial cell pellet was carefully and completely resuspended in 4 ml of resuspension buffer (R7), which was supplemented with RNase A. Next, the bacteria were lysed through the addition of 4 ml lysis buffer (L7) and by gentle inversion of the capped tube for five times. The tube was incubated for 5 min at RT. For protein denaturation, 4 ml of the precipitation buffer (N3) were added and the solution was immediately mixed again by inverting. The lysates were centrifuged at 10,000 x *g* for 10 min at 4°C and the supernatant was loaded onto the column and allowed to drain by gravity flow. After draining, the column was washed two times with 10 ml wash buffer (W8). The column was then transferred into a new tube and 5 ml elution buffer (E4) were added and left to drain by gravity flow. The eluate, which contains the purified pDNA was redistributed in five, 2 ml reaction tubes containing 1 ml 100 % isopropanol. To precipitate the pDNA, the tubes were incubated at -20°C overnight or for 20 min at -80°C. After the precipitation, the pDNA was pelleted by centrifugation at 13,000 rpm, at 4°C for 30

min. The supernatant was discarded and 200 µl 70 % ethanol were added for washing the pDNA and again centrifuged for 10 min at 13,000 rpm, at 4°C. After supernatant removal, the pDNA was dried at 55°C for 5 min and resuspended in ultrapure H_2O in an appropriate volume (20 µl total volume) for 10 min at 42°C and 1,100 rpm on a heating block. At the end, all isolated pDNA was pooled in one reaction tube with the final volume of 100 µl. Plasmid stocks were stored at -20°C.

2.15.2. Small-scale isolation of plasmid DNA and purification

For small-scale DNA plasmid purification, components of the PureLink®HiPure Plasmid Midiprep kit were used. Approximately 1.3 ml of a bacterial overnight culture (section 2.14.4) were transferred to a 1.5 ml reaction tube and the cells were pelleted by centrifugation for 5 sec at 13,000 rpm. After supernatant removal, 200 µl resuspension buffer (R7) supplemented with RNase A were added to the pellet and vortexed with short pulses until visibly homogeneous. Subsequently, 200 µl lysis buffer (L7) were added to the sample and the tube was gently inverted, after which 200 µl of precipitation buffer (N3) were added and the sample was once again inverted. The sample was pelleted by centrifugation at 13,000 rpm, at 4°C for 10 min and approximately 480 µl of the supernatant were transferred to a new 1.5 ml reaction tube containing 1 ml 99 % ethanol. The DNA was precipitated at -20°C for 1 h or at -80°C for 20 min and pelleted by centrifugation at 13,000 rpm, at 4°C for 30 min. The supernatant was discarded and 300 µl 70 % ethanol were added to the pellet and again centrifuged for 10 min at 13,000 rpm, at 4°C. After throwing out the supernatant, the pellet was dried at 55°C for 10 min and resuspended in ultrapure H_2O in an appropriate volume (50 – 100 µl) for 10 min at 42°C at 1000 rpm on a heating block. Plasmid stocks were stored at -20°C.

2.15.3. Isolation of DNA fragments from agarose gel

The extraction and purification of the DNA fragments from agarose gel was performed with a gel extraction Mini kit and followed up by PCR clean up (Table 5). DNA fragments were excised from the agarose gel under UV light with a sterile surgical blade, transferred in a tube and weighed. 200 µl of binding buffer (NTI) were added for each 100 mg of < 2 % agarose gel and were doubled for gels containing more than 2 % agarose. The samples were incubated for 8 min with NTI buffer on a heating block shaker set to 50°C and 500 rpm. After placing the NucleoSpin® Gel and PCR clean-up column into a 2 ml collection tube, 700 µl of the sample were loaded and centrifuged for 30 sec at 11,000 rpm. The flow through was discarded and 700 µl washing buffer (NT3) were added to the collection tube with the NucleoSpin® Gel and PCR clean-up column and the tube was centrifuged for 30 sec at 11,000 rpm. The flow through was discarded and this washing step was repeated twice. The column was additionally centrifuged for 1 min at 11,000 rpm to completely remove the NT3 and to dry the silica membrane. Next, the column was placed into a new sterile 1.5 ml tube and 15 – 30 µl of eluate buffer (NE) were added to the center of the column. After 1 min incubation at RT the tube was centrifuged for 1

min at 11,000 rpm and the flow through was pipetted back into the column and centrifuged again for 1 min at 11,000 rpm. The concentration of the isolated DNA fragment was measured as explained in section 2.15.6 and the samples were stored at -20°C until further use.

2.15.4. RNA Isolation from cell culture

Total RNA isolation was performed on ice and all applied equipment and surfaces were RNase-free. First, the cultured cells were washed twice with ice-cold 1x PBS and 1 ml TRIzol was added to each well of the 6-well culture plate. The cells were detached by repeated pipetting of the TRIzol-cell mixure, transferred into 2 ml reaction tubes, vortexed for 2 min at the highest setting and incubated for 5 min at RT. After addition of 200 µl of chloroform, each sample was again vortexed for 15 sec and incubated for 3 min at RT. Phase separation of the solution was achieved by 10 min centrifugation at 12,000 rpm at 4°C. The upper phase (500-600 µl) was placed in a new 2 ml reaction tube containing 700 µl of cooled isopropanol and the solution was gently inverted once. The precipitation was performed overnight at -20°C. The next day, the samples were centrifuged at 12,000 rpm at 4°C for 30 min. The supernatant was discarded, 700 µl of cooled 70 % ethanol were added and again centrifuged at 12,000 rpm, 4°C for 10 min. After the repetition of the last washing step, the pellets were dried at RT for approximately 1 hour. Finally, the pellets were resuspended in 20 µl ultrapure H_2O while shaking at 900 rpm for 10 min at 56°C on a heating block. The concentration of the isolated RNA was measured as explained in section 2.15.6 and the samples were stored at -80°C until further use.

2.15.5. RNA isolation from fibrous tissue

To isolate RNA from mouse tail skin (wild type C57BL6/N) and human skin samples (Patient No. 22) the RNeasy Fibrous Tissue Mini Kit (Table 5) was used. Briefly, 30 mg of tissue sample were added in 300 µl RLT-β-mercaptoethanol-buffer in 2 ml reaction tubes. The tissue was homogenized for 1 – 1.5 min. The homogenizer was disassembled and washed thoroughly with RLT-β-mercaptoethanol-buffer after every homogenization cycle. Next, 590 µl ultrapure H_2O and 10 µl proteinase K were added to the lysates and mixed thoroughly by pipetting. Afterward, the lysates were incubated for 10 min at 55°C and 350 rpm on a heating block shaker and centrifuged at 12,000 rpm for 3 min at RT. The supernatant (approx. 900 µl) was transferred into a new 2 ml tube, 450 µl 99 % ethanol were added and thoroughly mixed. 700 µl of the sample were transferred to an RNeasy Mini spin column that were placed in a 2 ml collection tube and centrifuged twice at 10,000 rpm at RT for 15 sec with discarding the flow-through between centrifuging. Next, 350 µl RW1 buffer were added to the column and the sample was centrifuged at 10,000 rpm at RT for 15 sec with discarding the flow-through. Then 70 µl RDD buffer and 10 µl DNase I were added onto the center of the column and the column was incubated at RT for 17 min. Next, 350 µl RW1 buffer were added, the column was centrifuged at 10,000 rpm at RT for 15 sec and the flow-through was discarded. The column was transferred in a new 2 ml collection tube supplied by the kit, 500 µl RPE buffer were added and the sample

was centrifuged at 10,000 rpm at RT for 15 sec with discarding the flow-through. Again, 500 µl RPE buffer were added and the column was centrifuged at 10,000 rpm at RT for 2 min with discarding the flow-through. After one more centrifugation at 12,000 rpm for 1 min the column was transferred to a new 1.5 ml collection tube, 30 µl ultrapure H_2O were added to the column and incubated for 1 to 3 min at RT. Then, the column was again centrifuged at 10,000 rpm for 1 min at RT. The last step was repeated twice to ensure high RNA concentration. The concentration of the isolated RNA was measured as explained in section 2.15.6 and the samples were stored at -80°C until further use.

2.15.6. Photometric quantification of nucleic acids

DNA and RNA concentration and purity measurements were performed with a Thermo Scientific NanoDrop 8000 Spectrophotometer. The DNA or RNA concentrations were determined by loading 1 µl of the sample and then measuring its optical density (OD) at 260 nm. An OD at 260 nm of 1.0 refers to 50 ng/µl pure dsDNA and 40 ng/µl pure RNA. The concentration of isolated nucleic acids was calculated by multiplying the measured values for OD at 260 nm with 50 (for DNA) or 40 (for RNA). Additionally, the OD at 230 nm (concentration of sugars and salts), 280 nm (concentration of proteins) and 340 nm (measure background signals) were determined for each sample. The purity of the isolated DNA or RNA samples was determined by calculating the optical density ratio of 260 and 280 nm (260 / 280) and also of 260 and 230 nm (260 / 230). The generally accepted 260 / 280 ratios for “pure” DNA and RNA are 1.8 and 2.0, and the 260 / 230 ratios should be between 1.8 and 2.2, respectively.

2.16. Immunohistochemical stainings

2.16.1. Immunocytochemistry

For immunocytochemistry, eukaryotic cells were seeded in 4-well chamber slides or directly on coverslips in 24-well plates, containing 500 µl of the respective growth medium. Following removal of the cell culture medium, the cells grown either in the slides or the coverslips were fixed by applying 500 µl 4 % PFA for 10 min at RT. The cells were then washed three times with 500 µl 1x PBS and incubated for 30 min at RT with 500 µl 0.5 % Triton X-100 dissolved in 1x TBS. Again, the cells were washed three times with 500 µl 1x PBS. Unspecific antigens were blocked by adding 500 µl 0.2 % I-Block in 1x TBS for 30 min at RT. Next, the cells were incubated with the primary antibody dissolved in 1x TBS (Table 8) at 4ºC overnight. Therefore, coverslips with attached cells were inverted and incubated on top of 20 µl, antibody-containing droplets on parafilm, while cells grown in the 4-well chambers were incubated in 100 µl antibody solution. Next, the coverslips and the 4-well chambers were washed three times with 1% Triton X-100 dissolved in 1x TBS. Afterwards, the cells were incubated in a dark environment for 1 h at RT with 200 µl 1x TBS solution containing the secondary, fluorescently-labeled antibody (Table 8). Unbound secondary antibodies were washed away with 1 % Triton X-100 dissolved in 1x TBS. Afterwards, DAPI-containing mounting media was applied onto the chamber slides.

In the case of coverslips, mounting medium droplets were applied onto a microscope slide on top of which the coverslips were mounted (cells facing the mounting medium).

2.16.2. Flow cytometry

Flow cytometry was applied to confirm the isolation of $CD4^+$ mouse splenocytes (section 2.13.11). 2 x 10^5 cells from input, $CD4^+$ and $CD4^-$ cells were stained with 1 µl CD4-FITC and 1 µl CD3-PE-Cy7 (Table 9) in 1ml 1x PBS for 30 min on ice at RT in dark. Afterwards the samples were washed with 1 ml 1x PBS and centrifuged at 300 x *g*, 4°C for 4 min, the supernatants were discarded and 500 µl 1x PBS were added. The samples were kept on ice until analysis on a BD™ LSR II flow cytometer (BD Biosciences, San Jose, CA, USA). The results are shown in Figure 8.

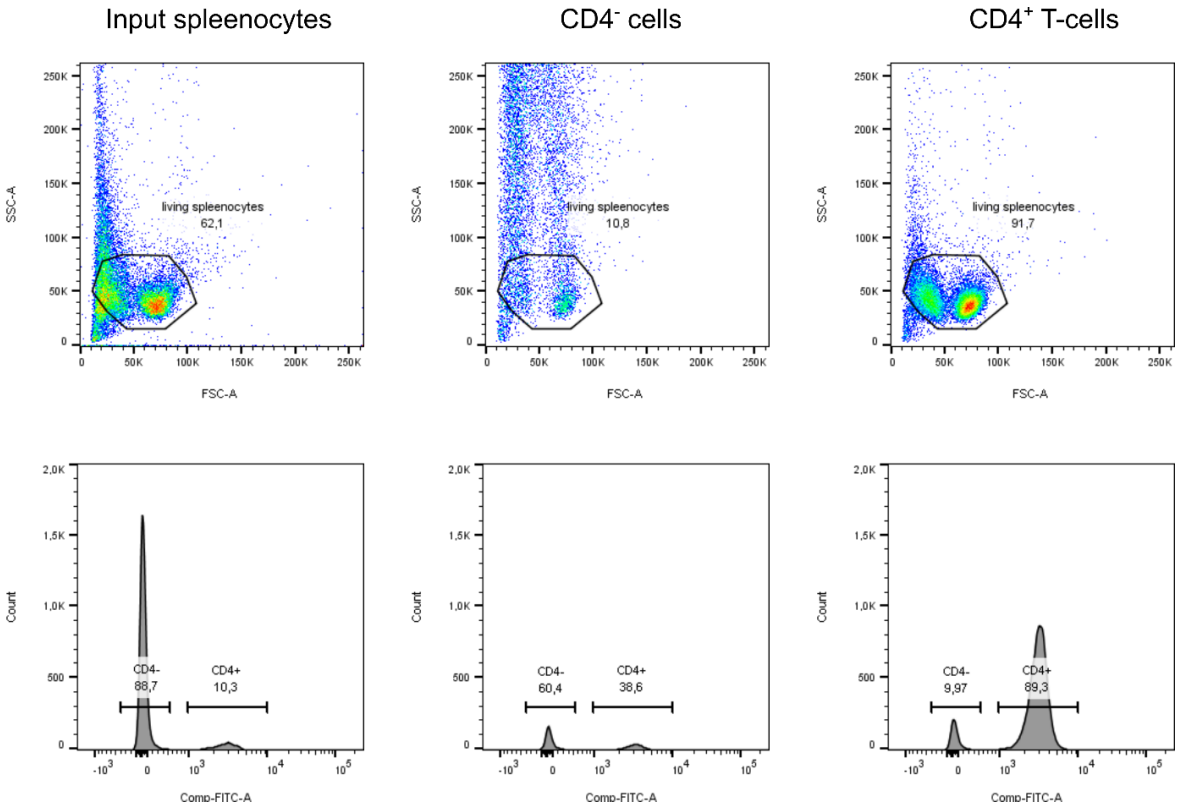

Figure 8: Flow cytometric analysis of $CD4^+$ splenocytes isolated using EasySep™ Mouse $CD4^+$ T Cell Isolation Kit. Side vs. forward scatter plots of input spleenocytes, $CD4^-$ and $CD4^+$ T cells revealed two immune cell populations, both of which were selected for further analysis (freehand selection in top row). Subsequent frequency distribution histograms of FITC intensity of the freehand selected populations identified $CD4^-$ and $CD4^+$ cells in all samples (bottom row). Based on the applied intensity gates, 10.3%, 38.6% or 89.3 % of the cells were $CD4^+$.

3. Results

The results section of this dissertation is divided into three parts: First, the results of *in vitro* differentiation and dedifferentiation experiments on human and murine keratinocyte cell lines are presented. Particular emphasis is placed on the dedifferentiation process itself and its verification. The second part describes the results of the attempt to create an inducible, stably transfected dedifferentiated keratinocyte cell line. The third part summarizes data from the analysis of transient transfection experiments to analyze the CD4 protein function in dedifferentiated basal keratinocytes.

3.1. Development of basal cell-like keratinocyte cell lines

3.1.1. Generation of a human and a murine basal cell-like, dedifferentiated keratinocyte cell line

To study CD4 protein function in basal cell-like keratinocytes *in vitro*, the human immortalized keratinocyte cell line HaCaT (Boukamp et al. 1988) and the murine keratinocyte cell line C5N (Zoumpourlis et al. 2003) were dedifferentiated by applying a culturing protocol adopted from Deyrieux and Wilson (2007) (Figure 9).

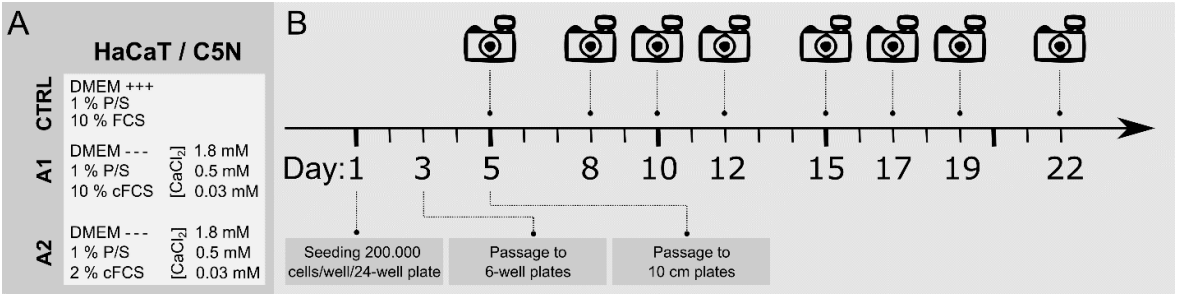

Figure 9: Experimental setup for the generation of basal cell-like dedifferentiated human HaCaT and murine C5N cells. (A) Compilation of the cell lines and the respective media used for cell culturing during the 3-week dedifferentiation period. **(B)** Timeline of the experimental dedifferentiation protocol. On day 1, cells were seeded in a 24-well plate (2 x 10^5 cells per well) and were transferred into 6-well plates on day 3. On day 5, the cells were transferred into 10 cm dishes and cultured for a total of 3 weeks in the respective medium (A). Pictures were taken on day 5, 8, 10, 12, 15, 17, 19 and 22 post-seeding.

In short, HaCaT and C5N cells were seeded in DMEM without L-glutamine, sodium pyruvate and $CaCl_2$ medium (DMEM ---) supplemented with 200 mM L-glutamine, 100 mM sodium pyruvate, 1 % P/S and 10 % (A1 medium) or 2 % cFCS (A2 medium), respectively, as well as defined $CaCl_2$ concentrations (1.8, 0.5 and 0.03 mM) (Figure 9A). As controls (CTRL), HaCaT and C5N cells were grown in DMEM+++ supplemented with 1 % P/S and 10 % FCS suitable to maintain HaCaT and C5N cells, but also contains $CaCl_2$ of a sufficient concentration to induce the expression of keratinocyte differentiation markers (e.g. Fujisaki et al. (2018)).

Initially, HaCaT and C5N cells maintained in CTRL medium were seeded in a 24-well plate in A1 (containing 10 % cFCS) or A2 medium (containing 2 % cFCS) at a rate of 2 x 10^5 cells per well and then transferred to 6-well plates on day 3. On day 5, the cells were passaged into 10 cm dishes (section 2.13.2). Cell morphology was

documented by phase-contrast microscopy recordings on day 5, 8, 10, 12, 15, 17, 19 and 22 (Figure 9B). The medium was exchanged every third day and the cells were split at 60 - 70 % confluency (see sections 2.13.1 and 2.13.2).
The cellular morphology of both HaCaT (Figure 10) and C5N (Figure 11) cells changed upon 3-week culturing in A1 or A2 medium compared to culture in CTRL medium. In particular, on day 5 HaCaT cells grow under all conditions with similar morphology as the cells were roundish, flat with higher cell-to-cell packaging (Figure 10, yellow arrows). However, beginning at day 22, HaCaT cells grown in medium supplemented with 0.03 mM $CaCl_2$ began to show morphological changes. They changed from the roundish, flattened to a spindle-shaped morphology, with an overall loose arrangement with their neighboring cells, accompanied by a reduction of cell-cell tight junctions (Figure 10, yellow arrows). HaCaT cells grown in CTRL media, A1 or A2 media supplemented with 1.8 and 0.5 mM $CaCl_2$ did not change their morphology in a similar manner. However, these analyses further revealed that on day 22, the low, 2 % cFCS amount in A2 media containing 1.8, 0.5 or 0.03 mM $CaCl_2$, respectively, lead to a reduction in cell proliferation rate. Similarly, at day 5 of the culture period, C5N cells grown in CTRL medium and in media containing 2 or 10 % cFCS and defined $CaCl_2$ concentrations (1.8, 0.5 and 0.03 mM) did not obviously differ in their cubical, flat morphology and their tightly arranged growth appearance (Figure 11, yellow arrows). However, and similar to HaCaT cells, C5N cells cultured for at least 22 days in A1 media containing 10 % cFCS and 0.03 mM $CaCl_2$, changed their morphology and their growth behavior to a more spindle shaped form and a less compact growth (Figure 11, yellow arrows). Nevertheless, C5N cells grown in CTRL media or in A1 media with 10 % cFCS and 1.8 or 0.5 mM $CaCl_2$, respectively, did not differ in their morphological appearance. C5N cells kept in A2 media with only 2 % cFCS and 0.5 or 0.03 mM $CaCl_2$ did not proliferate well and were discarded at day 8 or day 22, respectively.
Taken together, these results show that culture of HaCaT and C5N cells in media containing low [Ca^{2+}] concentrations induce morphological changes resembling a basal cell-like phenotype. However, both HaCaT and C5N cells do not proliferate well in A2 media containing low cFCS amounts. Thus, for subsequent experiments the cells were grown in 10 % cFCS containing A1 medium with defined $CaCl_2$ concentrations (1.8, 0.5 and 0.03 mM).

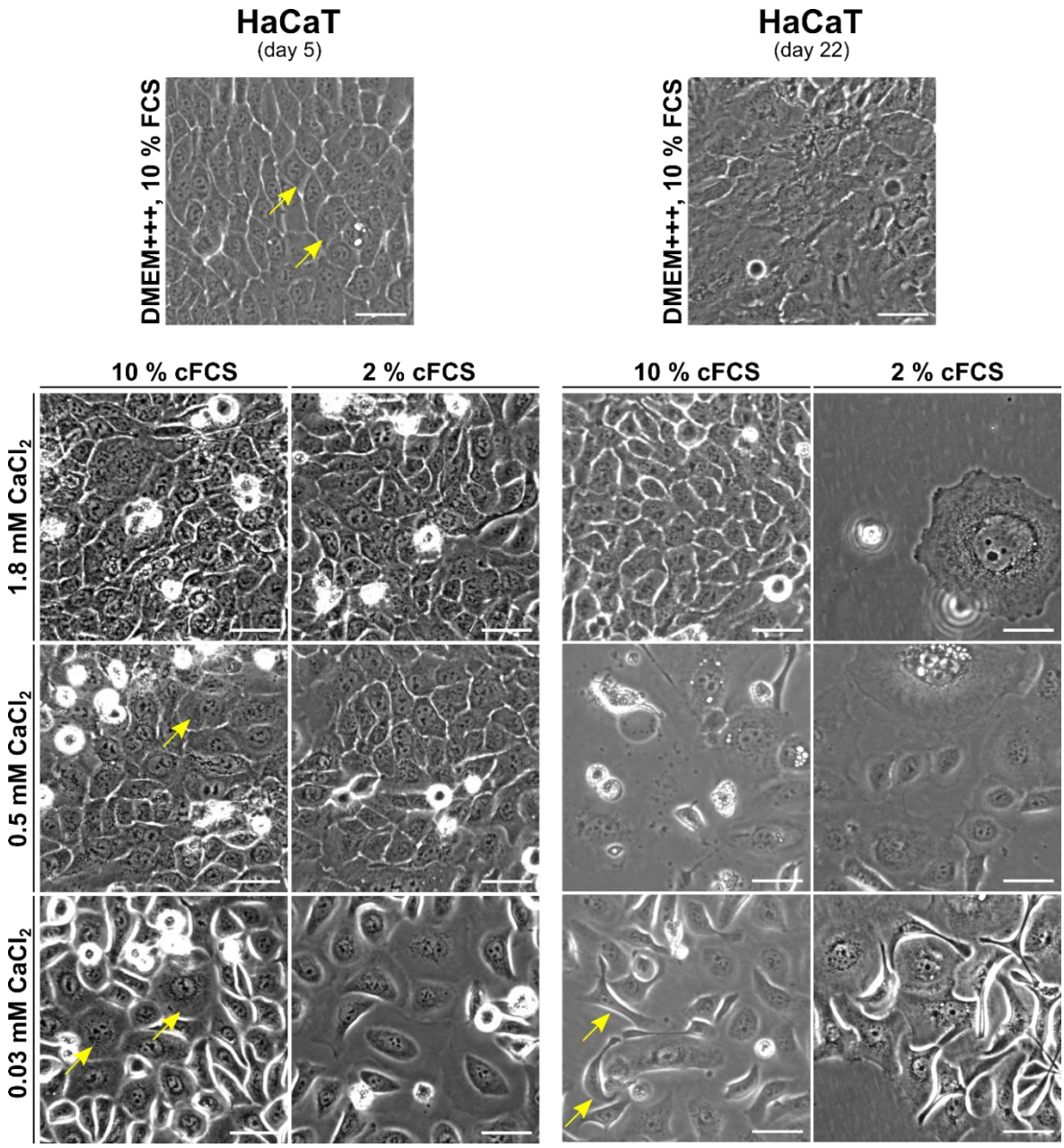

Figure 10: Morphological changes in HaCaT cells upon culture in low [Ca^{2+}] concentration medium. Phase contrast microscopy acquisitions of HaCaT cells grown in CTRL medium (DMEM+++, 10 % FCS; top) or in media containing 2 or 10 % cFCS (bottom) with defined [Ca^{2+}] levels ranging from 1.8, 0.5 and 0.03 mM $CaCl_2$ for 5 (left) or 22 days (right), respectively. Cell morphology changes to a more spindle shaped form under low [Ca^{2+}] conditions (yellow arrows) and upon increased culture period. Furthermore, cells cultured for 22 days show less cell-cell tight junctions then cells cultured only for 5 days in low [Ca^{2+}] concertation medium or in CTRL medium. Scale bars: 30 µm.

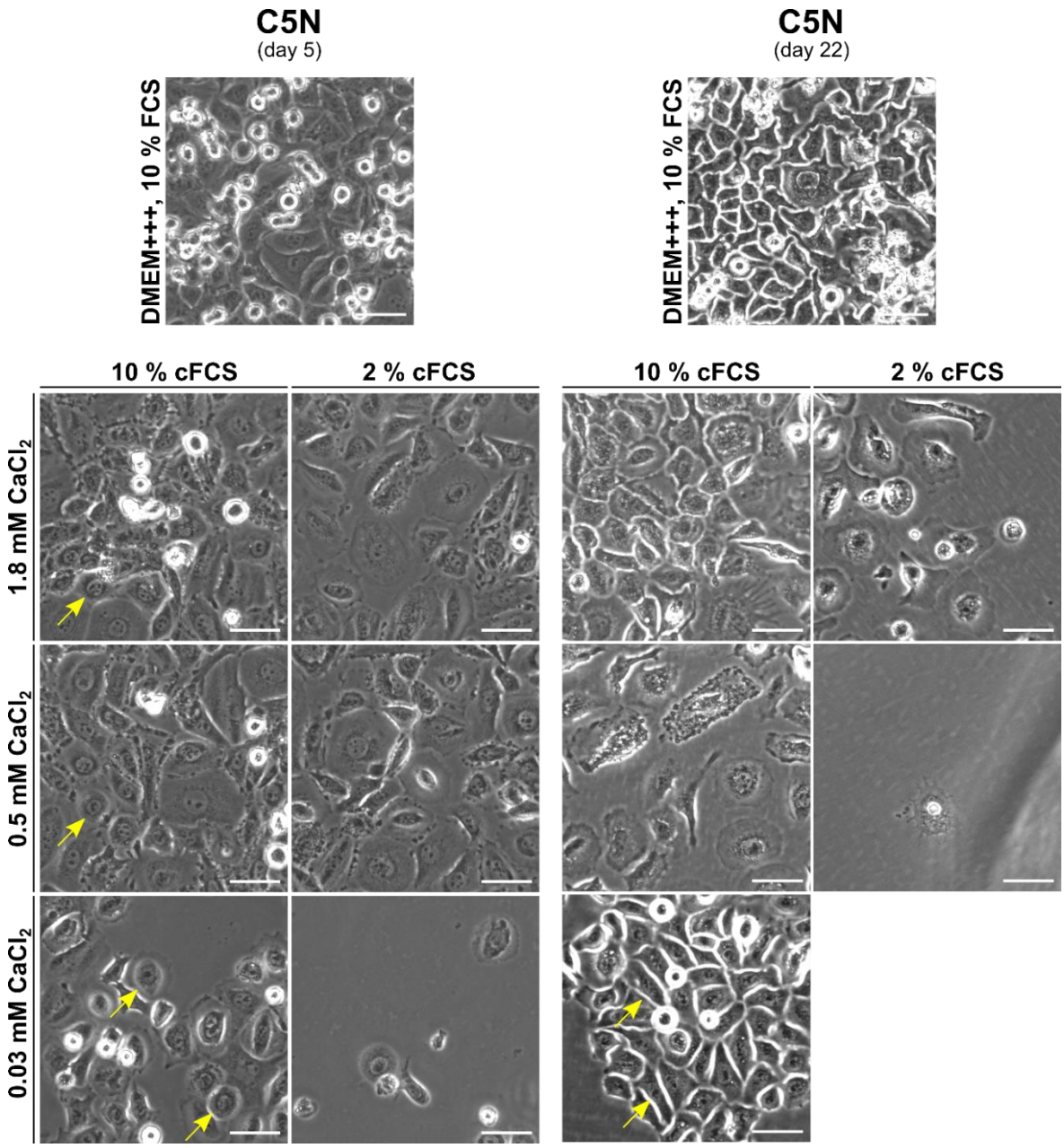

Figure 11: Morphological changes in C5N cells upon culture in medium with low [Ca^{2+}] concentrations. Phase contrast microscopy acquisitions of C5N cells grown in CTRL medium (DMEM+++, 10 % FCS; top) or in media containing 2 or 10 % cFCS (bottom) with defined [Ca^{2+}] levels ranging from 1.8, 0.5 and 0.03 mM for 5 (left) or 22 days (right), respectively. Cell morphology changes to a more spindle shaped form under low [Ca^{2+}] conditions (yellow arrows) and upon increased culture period. C5N cells kept in A2 media (2 % cFCS) with [Ca^{2+}] levels of 0.03 mM did not proliferate well and were discarded at day 8. Scale bars: 30 µm.

3.1.2. Characterization of the basal cell-like, dedifferentiated keratinocyte cell lines

3.1.2.1. Analysis of keratinocyte differentiation status by immunofluorescence antibody staining

In addition to morphological changes, the differentiation status of HaCaT and C5N cells cultured in media with different [Ca^{2+}] concentrations was investigated by immunofluorescence antibody staining against different keratins, whose expression is tightly regulated during keratinocyte cell differentiation (section 1.2.2).

For this purpose, HaCaT and C5N cells cultured in CTRL medium or in A1 media supplemented with different [Ca^{2+}] levels (1.8, 0.5 and 0.03 mM $CaCl_2$) were cultured in 4-chamber slides for 3 days. Subsequently, the cells were fixed and stained with antibodies against keratinocyte marker proteins.

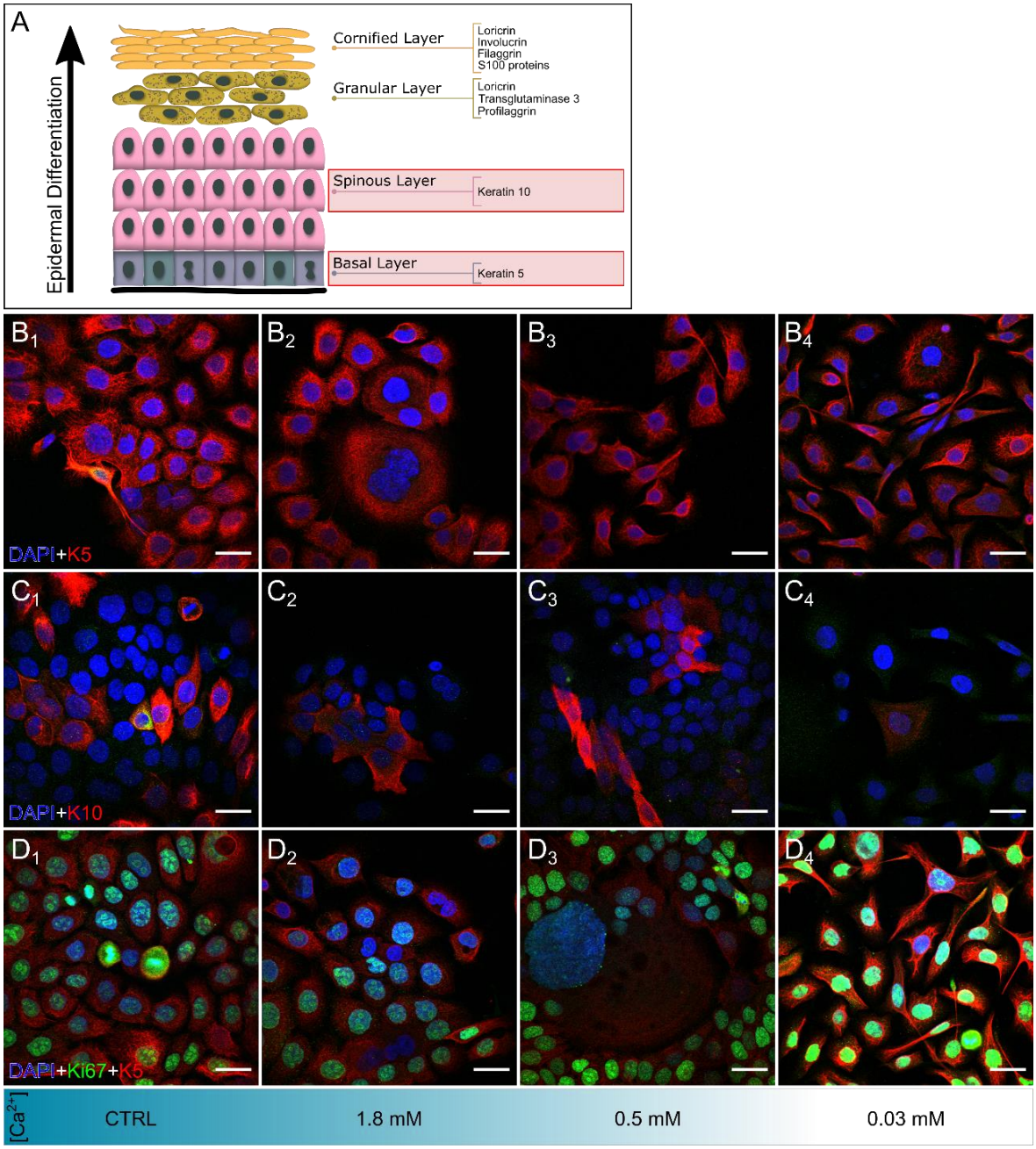

Figure 12: Low [Ca^{2+}] concentrations increase expression of the basal marker K5 and decrease the expression of differentiation marker K10 but does not impact proliferative activity of HaCaT cells. (A) Schematic representation of the epidermal differentiation and respective molecular markers of human skin. Red boxes indicate the marker keratins analyzed by immunofluorescent antibody staining. **(B-D)** Representative immunofluorescence antibody staining against the basal cell marker K5 (red, B1-4), the spinous cell marker K10 (red, C1-4) as well as K5 (red) and proliferation marker Ki67 (green, D1-4) of HaCaT cells cultured in CTRL medium (B1, C1, D1 all passage 8), in A1 medium containing 1.8 mM $CaCl_2$ (B2, C2, D2 all passage 4), in 0.5 mM $CaCl_2$ (B3, C3, D3 all passage 7) or 0.03 mM $CaCl_2$ (B4, C4, D4 all passage 8). Nuclei were counterstained with DAPI. Scale bar: 30 µm. For details regarding the immunocytochemistry and the used antibodies see section 2.16.1 and Table 8, respectively.

The immunofluorescence antibody staining revealed that HaCaT cells cultured in medium containing low [Ca^{2+}] concentrations increased the expression of the basal cell marker K5 (Figure 12B) and reduced the expression of the differentiation marker K10 (Figure 12C). Moreover, based on the constantly high expression of the proliferation marker Ki67 (Figure 12, D_1-D_4) the results furthermore indicated that the different media did not affect the proliferative activity of the HaCaT cells. Similarly, the immunofluorescence staining of C5N cells showed that culture in low [Ca^{2+}] concentrations media increases the K5 expression in comparison to culture in CTRL medium or in media with high [Ca^{2+}] concentrations (Figure 13).

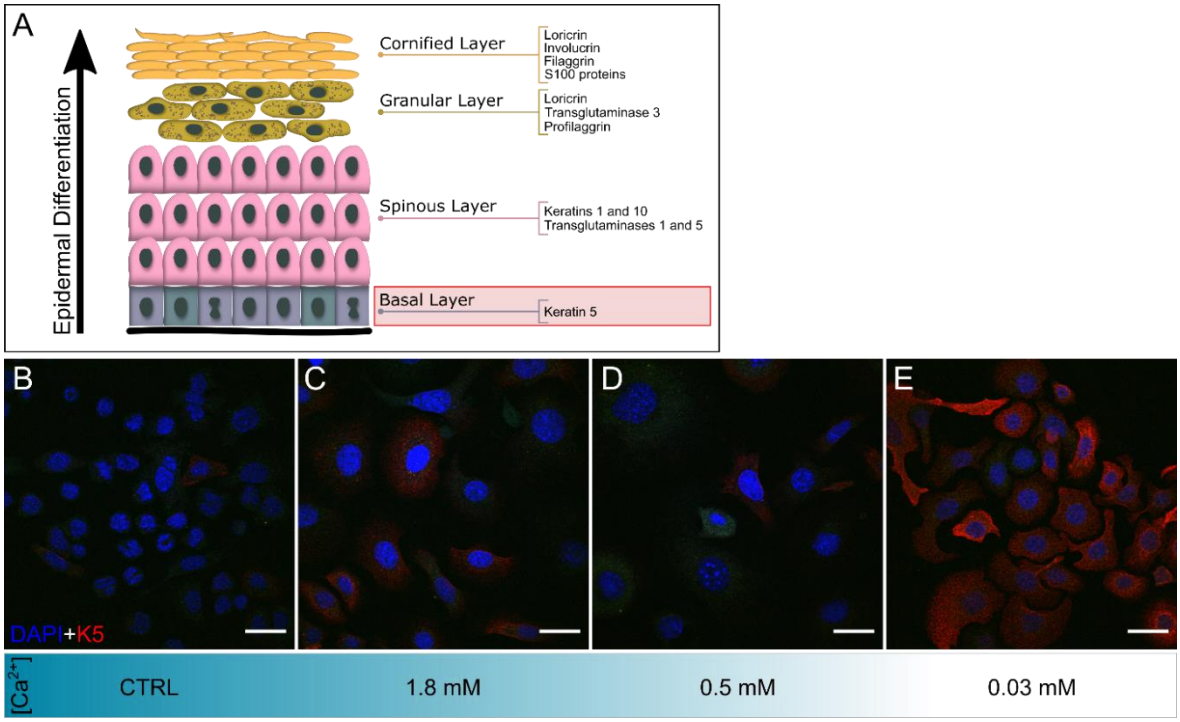

Figure 13: Culture of C5N cells in medium containing low [Ca^{2+}] concentrations induce the expression of the basal cell marker K5. (A) Schematic representation of the epidermal differentiation and respective molecular markers of murine skin. Red box marks the basal cell marker analyzed by immunofluorescence antibody staining. **(B-E)** Representative immunofluorescence antibody staining against the basal cell marker K5 (red) of C5N cells cultured in in CTRL medium (B; passage 7), in A1 medium containing 1.8 mM $CaCl_2$ (C, passage 7), in 0.5 mM $CaCl_2$ (D, passage 6) or 0.03 mM $CaCl_2$ (E, passage 4).

Nuclei were counterstained with DAPI. Scale bar: 30 µm. For details regarding the immunocytochemistry and the used antibodies see section 2.16.1 and Table 8, respectively.

Together, these results confirmed the previously made observation that low [Ca^{2+}] levels induce a dedifferentiation of HaCaT and C5N cells to a more basal cell-like phenotype. Thus, in the following text, HaCaT and C5N cells cultured for a period of at least 3 weeks in medium containing low [Ca^{2+}] concentrations are named dedifferentiated HaCaT (ddHaCaT) or dedifferentiated C5N (ddC5N) cells.
According to Deyrieux and Wilson (2007), the differentiation potential of ddHaCaT cells need to be verified. For this purpose, ddHaCaT cells (cultured in A1 medium containing 0.03 mM $CaCl_2$, passage 7) were transferred and cultured for 72 h in high [Ca^{2+}] levels medium (DMEM--- medium containing 200mM L-glutamine, 100 mM sodium pyruvate, 1% P/S, 10 % cFCS and 2.8 mM $CaCl_2$) (Deyrieux and Wilson 2007) (Figure 14A). Subsequently the cells were fixed and stained with antibodies against K5, K10 and Ki67. As a control also ddHaCaT cells cultured in A1 medium with low [Ca^{2+}] concentration (0.03 mM $CaCl_2$) were simultaneously analyzed. As shown in Figure 14C-E, ddHaCaT cells grown in medium containing low [Ca^{2+}] concentration continue to express high levels of the basal layer marker K5 (Figure 14C1) whereas ddHaCaT cells grown in 2.8 mM $CaCl_2$ containing medium (Figure 14C2) showed a reduced K5 expression indicating that high [Ca^{2+}] levels suppress the basal cell-like phenotype of ddHaCaT cells efficiently. Moreover, ddHaCaT cells grown in high [Ca^{2+}] concentration medium showed an increased expression of the spinous cell marker K10 (Figure 14D1-D2). However, the proliferative activity of ddHaCaT cells did not differ between culture in low and high [Ca^{2+}] levels medium (Figure 14E1-E2).

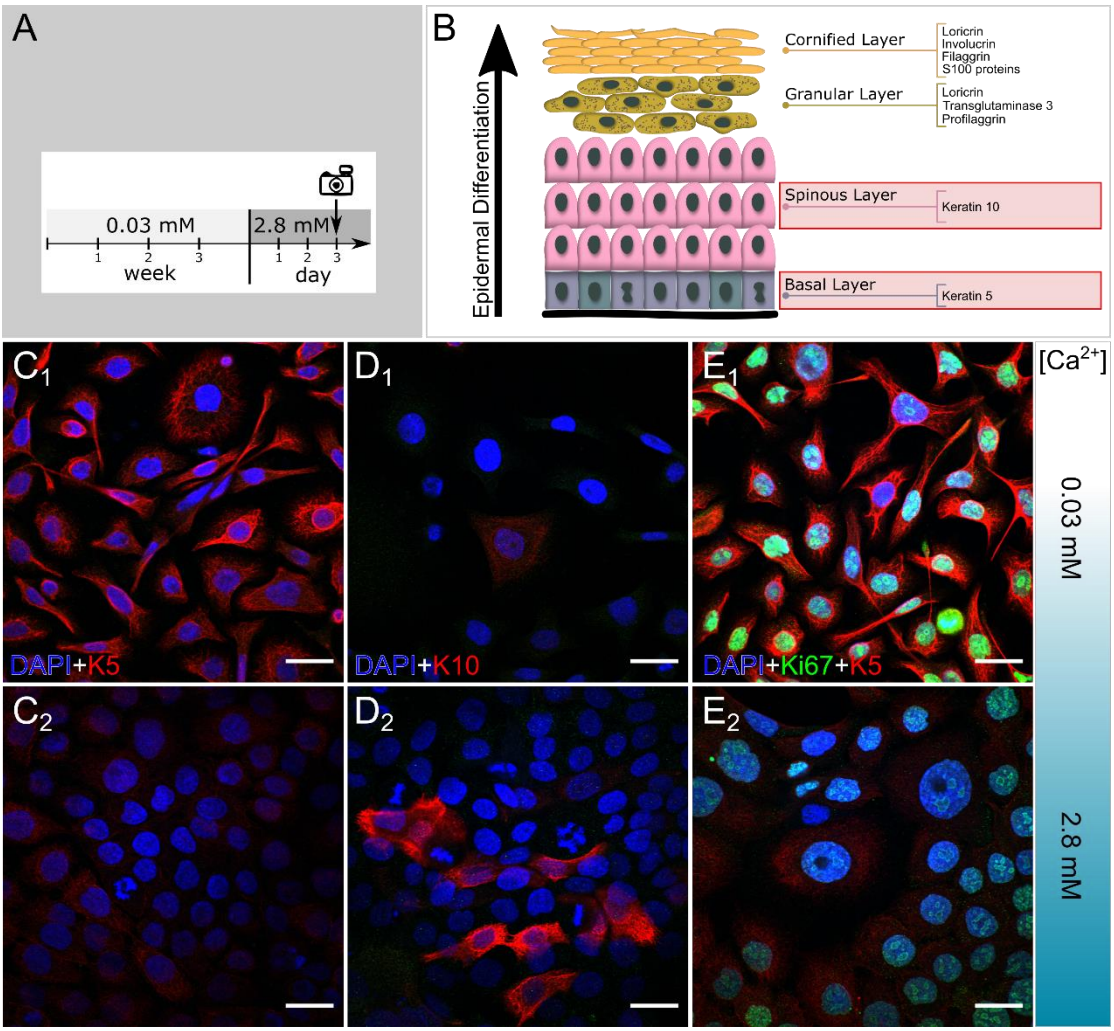

Figure 14: Phenotype switch of ddHaCaT cells upon culture in high [Ca^{2+}] concentration medium. (A) Schematic representation of the experimental setup for analyzing the effect of high [Ca^{2+}] concentration upon ddHaCaT cells: ddHaCaT cells were cultivated for 72 h in high [Ca^{2+}] concentration media (2.8 mM $CaCl_2$), fixed and stained against K5, K10 or K5/Ki67. **(B)** Schematic representation of the epidermal differentiation and respective molecular markers of human skin. Red boxes mark the cell markers analyzed by immunofluorescent antibody staining. **(C-E)** Representative immunofluorescent antibody staining against the basal cell markers K5 (red, C), K10 (red, D) and K5 (red) / Ki67 (green, E) of HaCaT cells cultured in A1 medium with low [Ca^{2+}] concentration (0.03 mM $CaCl_2$) (C1, D1, E1; all passage 7) and ddHaCaT cells cultured for 72 h in A1 medium with high [Ca^{2+}] concentration (2.8 mM $CaCl_2$) (C2, D2, E2; all passage 1). Nuclei were counterstained with DAPI. Scale bar: 30 µm. For details regarding the immunocytochemistry and the used antibodies see section 2.16.1 and Table 8, respectively.

These data confirmed our previous findings that HaCaT cells cultured in medium containing low [Ca^{2+}] levels proliferate and show a basal cell-like phenotype with a high K5, but low K10 expression level. Beyond that, the results furthermore demonstrate that high [Ca^{2+}] levels induce a reduced K5 and an increased K10 expression in ddHaCaT cells and thus are able to switch from the basal cell-like phenotype to a more differentiated one.

3.1.2.2. Analysis of the keratinocyte differentiation status by qRT-PCR

Next, the differentiation status of ddHaCaT and ddC5N cells maintained in A1 medium containing low [Ca^{2+}] levels (0.03 mM $CaCl_2$) and their phenotype switch upon culture to high [Ca^{2+}] levels (2.8 mM $CaCl_2$) was analyzed by qRT-PCR. For this purpose, ddHaCaT and ddC5N cells were cultured for 5 days in A1 medium containing either 0.03 mM $CaCl_2$ or 2.8 mM $CaCl_2$, respectively. Subsequently, the RNA was isolated, cDNA was synthesized and keratinocyte marker expression was analyzed. HaCaT and C5N cells cultured in CTRL medium served as controls.

Generally these analyses revealed, that ddHaCaT as well as C5N cells cultured in A1 medium supplemented with high [Ca^{2+}] levels (2.8 mM $CaCl_2$) showed a more differentiated expression profile than their counterparts cultured in low [Ca^{2+}] level (0.03 mM $CaCl_2$) containing medium (Figure 15 and Figure 16).

Interestingly, the *K5* expression levels were similarly low in ddHaCaT cells cultured in 0.03 mM $CaCl_2$ containing medium as in ddHaCaT cells cultured in 2.8 mM $CaCl_2$ containing medium (Figure 15A). However, the generally high expression level of the basal cell marker *K15* in ddHaCaT cells cultured in 0.03 mM $CaCl_2$ containing medium significantly decreased upon switch to 2.8 mM $CaCl_2$ containing medium (Figure 15A). Moreover, the expression levels of the keratinocyte differentiation markers *K1* and *K10*, that are very low in ddHaCaT cells (Figure 15B), as well as *Involucrin* significantly increase upon culture in 2.8 mM $CaCl_2$ containing medium (Figure 15B).

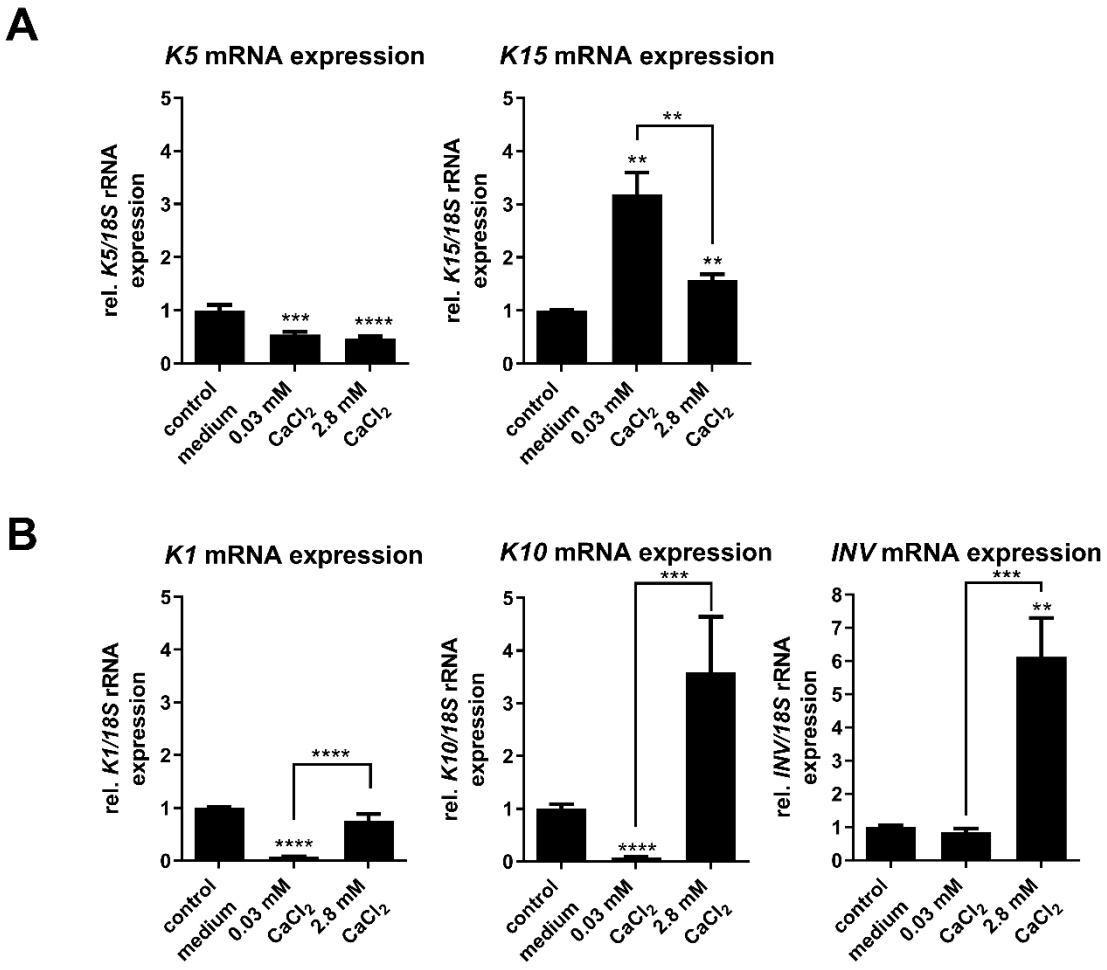

Figure 15: Culture of ddHaCaT cells in medium containing high [Ca^{2+}] concentrations induce a phenotype switch from a basal cell-like to a more differentiated expression profile. qRT-PCR-based quantification of *K5* and *K15* **(A)** and *K1, K10* and *Involucrin* **(B)** mRNA expression levels of HaCaT cells cultured in CTRL medium (passage 18) or ddHaCaT cells cultured in A1 medium supplemented with 0.03 mM (passage 13) or 2.8 mM $CaCl_2$ (passage 1), respectively. Gene expression levels were measured in technical triplicates. Keratinocyte marker expression was normalized to *18S* rRNA expression level. Normalized expression levels of HaCaT cells cultured in CTRL medium were subsequently set to one. Statistical analyses were performed by a non-parametric Mann-Whitney t-test. **p<0.01, ***p<0.001****p< 0.0001.

Similarly to HaCaT, ddC5N cells cultured in A1 medium supplemented with high [Ca^{2+}] levels (2.8 mM $CaCl_2$) led to a significant decreased expression of the basal cell marker *K5* (Figure 16A) and to a significant increased expression of the differentiation marker *Involucrin* (Figure 16B) compared to cells cultured in 0.03 mM $CaCl_2$ containing A1 medium or/and in CTRL medium, respectively.

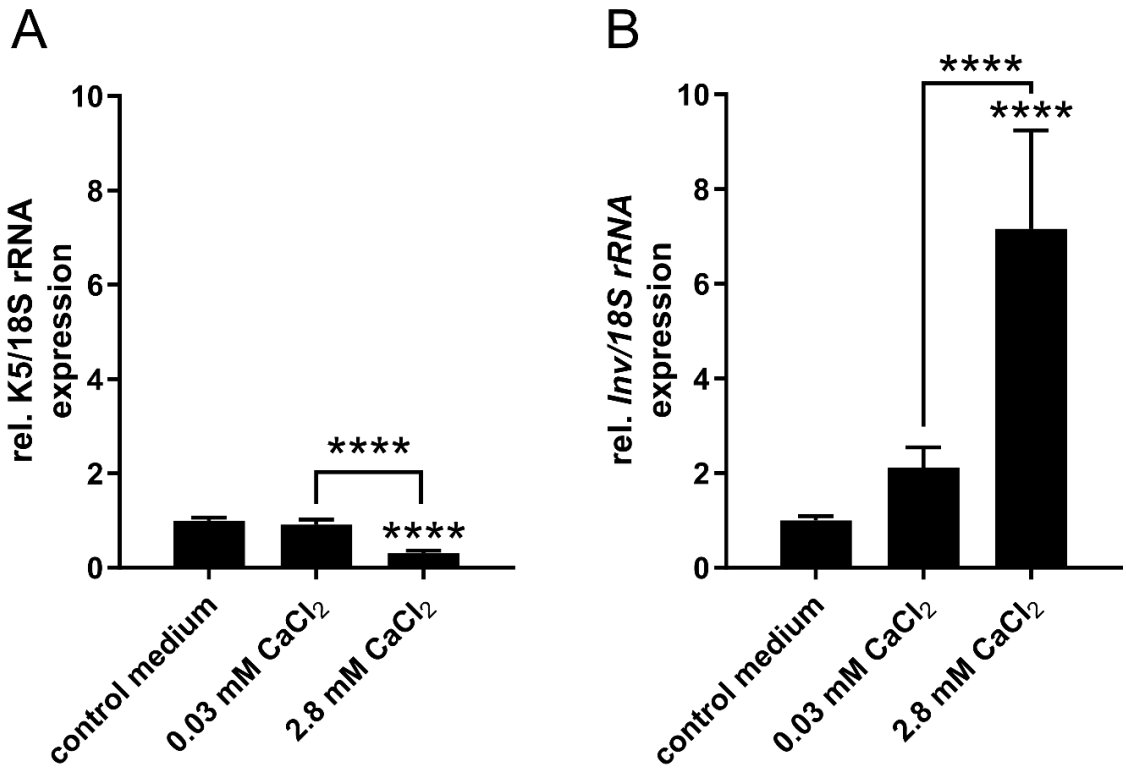

Figure 16: Culture of ddC5N cells in medium containing high [Ca^{2+}] concentrations induce a phenotype switch from a basal cell-like to a more differentiated expression profile. qRT-PCR-based quantification of *K5* **(A)** and *Involucrin* **(B)** mRNA expression levels of C5N cells cultured in CTRL medium (passage 26) or ddC5N cells cultured in A1 medium supplemented with 0.03 mM (passage 8) or 2.8 mM $CaCl_2$ (passage 1), respectively. Gene expression levels were measured in technical triplicates. Keratinocyte marker expression was normalized to *18S* rRNA expression level. Normalized expression levels of C5N cells cultured in CTRL medium were subsequently set to one. Statistical analyses were performed by a non-parametric Mann-Whitney t-test. ****p< 0.0001.

Taken together, these results confirmed that ddHaCaT and ddC5N cells lose their basal cell-like phenotype and start to differentiate upon culture in medium supplemented with high [Ca^{2+}] concentrations.

3.1.2.3. Analysis of the keratinocyte differentiation status via immunofluorescent-based quantification of protein expression

For further verification of the keratinocyte differentiation status quantitative analyses of anti-K5 and anti-K10 antibody stained HaCaT cells cultured in CTRL medium or ddHaCaT cells cultured in A1 medium containing 0.03 mM or 2.8 mM $CaCl_2$ were performed. For this purpose, the cells were cultured in the respective medium for 3 days in 4 well-chamber slides. Subsequently, the cells were fixed and stained against the basal cell marker K5 and the keratinocyte differentiation marker K10. Finally, images of the respective staining were acquired and analyzed with an automated image analysis workflow to quantify the K5 and K10 protein expression levels. For this purpose, multichannel, confocal images of the stained cells were acquired with a fully automated, inverted Nikon Eclipse Ti microscope equipped with

a Yokogawa CSU W1 spinning disk unit. The same acquisition settings were used to acquire 10 fields of view within each well (Figure 17).

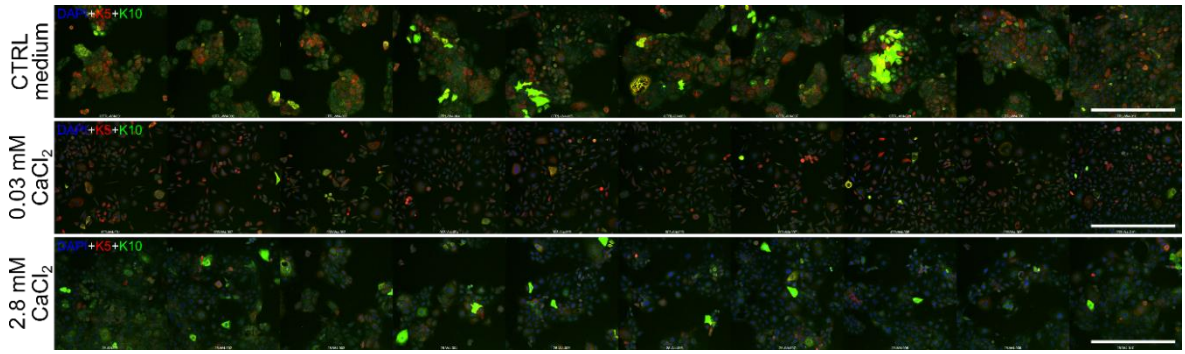

Figure 17: Panoramic pictures of immunofluorescent anti-K5/anti-K10 antibody stained HaCaT and ddHaCaT cells. 10 visual fields of anti-K5 (red)/anti-K10 (green) immunofluorescent antibody stainings of HaCaT cells grown in CTRL medium (passage 12, top) and ddHaCaT cells grown in A1 medium supplemented with 0.03 mM (passage 10, middle) or 2.8 mM $CaCl_2$ (passage 1, bottom), respectively, were merged to the respective panoramic pictures. Nuclei were counterstained with DAPI (blue). Scale bar: 500 µm. The applied Nikon Plan Apo 20x/0.75 NA air objective and the Andor iXon Ultra 888 camera resulted in images sized 668.03 x 668.03 µm (0.65 µm/pixel).

For this purpose, the fluorescent emissions of the DAPI, Cy3 and Alexa Fluor 488 fluorophores for visualization of the nuclei and the anti-K5 or anti-K10 antibody staining, respectively, were acquired sequentially. To reduce artefacts, the identical objective-to-cell distance was kept at each position through application of the hardware autofocus (Nikon Perfect Focus). Additionally, intensity measurements on previously acquired time series for each fluorophore were used to optimize acquisition settings so that bleaching levels were kept below 0.5 %. The Cy3 and Alexa Fluor 488 mean intensities were extracted automatically on a per cell basis with the CellProfiler™ image analysis software (https://cellprofiler.org/). In particular, a custom-made CellProfiler™ pipeline separated the three acquired emission channels and used the DAPI channel as a basis for the segmentation of each cell nucleus (Figure 18). Cells whose nuclei were located at the edge of the field of view were excluded. Afterwards, a mask resembling a perinuclear ring was generated automatically for each nucleus (Figure 18C). The same perinuclear mask was then applied to measure the respective, mean anti-K5 (Cy3) and anti-K10 antibody (Alexa Fluor 488) fluorescence intensity (Figure 18D, E).

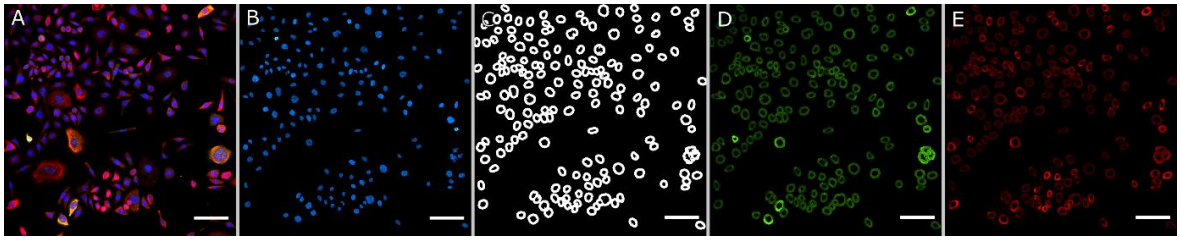

Figure 18: Image analysis workflow for the quantification of the K5 and K10 protein expression level analysis. (A) Representative three-channel image of HaCaT cells. The

automated image analysis workflow extracts the DAPI-stained nuclei channel **(B)** from the three-channel image and generates the corresponding perinuclear masks **(C)** that were applied to the Cy3 **(D)** and the Alexa Fluor 488 **(E)** channels to obtain the respective mean fluorescence intensity of the anti-K5 and the anti-K10 antibody staining on a per cell basis. Scale bar: 100 µm.

Background values were defined as being lower than the lower quartile of the respective channel and excluded from final quantifications. The relative fluorescence intensities were then extracted from fluorescence images and were afterwards analyzed by GraphPad Prism 6 software.
Figure 19 summarizes the results of the automated immunofluorescent-based quantification of K5 and K10 protein expression. In particular, ddHaCaT cells cultured in A1 medium supplemented with 0.03 mM $CaCl_2$ showed significantly higher levels of K5 protein expression than cells cultured in 2.8 mM $CaCl_2$ containing A1 medium (Figure 19A). Furthermore, the expression of K10 which was significantly lower in ddHaCaT cultured in 0.03 mM $CaCl_2$ containing medium and increased significantly upon medium switch to 2.8 mM $CaCl_2$ containing medium (Figure 19B).

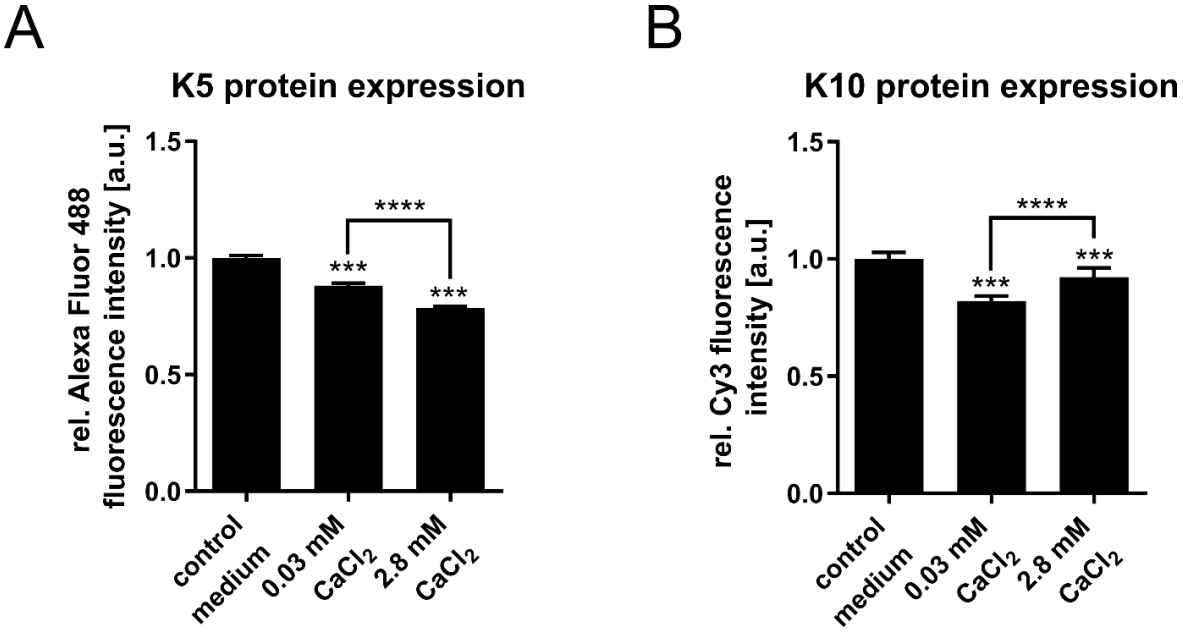

Figure 19: Culture of ddHaCaT cells in medium containing high [Ca^{2+}] concentrations induce a phenotype switch from a basal cell-like to a more differentiated protein expression profile. Immunofluorescence-based quantification of the **(A)** K5 and **(B)** K10 protein expression levels of HaCaT cells cultured in CTRL medium (passage 10) or ddHaCaT cells cultured in A1 medium supplemented with 0.03 mM (passage 10) or 2.8 mM $CaCl_2$ (passage 1), respectively. Relative fluorescence intensities of two independent biological replicates were measured. Keratinocyte marker expression of HaCaT cells cultured in CTRL medium was set to one. Statistical analyses were performed by a non-parametric Mann Whitney t-test. ***p<0.001, ****p<0.0001. For details to the automated image analysis workflow, please see main text.

Together these data confirm our previous findings that the culture of ddHaCaT cells in medium containing high [Ca^{2+}] levels is sufficient to induce a phenotype switch from a basal cell-like to a more differentiated expression profile.

3.1.2.4. Analysis of the proliferative behavior

To compare the proliferative behavior of ddHaCaT cells cultured in medium with low and high [Ca^{2+}] concentrations the cells were grown for 3 days in 4 well-chamber slides in A1 medium containing 0.03 mM or 2.8 mM $CaCl_2$. Afterwards, the cells were fixed and stained with antibodies against the basal cell marker K5 and the proliferation marker p63 (Truong et al. 2006; Wu N et al. 2012). This approach revealed that ddHaCaT cells grown in media with low (Figure 20A) or high (Figure 20B) [Ca^{2+}] levels show comparably strong p63 staining pattern. Similarly to the previously made observation, where the Ki67 staining pattern of ddHaCaT cells cultured in A1 medium containing 0.03 mM and 2.8 mM $CaCl_2$ does not differ grossly (Figure 12 and Figure 14), the p63 immunofluorescence staining substantiates the finding that although high [Ca^{2+}] concentrations induces a more differentiated phenotype in ddHaCaT cells (see chapter 3.1.2), it has no obvious influence on the highly proliferative activity of these cells.

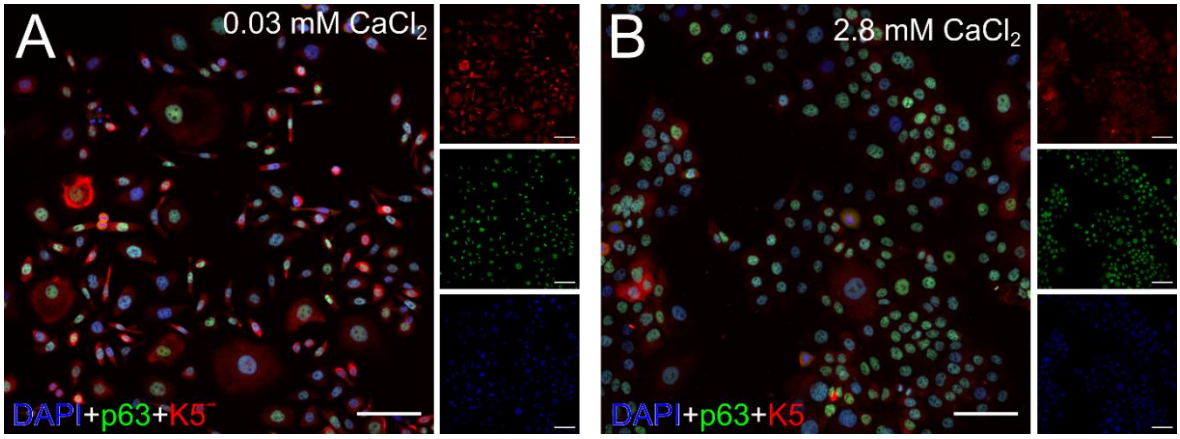

Figure 20: The p63 expression pattern of ddHaCaT cells is not influenced by culture in high [Ca^{2+}] level medium. Representative immunofluorescence staining of ddHaCaT cells cultured in **(A)** 0.03 mM (passage 10) and **(B)** 2.8 mM (passage 1) $CaCl_2$-containing A1 medium with antibodies against the basal cell marker K5 and proliferation marker p63. Nuclei were counterstained with DAPI. Scale bar: 100 µm. For details regarding the immunocytochemistry see section 2.16.1 and for details regarding the used antibodies see Table 8.

To quantify the proliferative activity of ddHaCaT and ddC5N cells cultured in different $CaCl_2$ levels-containing media, BrdU incorporation assays were performed. For this purpose, HaCaT and C5N cells grown in CTRL medium and ddHaCaT, ddC5N cells cultured in 0.03 mM or 2.8 mM $CaCl_2$-containing A1 medium were pulsed with BrdU for 22 h before analysis. 70 h and 94 h after seeding, the cellular proliferation rates of the last 22 h of the culture period were determined (Figure 21A). This revealed that independently on the analyzed time point, ddHaCaT and ddC5N cells cultured in 0.03 mM or 2.8 mM $CaCl_2$-containing A1 medium proliferate significantly less compared to HaCaT or C5N cells cultured in CTRL medium, respectively (Figure 21B,C). Except for the proliferation rate of ddHaCaT grown in 2.8 mM $CaCl_2$-containing A1 medium measured 94 h after seeding, both ddHaCaT and ddC5N

cells cultured in 2.8 mM $CaCl_2$-containing A1 medium proliferate less than cells cultured in 0.03 mM $CaCl_2$-containing A1 medium irrespectively of the analyzed time point. However, the proliferation rate of ddHaCaT and ddC5N cells cultured for 94 h was either higher (Figure 21B) or lower (Figure 21C), respectively, when compared to that of the respective 70 h culture period. Taken together these results demonstrate that the proliferation rate of ddHaCaT and ddC5N cells is generally lower than those of HaCaT and C5N cells grown in CTRL medium and that both cell lines proliferate less in culture medium containing high [Ca^{2+}] levels compared to low [Ca^{2+}]-containing media.

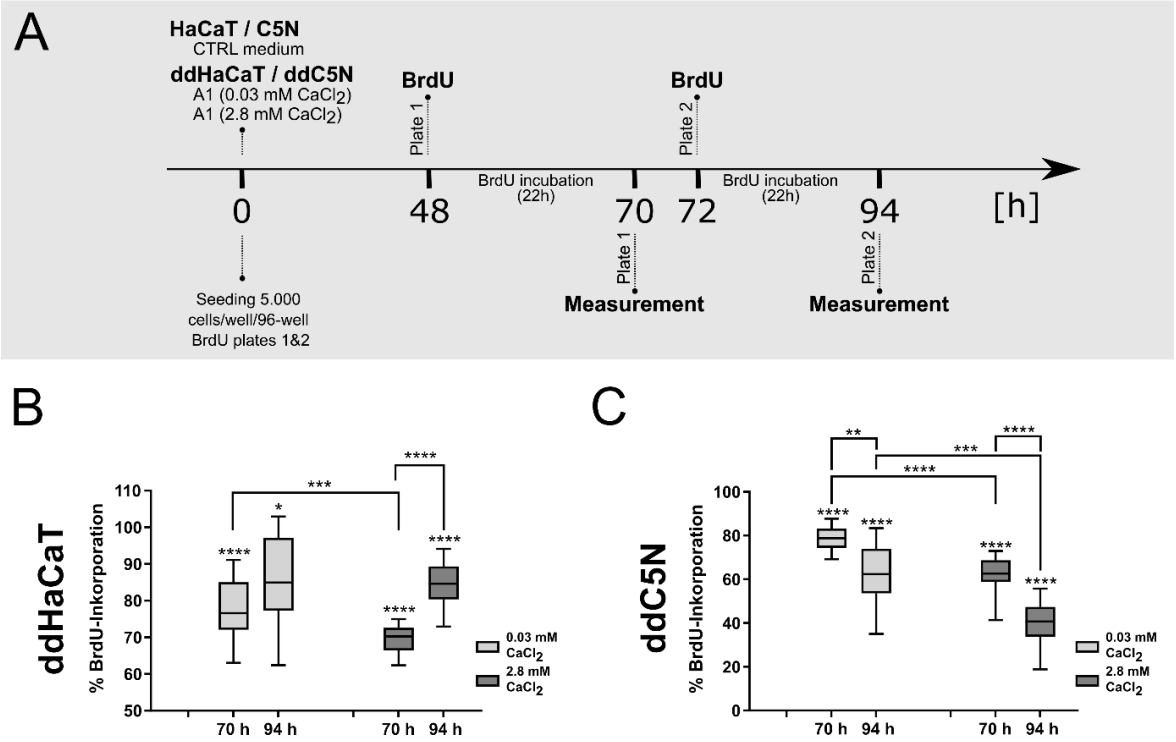

Figure 21: The proliferation rate of ddHaCaT and ddC5N cells is reduced compared to HaCaT and C5N CTRL cells and decreases further upon culture in high [Ca^{2+}]-containing medium. (A) Schematic representation of the experimental setup: cells were seeded and cultivated for 48h and 72h in CTRL, low [Ca^{2+}] concentration (0.03 mM $CaCl_2$) or high [Ca^{2+}] concentration (2.8 mM $CaCl_2$) A1 media, respectively. After 48 h and 72 h the cells were pulsed with BrdU for 22 h and the proliferative activity was analyzed. **(B-C)** Percentual proliferation rate of **(B)** ddHaCaT and **(C)** ddC5N cells cultured in A1 medium supplemented with 0.03 mM (ddHaCaT cells, passage 15; ddC5N cells, passage 18; light grey boxes) or 2.8 mM $CaCl_2$ (ddHaCaT cells, passage 1; ddC5N cells, passage 1; dark grey boxes) respectively, measured by means of BrdU-incorporation assays. BrdU-incorporation was measured in technical triplicates and the depicted proliferation rates were normalized to that of simultaneously analyzed HaCaT or C5N cells, respectively, cultured in CTRL medium that were set to 100% (HaCaT cells, passage 18; C5N cells, passage 40). Statistical analyses were performed by a non-parametric Mann Whitney t-test. *p<0.05, ***p<0.001, ****p<0.0001.

3.2. Generation of an *in vitro* system for inducible expression of human *CD4*

After establishment of ddHaCaT and ddC5N keratinocyte cell lines with a basal cell-like phenotype, the cells were used to stably transfect a plasmid containing an inducible *CD4*-expression system allowing for the study of CD4 function in these cells. Due to lack of sufficient data in the literature concerning C5N cells, the further experiments were only performed in HaCaT cells.

For the generation of the stably transfected keratinocytes, the Tet-On® Advanced Inducible Gene Expression System from Clontech (Table 5) was utilized, which has been described as a tightly regulated and highly responsive system for the doxycycline (Dox)-inducible robust expression of a gene of interest (GOI) in target cells. The components and the mechanism of the system are depicted in Figure 22. The Tet-ON Advanced protein (Figure 22, grey circle) is based on tetracycline-regulated transcriptional transactivators (Gossen and Bujard 1992; Gossen et al. 1995) but with optimized sensitivity and expression in mammalian cells (Urlinger et al. 2000). It consists of a mutant *E. coli* tetracycline repressor protein (reverse TetR, rTetR) fused to three minimal "F"-type activation domains derived from the *Herpes simplex* virus VP16 protein (Baron et al. 1997; Triezenberg et al. 1988). In the presence of Dox, the Tet-On Advanced protein binds to the P_{Tight} promoter (Figure 22), consisting of a modified tetracycline response element (TRE_{mod}) with seven repeats of the *Escherichia coli* tetracycline operator sequence upstream of a minimal CMV promoter sequence ($CMV_{min\Delta}$), and activates the transcription of the downstream GOI (Figure 22) (Baron and Bujard 2000).

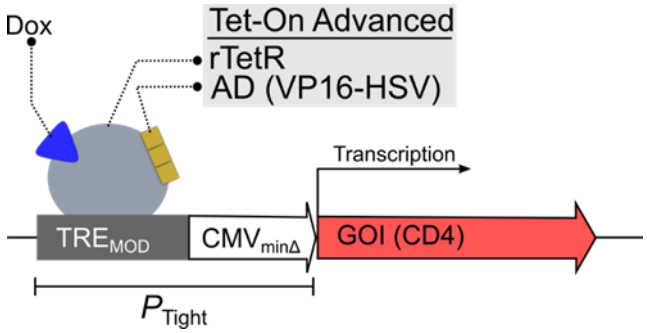

Figure 22: Inducible expression of a gene of interest (GOI) using the Tet-On Advanced System from Clontech. The Tet-On advanced system is composed of a transactivator protein (grey circle) consisting of the reverse tetracycline repressor protein from *Escherichia coli* (rTetR) combined with activation domains (AD, yellow boxes) from the *Herpes simplex* virus VP16 protein (VP16-HSV). In presence of doxycycline (Dox, blue triangle) the Tet-On Advanced protein binds to the modified tetracycline response element (TRE_{mod}, dark gray box) of the P_{Tight} promoter and induces the expression of the downstream cloned GOI (red arrow). (Scheme adapted from Clontech (2012)).

To establish a cell line in which the expression of a GOI can be controlled by Tet-On® Advanced Inducible Gene Expression System the plasmid encoding the Tet-On advanced protein (*pTet-DualON*) and the plasmid containing the GOI controlled by the P_{Tight} promoter (customized *pTRE-Dual2-GOI*, here *pTRE-Dual2-hCD4*) have

to be consecutively transfected into the cells followed by an antibiotic selection of cells that stably integrated the respective plasmid (Figure 23, step 1 and 3). After picking, expanding and analyzing independent clones (Figure 23, step 2 and 4) either the second plasmid can be transfected into the best clone (Figure 23, step 3) or the best double-transfected clone can be used for further analysis (Figure 23, step 4), respectively.

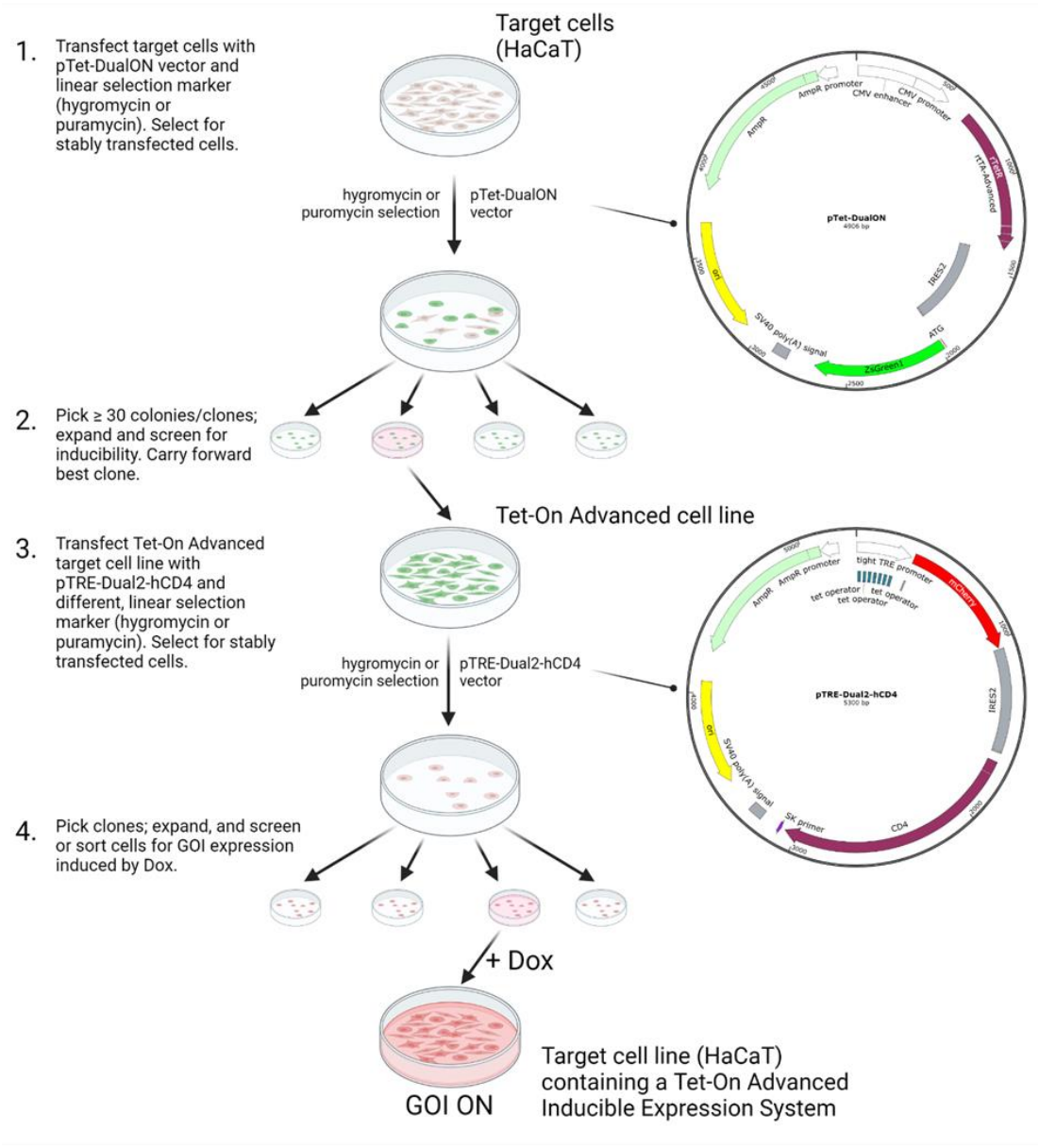

Figure 23: Schematic representation of the generation of a cell line harboring the Tet-On® Advanced Inducible Gene Expression System. HaCaT cells, stably transfected with the doxycycline (Dox)-inducible expression of a gene of interest (GOI), were generated with consecutive transfections, each of which was followed by an antibiotic selection step. For this purpose, the cells are simultaneously transfected with a plasmid encoding the Tet-ON Advanced protein (*pTet-DualON*) and a linear selection marker (hygromycin or purmoycin) (step 1). After selection of stably transfected cells, independent clones are picked, expanded and analyzed for their expression of the Tet-ON Advanced protein or rather of the green fluorescent protein ZsGreen1, which is simultaneously expressed with the Tet-ON

Advanced protein, since both genes are linked via an internal ribosomal entry site 2 (*IRES2*) (step 2). Secondly, the Tet-ON Advanced protein-expressing cell line is simultaneously transfected with a plasmid containing the GOI (here the human *CD4* gene, *hCD4*) controlled by the P_{Tight} promoter (*pTRE-Dual2-hCD4*) and a linear antibiotic selection marker (hygromycin or purmoycin) (step 3). After selection, picking and expansion, the cells are analyzed for their Dox-inducible expression of the red fluorescent protein mCherry and of the *IRES2*-linked GOI (step 4). The resulting cell line can then be used for further experiments. (Scheme adapted from Clontech (2012)).

Here the target cell line HaCaT was transfected with the *pTet-DualON* plasmid which is supplied with the Tet-On® Advanced Inducible Gene Expression System (Table 5, Figure 23, step 1). The transfection conditions, number of cells used and plasmid quantities are described in section 2.13.6. Since the *pTet-DualON* plasmid encodes for the cytomegalovirus (*CMV*) promoter-driven expression of the Tet-On Advanced protein and the internal ribosomal entry site 2 (*IRES2*)-linked green fluorescent protein ZsGreen1 (Matz et al. 1999), the ZsGreen1 expression serves as an indicator of transfection and expression efficiency of the *pTet-DualON* plasmid (Figure 23, step 1). The *ColE1* origin of replication and the ampicillin resistance (*AmpR*) cassette enables the selection and isolation of high amounts of the *pTet-DualON* plasmid in *E. coli*. For the selection of HaCaT cells that stably integrated the *pTet-DualON* plasmid into their genome, a linear double-stranded DNA encoding for antibiotic selection marker (either hygromycin or puromycin) was cotransfected in a vector-to-marker molar ratio of 20:1. After a 4 to 7 day antibiotic selection period, depending on the transfected linear marker and its maintenance in the cells, colonies expressing ZsGreen1 and thus the Tet-On Advanced protein were selected (Figure 23, step 1). Next, >30 green fluorescent colonies should be picked, expanded and screened for ZsGreen1/Tet-On Advanced protein expression level (Figure 23, step 2). The best clones should be chosen for the transfection with the customized *pTRE-Dual2-GOI* plasmid (here *pTRE-Dual2-hCD4*) and a linear double-stranded DNA encoding for different antibiotic selection marker used for the first selection (either hygromycin or puromycin, see above) (Figure 23, step 3). After antibiotic selection for 4 to 7 days, depending on the transfected linear marker and its maintenance in the cells, colonies should appear (Figure 23, step 3). The *pTRE-Dual2-GOI* plasmid used in this work encodes for the expression of the red fluorescent protein mCherry and an *IRES2*-linked *CD4* gene under the control of the P_{Tight} promotor (Figure 23, step 3; *pTRE-Dual2-hCD4*; for details about the generation of the *pTRE-Dual2-hCD4* plasmid please see section 2.14.3), which enables the use of mCherry expression as an indicator for the CD4-expression upon Dox-treatment. Thus, for screening of clones the mCherry/GOI protein expression level after Dox-treatment should be analyzed (Figure 23, step 4). Afterwards the best clones should be used for further experiments (Figure 23, step 4). Similarly to the *pTet-DualON* also *pTRE-Dual2-hCD4* plasmid can be also selected and isolated in high amounts in *Escherichia coli* by its *ColE1* origin of replication and *AmpR* cassette.

3.2.1. Generating of HaCaT cells with stable expression of Tet-ON Advanced protein

For the generation of a HaCaT cell line stably expressing the Tet-ON Advanced protein (see Figure 23), ddHaCaT cells cultured in A1 medium containing 0.03 mM $CaCl_2$ and HaCaT cells cultured in CTRL medium were transfected with the *pTet-DualON* plasmid and one of the provided linear selection markers (hygromycin or puromycin) in a vector-to-marker molar ratio of 20:1 by electroporation or magnet-assisted transfection. For details of the method, conditions of transfection, number of cells and plasmid quantities please see section 2.13.6. Subsequently, the cells were seeded in 10 cm dishes in complete culture medium without selective antibiotics and kept under constant conditions (37°C, 5 % CO_2, humidified atmosphere) in a CO_2-incubator for a period of 48 h. Afterwards, the media of the transfected ddHaCaT and HaCaT cells were switched to A1 medium containing 0.03 mM $CaCl_2$ or CTRL medium, respectively, supplemented with high concentration (selection concentration, see Table 24) of either puromycin or hygromycin, dependent on the respective transfected marker. The antibiotic concentrations were determined by dose response experiments in which the cells were subjected to increasing amounts of the respective antibiotic to define the lowest antibiotic concentration that kills all cells in a specific time period (for the puromycin 4 days, for hygromycin 7 days). The antibiotic selection using high antibiotic levels was performed for 4-7 days, while refreshing the culture medium every 2 days to remove dead cells. The cells were not passaged during the antibiotic selection period. Following the initial selection with high antibiotic concentration, the cells were further cultured in their respective media supplemented with lower concentrations of the respective antibiotic (see Table 24) for an additional 2-3 weeks, within which resistant colonies expressing ZsGreen1 should have grown. However, neither the use of the puromycin nor the hygromycin resistance marker generated ZsGreen1$^+$ ddHaCaT or ZsGreen1$^+$ HaCaT colonies (data not shown).

Table 24. Antibiotic concentrations for selection and maintenance of ddHaCaT and HaCaT cells after transfection with linear selection markers for hygromycin or puromycin resistance.

Cell type	Puromycin		Hygromycin	
	Selection concentration	Maintenance concentration	Selection concentration	Maintenance concentration
dd HaCaT	0.5 µg/ml	0.25 µg/ml	80 µg/ml	20 µg/ml
HaCaT	2.5 µg/ml	1.0 µg/ml	100 µg/ml	50 µg/ml

The transfection of HaCaT cells with circular plasmids is known to be difficult and the efficiency only reaches 20-30 %, maximal 50 % (Deyrieux and Wilson 2007; Deyrieux et al. 2007; Wang et al. 2015). Moreover, as shown by Deyrieux *et al.* (2007) and by our own experiments (data now shown), the transfection efficiency and survival rate after transfection of ddHaCaT is even lower than that of HaCaT cells. Thus, we assumed that the failed establishment of stable ZsGreen1 expres-

sion or Tet-ON Advanced expressing colonies is due to the low ddHaCaT and HaCaT cell transfection rate with circular plasmids using the transfection and selection strategy described above.

To optimize the transfection efficiency as well as the probability of genomic integration of transfected DNA, the *AseI*-linearized *pTet-DualON* plasmid was cotranfected with one of the linear hygromycin selection markers into HaCaT cells (passage 55) by electroporation (see section 2.13.6). The experiments using ddHaCaT were suspended due to the low survival rate after transfection. 48 h after transfection, the cells were cultured in 100 µg/ml hygromycin containing CTRL medium (see Table 24) for 7 days. After passaging, the cells were then cultured for an additional 2 weeks in CTRL medium supplemented with 50 µg/ml hygromycin (see Table 24). The analysis of the remaining cells via brightfield and fluorescence microscopy revealed that approximately 40-50% of one colony consisted of ZsGreen1-expressing HaCaT cells (Figure 24), indicative of the TetON-Advanced protein expression in these cells (see section 3.2). However, the analyzed colony also contained many ZsGreen1^{neg} HaCaT cells (Figure 24) which presumably harbored only the linear hygromycin resistance marker but not the *pTet-DualON* plasmid and thus were resistant against the hygromycin selection without expressing ZsGreen1 or the TetON-Advanced protein. Moreover, the transfection efficiency of the ddHaCaT cells with the *pTet-DualON* plasmid fallen short of expectations since it only yielded 10 – 20 % ZsGreen1^{+} cells after transfection, even when using more gentle transfection protocols like magnet-assisted transfection (data not shown).

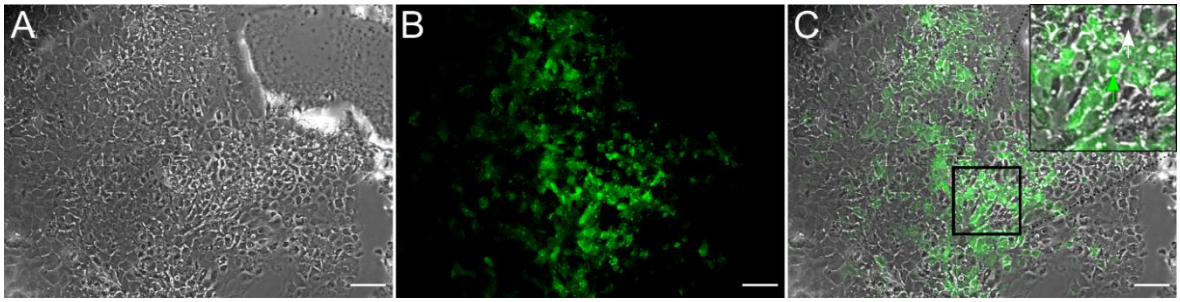

Figure 24: Generation of TetON-Advanced protein-expressing HaCaT cells. (A) Brightfield and **(B)** fluorescence microscopy-based analysis of HaCaT cells (passage 55) transfected with *Ase*I-linearized *pTet-DualON* plasmid and a linear hygromycin resistance marker (vector-to-marker molar ratio of 20:1) after antibiotic selection, passaging and additional 2 weeks culture in CTRL medium supplemented with hygromycin, as described in the main text. **(C)** Overlay of the images shown in (A) and (B). Black-framed box indicates the zoom-in area of the higher magnification shown in the in upper right corner. Green arrow in the inset (C) marks a ZsGreen1^{+} cell, white arrow marks a ZsGreen1^{neg} cell. ZsGreen1 expression is indicative for the presence of the *pTet-DualOn* sequence in the cells and for the expression of the TetON-Advanced protein (see main text for details). Scale bar: 100µm.

3.2.2. Isolation and establishment of a homogeneous HaCaT cell line with stable expression of Tet-ON Advanced protein

Due to the observation that the used strategy for generation of Tet-ON Advanced-expressing HaCaT cells failed to result in a homogeneous ZsGreen1^{+} population

(see Figure 24), next ZsGreen1$^+$ cells of HaCaT cells transfected with *Ase*I-linearized *pTet-DualON* plasmid and a linear hygromycin resistance marker were picked 4 weeks after transfection and subsequently expanded with the attempt to establish a homogeneous ZsGreen1/Tet-ON Advanced-expressing HaCaT cell line. For this purpose, three picking strategies were performed.

First, ZsGreen1$^+$ colonies were scraped-off the petri dish with a glass Pasteur pipette, whose tip was transformed to a tiny "hook" (Cerbini et al. 2015). Each colony was transferred into a well of a 96-well plate containing 100 µl CTRL medium supplemented with 50 µg/ml hygromycin (see Table 24). The cells were cultured until reaching 60-70 % confluency with media exchange every 2nd to 3rd day.

In a second approach ZsGreen1$^+$ colonies were picked using trypsin for enzymatic detachment of the cells as described previously (Strukov and Belmont 2008). For this purpose, the cell culture medium was discarded, the cells were washed with PBS and the excess liquid was removed. Then, sterilized circular filter papers were dipped into TrypLE Express (Table 13) and were incubated atop on ZsGreen1$^+$ colonies for 3-5 min at 37°C. Subsequently, the filter papers were gently deducted and individually transferred into wells of a 96-well plate containing 100 µl CTRL medium supplemented with 50 µg/ml hygromycin (see Table 24). After 48 h, the filter papers were removed from the wells and the cells were further cultured until reaching 60-70 % confluency.

Third, ZsGreen1$^+$ colonies were isolated by using agarose gel. For this purpose, the cell culture medium was discarded, the cells were washed with PBS, excess liquid was removed and the plate was poured with a hand-warm agarose/medium mixture consisting of 1 part of 2 % agarose gel in a sterile water and one part CTRL medium. After gel hardening, ZsGreen1$^+$ colonies were picked using truncated pipette tips and individually transferred into wells of a 24-well plate 500 µl of CTRL medium supplemented with 50 µg/ml hygromycin (see Table 24) by up-and-down pipetting. Subsequently, the cells were cultured for 1 week.

Unfortunately, none of the applied colony picking techniques was sufficient for establishing a homogeneous ZsGreen1/Tet-ON Advanced-expressing HaCaT cell line. Instead, the colonies grown from the picked cells were still ZsGreen$^+$ or ZsGreen^{neg} (data not shown), respectively, indicating that all techniques isolated a mixture of ZsGreen$^+$ and ZsGreen^{neg} cells. Moreover, ZsGreen^{neg} cells overgrow ZsGreen$^+$ cells and thus seem to have a higher proliferative rate than the latter ones. However, these results furthermore substantiate the previously made observation that the Tet-On® Advanced Inducible Gene Expression System from Clontech generates cells harboring the *pTet-DualON* plasmid and a linear hygromycin resistance marker, as well as cells that only harbor the linear hygromycin resistance marker. This obstacle may be resolved in the future by transfecting a plasmid that combines the *Tet-ON Advanced*-encoding sequence and an antibiotic resistance cassette for clone selection.

3.3. Analyzing the function of CD4 in ddHaCaT cells

The rational for generation of *Tet-ON Advanced*-expressing ddHaCaT or HaCaT cells (see section 3.2) was to investigate the function of CD4 in these cells upon induction of *CD4*-expression in virtually every cell. However, the generation of *Tet-ON Advanced*-expressing HaCaT cells by transfecting the *pTet-DualON* plasmid together with a linear resistance marker failed (see section 3.2) and sufficient time was lacking to implement alternative strategies for establishing HaCaT cells stably expressing CD4 in an inducible manner. Therefore, in order to gain a first impression of CD4 function in keratinocytes, the cAMP levels after MHCII stimulation, the proliferation rate after MHCII and IL1-α treatment, *CD4*-expression upon IL1-α treatment and the influence of TNFα on the migration of ddHaCaT cells after transient transfection with the *pCR3.1-hCD4* vector, were investigated.

3.3.1. MHCII treatment decreases cAMP levels of CD4-expressing ddHaCaT cells

Based on the role of CD4 in MHCII-stimulated TCR/CD3^{neg} immune cells (see section 1.3.2 and Figure 4), activation of the CD4 signaling pathway was hypothesized upon MHCII ligation in basal cell-like cells (Figure 4). As a consequence, the MHCII treatment of CD4-expressing ddHaCaT cells should result in decreased cAMP levels (see Figure 4B). To evaluate this hypothesis, changes in cAMP levels over time were analyzed in CD4-expressing ddHaCaT (transient *pCR3.1-hCD4* transfected, Figure 25) cells cultured in presence of MHCII molecules in 0.03 mM $CaCl_2$-containing A1 medium.

For this purpose, *pCR3.1-hCD4* transfected cells (section 2.13.6) were seeded in 6-well plates containing A1 medium supplemented with 0.03 mM $CaCl_2$. 26 h after transfection, A1 medium supplemented with 0.03 mM $CaCl_2$ and 1 µg/ml MHCII (Table 3) was applied to the cells which were then harvested at specific time points after MHCII stimulation (30, 120, 180, 240, 300, 360, 1080 and 1440 min or 0.5, 2, 3, 4, 5, 6, 18 and 24 h, Figure 25). Finally, the cAMP levels of the cell lysates were analyzed by using the Cyclic AMP XP® Chemiluminescent Assay Kit (see section 2.13.8.). Untransfected cells and cells transfected with empty *pCR3.1* vector served as baseline controls. Untransfected ddHaCaT cells stimulated with 10 µM forskolin in A1 medium containing 0.03 mM $CaCl_2$ for 30 min served as a positive control (Mammone et al. 1998). cAMP levels in murine CD4$^+$ T cells (section 2.13.11) treated either with or without 1 µg/ml MHCII molecules for 30 min served as an assay control experiment (Baroja et al. 1999; Conche et al. 2009). The experiment was performed two times each in biological duplicates and measured in technical duplicates.

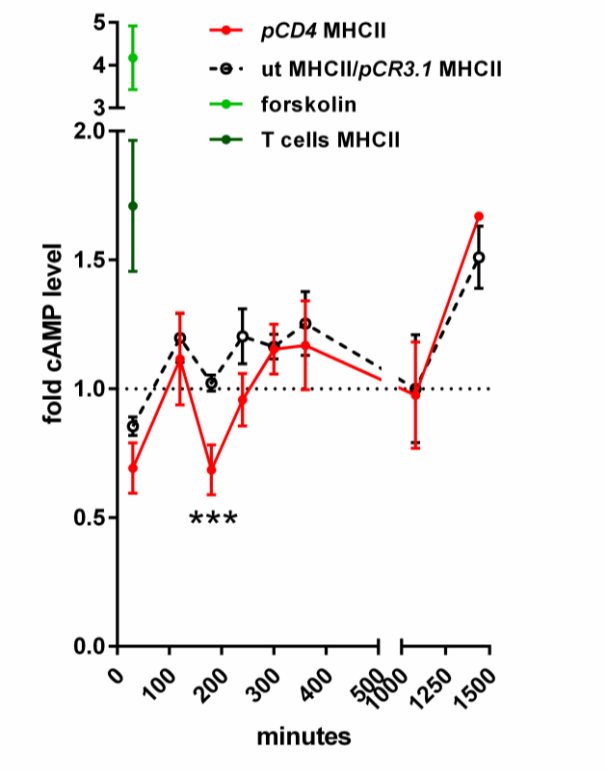

Figure 25: cAMP levels of CD4-expressing ddHaCaT cells decrease 180 minutes after MHCII stimulation. ELISA-based analyses of cAMP levels of murine splenic T cells stimulated for 30 min with 1 µg/ml MHCII (dark green), of untransfected ddHaCaT cells stimulated for 30 minutes with 10 µM forskolin (light green) or untransfected or transiently *pCR3.1* (dotted black) or *pCR3.1-hCD4* (red) transfected ddHaCaT cells stimulated with 1 µg/ml MHCII for 30, 120, 180, 240, 300, 360, 1080 and 1440 minutes. cAMP levels were normalized to respective unstimulated or vehicle-treated cells (dotted horizontal line). Represented data summarize two independent experiments each performed in biological duplicates and measured in technical duplicates shown as mean +/- SEM. Statistical analyses were performed by using unpaired t-test according to the Holm-Sidak-method. ***, $p<0.001$.

As shown in Figure 25, both, MHCII-stimulation of murine splenic T cells and forskolin-treatment of ddHaCaT cells resulted in cAMP increase compared to the respective untreated cells (1.7- or 4.1-fold, respectively). This verified that the used MHCII concentration and treatment protocol resulted in increased cAMP levels in T cell response as a response to MHCII ligation with the TCR/CD3/CD4 complex. On the other hand, it also confirmed that cAMP levels of HaCaT cells can be modulated upon treatment with small molecules, e.g. foskolin, an adenyl cyclase activator that induces increase in the cAMP levels (Mammone et al. 1998). The cAMP levels of ddHaCaT cells treated with MCHII molecules remained similar to each other and to the respective baseline cAMP levels (dotted horizontal line in Figure 25) within almost every analyzed treatment period (except after 1440 minutes) regardless of the transfected plasmid (Figure 25). However, one exception of this trend was observed upon 180 minutes MHCII-treatment, when CD4-expressing ddHaCaT cells showed significantly less cAMP levels compared to untransfected or control vector transfected ddHaCaT cell (Figure 25). This result indicates that similar to monocytes (see

Figure 4, (Zhen et al. 2014)) also in basal-like keratinocytes MHCII/CD4-ligation leads to reduced cAMP levels.

3.3.2. MHCII treatment decreases the proliferation rate of CD4-expressing ddHaCaT cells

The decreased cAMP levels in MHCII-stimulated CD4-expressing ddHaCaT cells suggested a role of MHCII/CD4-ligation in basal-like keratinocytes comparable to monocytes. To study whether CD4 activation via MHCII molecules might furthermore impact the proliferation rate in keratinocytes we next employed BrdU-incorporation assays. First it was investigated whether MHCII molecules influence the general proliferative behavior of ($CD4^{neg}$) ddHaCaT and HaCaT cells. In particular, ddHaCaT cultured in A1 medium containing 0.03 mM $CaCl_2$ (passage 19) and HaCaT cells cultured in CTRL medium (passage 17) were treated with 1 µg/ml MHCII for 6, 10, 12 and 24 h. Untreated cells served as baseline controls. As shown in Figure 26A, the proliferation of the keratinocyte cell lines was almost not influenced by MHCII treatment with exception of HaCaT cells treated for 10 h whose proliferation rate dropped significantly below the control baseline (Figure 26A right panel). Next, the effect of MHCII on the proliferative behavior of CD4-expressing ddHaCaT cells was assessed. For this purpose, ddHaCaT cells were transfected with the *pCR3.1-hCD4* plasmid (for details about the transfection method and created *pCR3.1-hCD4* vector see sections 2.14.3 and 2.13.6) and cultured in A1 medium containing 0.03 mM $CaCl_2$ for 26 h. The cells were then treated with 1 µg/ml MHCII molecules for 24 or 48 h with a BrdU pulse for the last 22 h of the respective end point analysis. Untreated ddHaCaT cells, that were either only electro-pulsed, transfected with *pCR3.1* empty vector or the *pCR3.1-hCD4* plasmid served as controls. Figure 26B shows that in contrast to the previous experiment, the MHCII-treatment this time significantly increased the general proliferation rate of ddHaCaT cells irrespectively of the transfection status of the cells (electro-pulsed, *pCR3.1* or *pCR3.1-hCD4* transfected ddHaCaT). However, the proliferation rate of CD4-expressing ddHaCaT cells significantly decreased upon 48 h MHCII-treatment in comparison to control vector transfected MHCII-treated ddHaCaT cells (Figure 26B). These data suggest that MHCII/CD4-ligation result in decreased proliferation of basal cell-like keratinocytes.

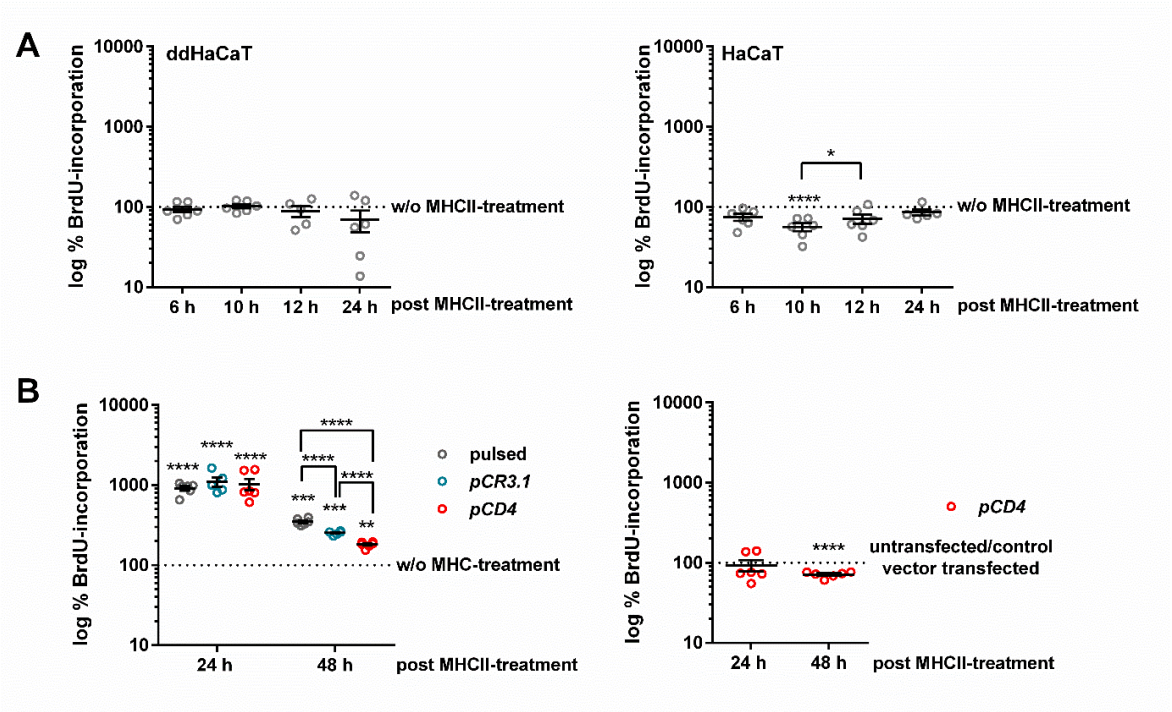

Figure 26: MHCII-treatment decreases the proliferation rate of CD4-expressing ddHaCaT cells. (A, B) BrdU-incorporation assay-based analyses of the proliferation rate **(A)** of ddHaCaT (left) and HaCaT cells (right) after 6,10,12 and 24 h MHCII-treatment and **(B)** of electro-pulsed (grey circles, pulsed), *pCR3.1* (blue circles) and *pCR3.1-hCD4*-transfected ddHaCaT (red circles, *pCD4*) 24 and 48 h after MHCII-treatment. Values of untransfected (A), electro-pulsed, *pCR3.1* and *pCR3.1-hCD4*-transfected ddHaCaT without MHCII-treatment (B, left) or electro-pulsed and *pCR3.1*-transfected ddHaCaT cells with MHCII-treatment (B, right), respectively, were set to one (dotted horizontal lines). Represented data summarize one experiment performed in biological hexaplicates shown as mean +/- SEM. Statistical analyses were performed by using unpaired t-test according to the Holm-Sidak-method. **, $p<0.01$; ***, $p<0.001$; ****, $p<0.0001$.

3.3.3. The influence of IL-1α and TNFα on basal cell-like keratinocytes *in vitro*

The mobilization of resident stem/progenitor cells and the promotion of epidermal cell proliferation and differentiation during telogen-to-anagen transition (Lee P et al. 2017; Wang X et al. 2017), epidermal wound healing (Larouche et al. 2018) and formation of psoriatic plaques and acanthosis of the skin (Albanesi et al. 2018; Benhadou et al. 2019; Bocheńska et al. 2017; Rendon and Schäkel 2019) are regulated by the proinflammatory cytokines IL-1α and TNFα. Besides, IL-1α also induces the expression of CD4 in microglia (Yu et al. 1998). Thus, it is likely that IL-1α and/or TNFα are involved in proliferation, *CD4*-expression or migration of basal cell-like keratinocytes. To investigate these hypotheses, we next analyzed the proliferative rate and the *CD4*-expression level of IL-1α-treated ddHaCaT cells (see section 3.3.3.1) and the migration of CD4-expressing ddHaCaT cells in the presence of TNFα (see section 3.3.3.2).

3.3.3.1. IL-1α does not impact the proliferation rate but decreases the *CD4*-expression of ddHaCaT cells

IL-1α has been shown to induce the proliferation of keratinocyte stem cells (Larouche et al. 2018; Lee P et al. 2017; Wang X et al. 2017) and also the *CD4*-expression in microglia (Yu et al. 1998). To investigate whether IL-1α also influences the proliferation rate and *CD4*-expression in basal cell-like ddHaCaT cells, BrdU-incorporation assays and *CD4*-expression analyses of ddHaCaT cells after IL-1α-treatment were conducted. For this purpose, ddHaCaT cells cultured in A1 medium supplemented with 0.03 mM $CaCl_2$ (passage 19) and HaCaT cells cultured in CTRL medium (passage 17) were treated with 1 ng/ml IL-1α (dissolved in 1xPBS containing 1 % BSA). After 6, 10, 12 and 24 h, as well as 6 and 24 h, the proliferation rate and the *CD4*-exression were assessed, respectively. Untreated cells were used as controls.

As shown in Figure 27, the IL-1α treatment did not impact the proliferation rate of ddHaCaT or HaCaT cells over a time period of 24 h. Moreover, albeit IL-1α-treatment significantly increases the expression of S100A7 (Yano et al. 2008) it did not increase the expression of *CD4* mRNA. Instead, IL-1α-treatment decreased *CD4*-expression (Figure 28). Together these data rebut the hypothesis, that IL-1α induces the proliferation and *CD4*-expression of basal cell-like keratinocytes (e.g. ddHaCaT cells) *in vitro*.

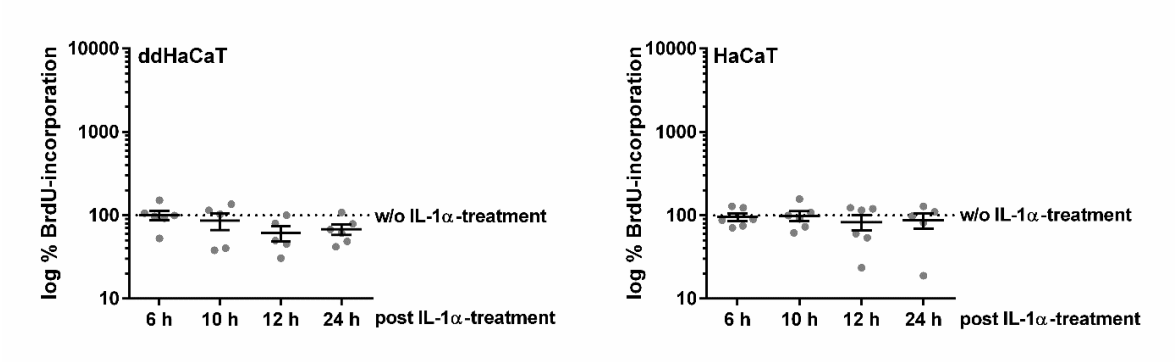

Figure 27: IL-1α-treatment does not impact the proliferation rate of ddHaCaT and HaCaT cells. BrdU-incorporation assay-based analyses of the proliferation rate of ddHaCaT (left) and HaCaT cells (right) after 6, 10, 12 and 24 h IL-1α-treatment. Values of untreated ddHaCaT or HaCaT cells, respectively, were set to one (dotted horizontal lines). Represented data summarize one experiment performed in biological hexaplicates shown as mean +/- SEM. Statistical analyses were performed by using unpaired t-test according to the Holm-Sidak-method.

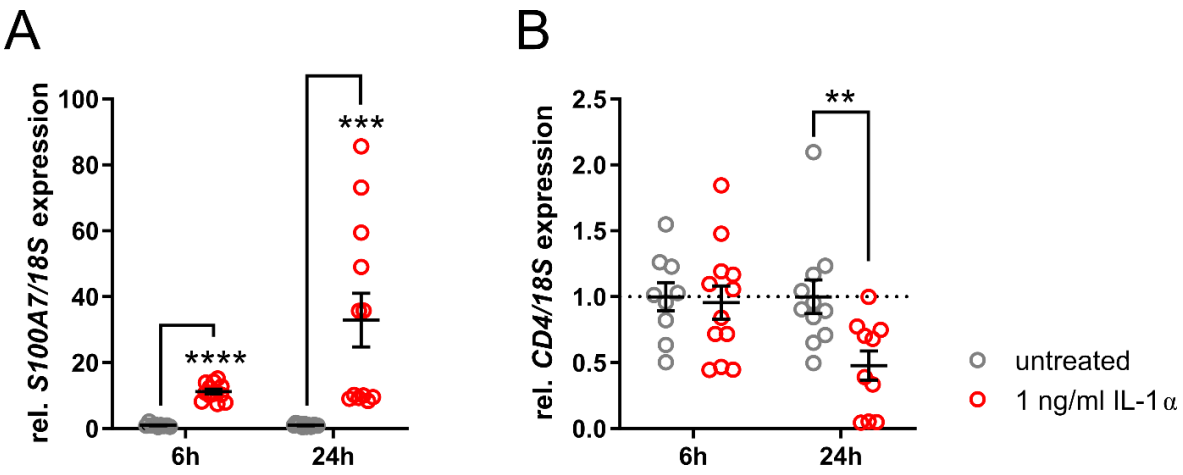

Figure 28: IL-1α reduces *CD4*-expression in ddHaCaT cells. qRT-PCR-based *S100A7* and *CD4*-expression analyses of ddHaCaT after 6 and 24 h IL-1α-treatment. Gene expression values were normalized to *18S* rRNA expression levels. Values of untreated ddHaCaT cells were set to one (dotted horizontal lines). Represented data summarize two independent experiments performed in biological duplicates and measured in technical triplicates shown as mean +/- SEM. Statistical analyses were performed by using unpaired t-test according to the Holm-Sidak-method. **, $p<0.01$; ***, $p<0.001$; ****, $p<0.0001$.

3.3.3.2. TNFα influences the cellular migration of CD4-expressing ddHaCaT cells

Due to the known role TNFα plays in the migration of epidermal stem/progenitor cells (Albanesi et al. 2018; Benhadou et al. 2019; Bocheńska et al. 2017; Larouche et al. 2018; Rendon and Schäkel 2019; Wang X et al. 2017), we hypothesized that this proinflammatory cytokine may influence the migration of CD4-expressing basal cell-like keratinocytes *in vitro*. To investigate this issue, the migration of single CD4-expressing ddHaCaT cells was tracked using 2D chemotaxis *µ-slide* (Ibidi GmbH, Germany) as described in chapter 2.13.10.

First, the co-transfection of ddHaCaT cells with *pCR3.1-hCD4* and *pEGFP-N1* plasmid by electroporation was established to enable the tracking of $CD4^+$ $EGFP^+$ cells. For this purpose, ddHaCaT cells (passage 36) cultured in A1 medium supplemented with 0.03 mM $CaCl_2$ were co-transfected with 1 µg *pCR3.1-hCD4* and either 400 ng or 500 ng *pEGFP-N1*. Then the cells were seeded on coverslips in 6-well plates containing A1 medium supplemented with 0.03 mM $CaCl_2$. 26 h after seeding the cells were fixed, stained with antibodies against CD4 and the number of EGFP-/CD4-co-expressing cell was determined.

This approach revealed that co-transfection of 1 µg *pCR3.1-hCD4* with 400 ng *pEGFP-N1* yielded only an efficiency of 50% CD4/EGFP-co-expression (Figure 29, left panel), whereas using 1 µg *pCR3.1-hCD4* and 500 ng *pEGFP-N1* resulted in 70 % CD4/EGFP-co-expression (Figure 29, right). Since these results showed that $EGFP^+$ ddHaCaT cells co-transfected with 1 µg *pCR3.1-hCD4* and 500 ng *pEGFP-N1* also express CD4 with a probability of 70%, the following chemotaxis experiments were performed using ddHaCaT cells co-transfected with these conditions to efficiently track $EGFP^+$ and thus primarily $CD4^+$ cells.

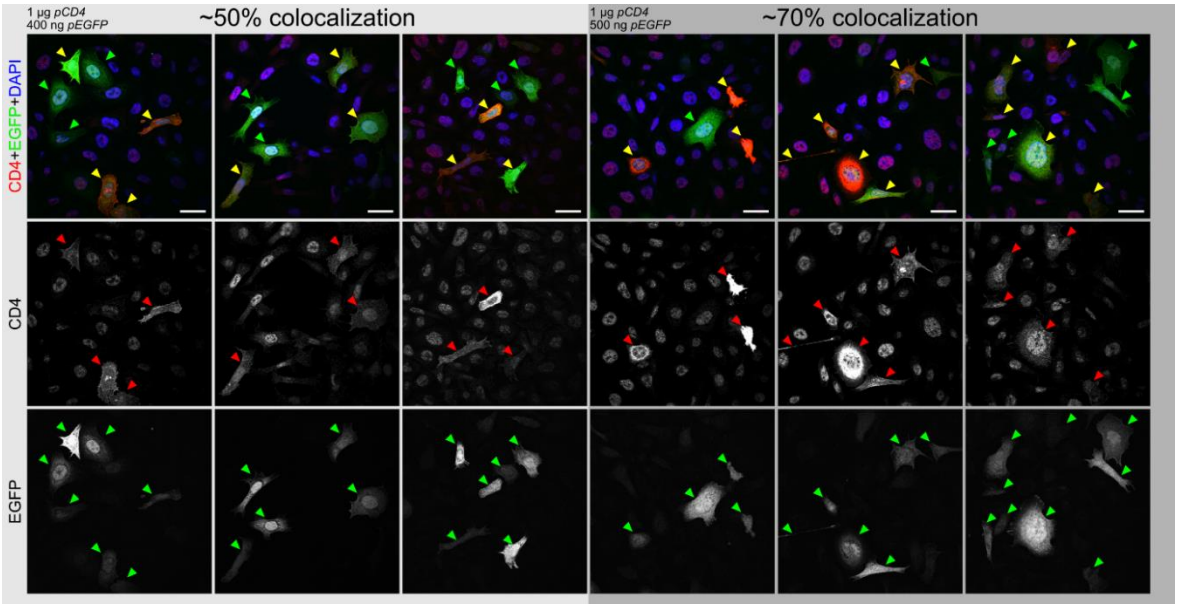

Figure 29: Co-transfection of ddHaCaT cells with *pCR3.1-hCD4* and *pEGFP-N1*. Immuno- fluorescence analyses of ddHaCaT cells 26 h after electroporation-based co-transfection of 1 µg *pCR3.1-hCD4* and either 400 ng (left) or 500 ng *pEGFP-N1* (right) and following anti-CD4 antibody staining (red). Co-expressing $CD4^+$ $EGFP^+$ cells are marked with yellow arrow heads, single CD4-expressing or EGFP-expressing cells are indicated with red or green arrow heads, respectively. For details regarding the immunocytochemistry refer to section 2.16.1 and Table 8 for details regarding the antibodies used. Scale bars: 30 µm.

Next, it was assessed whether *pCR3.1-hCD4*-transfected ddHaCaT cells overexpress CD4 during the entire period of the chemotaxis experiment. For this purpose, *pCR3.1-hCD4*-transfected ddHaCaT cells (passage 34) were seeded on coverslips in 6-well plates containing A1 medium supplemented with 0.03 mM $CaCl_2$. 26, 32 and 56 h after seeding, the cells were fixed and stained with antibodies against CD4 (Figure 30A shows the typical *CD4*-expression pattern of a ddHaCaT cell) and the basal cell marker CD29. The analyzed end points correspond to the initial *CD4*-expression 26 h post transfection and to the analysis times of the chemotaxis experiments at 6 h (32 h post transfection) and 30 h (56 h post transfection) post seeding in the chemotaxis *µ-slide* (summarized in Figure 30B). As shown in Figure 30C, *pCR3.1-hCD4*-transfected ddHaCaT cells overexpress *CD4* at all analyzed time points. Thus, the chemotaxis experiments were performed next by subsequent automated tracking of $EGFP^+$ *pCR3.1-hCD4/pEGFP-N1*-co-transfected ddHaCaT cells (see experimental setup in Figure 30B).

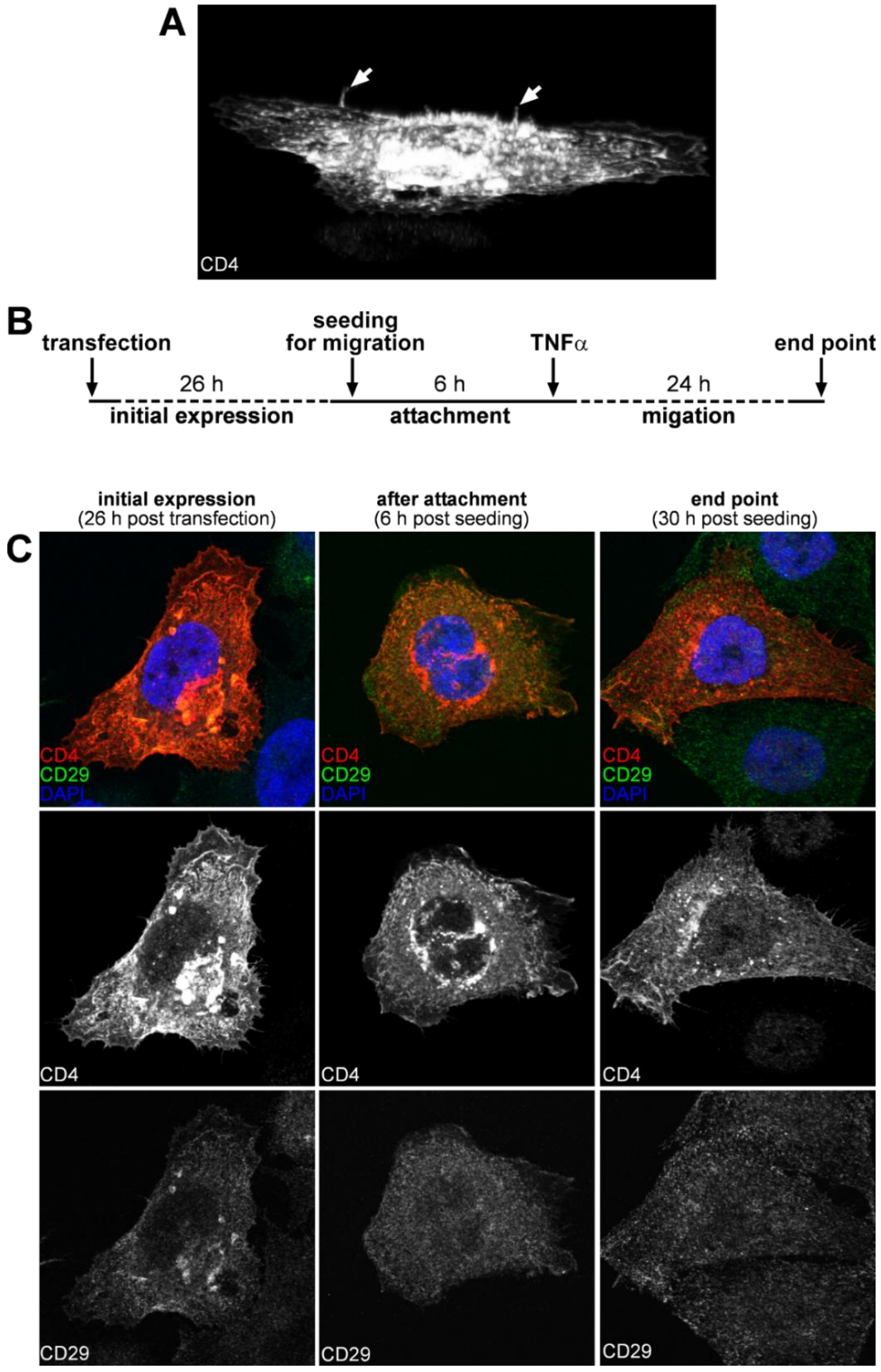

Figure 30: Immunofluorescence analysis of *CD4*-expression in *pCR3.1-hCD4*-transfected ddHaCaT cells within the time schedule of the migration experiment. Shown in **(A)** is an anti-CD4 antibody-stained *pCR3.1-hCD4*-transfected ddHaCaT cell. The experimental setup for analyzing *CD4*-expression in ddHaCaT cells after *pCR3.1-hCD4*-transfection and of the following migration experiment is shown in **B**. Representative examples of immunofluorescent anti-CD4/anti-CD29 antibody stainings of ddHaCaT cells 26, 32 and 56 h post *pCR3.1-hCD4*-transfection are shown in **C**. White arrows in (A) mark morphological features of cellular *CD4*-expression pattern. For details regarding the immunocytochemistry refer to section 2.16.1 and for details regarding the used antibodies see Table 8. Scale bars: 3,3 µm.

For this purpose, first the mitotic activity of ddHaCaT cells was blocked with mitomycin C treatment (2.13.9) to avoid excess proliferation during the migration experiment. Then the cells were co-transfected with *pCR3.1-h*CD4 and *pEGFP-N1* and seeded in 6-well plates as described above. After 26 h, the cells were detached (see section 2.13.7), seeded in chemotaxis *µ-slide* chambers in A1 medium containing 0.03 mM $CaCl_2$ and incubated for an additional 6 h to allow them to attach to the slide. Thereafter, the medium of the cells was refreshed by exchanging it with experimental medium (DMEM --- supplemented with 200 mM L-glutamine, 100 mM sodium pyruvate, 1 % P/S, 10mM HEPES buffer, 0.03 mM $CaCl_2$) and the chemoattractant was added in one reservoir to establish the stable chemotactic gradient (see Figure 31). Afterwards, the migration of $EGFP^+$ cells was acquired over a period of 24 h and then quantified via automated tracking (see section 2.13.10). As negative and positive controls, the migration was quantified in ddHaCaT cells co-transfected with *pCR3.1-h*CD4 and *pEGFP-N1* cultured in experimental medium either without chemoattractant or by adding 20% FCS to one reservoir of a *µ-slide*, respectively (Figure 31A). FCS is known to efficiently induce migration of different cell types due to its composition of enzymes, hormones and growth factors (Bagati et al. 2015; Brennan et al. 2008). To establish whether CD4-expressing ddHaCaT cells migrate towards a TNFα gradient, as it is described for keratinocytes *in vivo* (Albanesi et al. 2018; Benhadou et al. 2019; Bocheńska et al. 2017; Larouche et al. 2018; Rendon and Schäkel 2019; Wang X et al. 2017), both reservoirs of a *µ-slide* were filled with experimental medium with or without 2 % FCS, respectively (Figure 31A), and 50 ng/ml TNFα were added into one reservoir as a chemoattractant (Figure 31A). Since all *µ-slides* were only filled in one reservoir with a chemoattractant gradient (positive control or TNFα, Figure 31A) the second reservoir without chemoattractant served as an internal negative control. After applying the chemoattractant, automated, multi-position time lapse imaging of the slides was conducted using a Nikon Eclipse Ti2 inverted microscope equipped with an Okolab incubation chamber (37°C, 5 % CO2, humidified atmosphere) for 24 h with a 10 min time-lapse interval. Cell movement was analyzed with a workflow based on the FIJI (Schindelin et al. 2012), TrackMate (Tinevez et al. 2017) and the Chemotaxis and Migration Tool (Ibidi GmbH) software packages. All experiments were performed in biological triplicates.

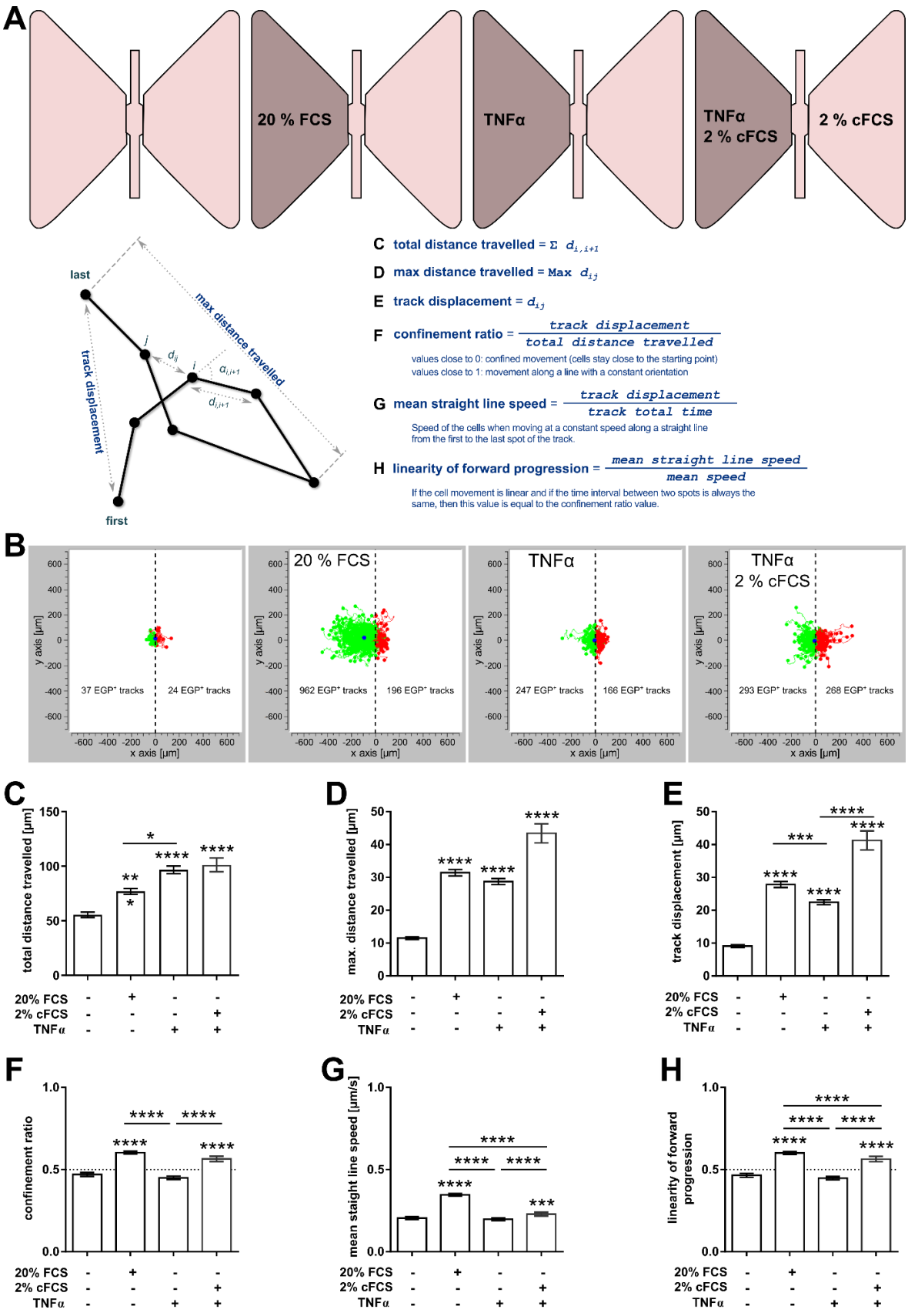

Figure 31: CD4-expressing ddHaCaT cells migrate towards a TNFα gradient. Schematic representation of the experimental setup of the *µ-slide* migration analysis of CD4-expressing ddHaCaT cells (top) and of the analyzed single cell-tracking parameters (bottom). **Top:** Each of the 4 graphs represent one *µ-slide* filled either with experimental me-

dium only in both reservoirs (left) or with experimental medium containing 20 % FCS (middle-left), TNFα (middle-right) in experimental medium without cFCS or TNFα in experimental medium with 2 % cFCS (right) in the left reservoir and experimental medium without chemoattractant in the right reservoirs. **Bottom:** Graphical scheme showcasing the tracked features of each cell and the respective parameters describing its movement behavior (left), as well as the description and associated formulas for determining the respective parameters analyzed (right). **(B)** Visualization of the automated tracking (similar arrangement as shown in top row of (A)), total distance traveled **(C)**, maximal distance traveled **(D)**, track displacement **(E)**, confinement ratio **(F)**, mean straight line speed **(G)** and linearity of forward progression **(H)** of single cell-tracked EGFP$^+$ *pCR3.1-hCD4/pEGFP-N1*-co-transfected ddHaCaT cells in presence of 50 ng/ml TNFα or 50 ng/ml TNFα in experimental medium with 2 % cFCS, respectively. Experimental medium with 2 % cFCS without chemoattractant served as negative control, 20 % FCS gradient served as positive control. Cell movement was analyzed with a workflow based on the FIJI (Schindelin et al. 2012), TrackMate (Tinevez et al. 2017) and the Chemotaxis and Migration Tool (Ibidi GmbH) software packages. All experiments were performed in biological triplicates. Statistical analyses was performed using a non-parametric 1way ANOVA (Kruskal-Wallis test). *, p<0.05; *** p<0.001; ****, p<0.0001.

Figure 31A-H summarizes the results of the chemotaxis of single cell-tracked EGFP$^+$ *pCR3.1-hCD4/pEGFP-N1*-co-transfected ddHaCaT cells in presence of 50 ng/ml TNFα or 50 ng/ml TNFα in experimental medium with 2 % cFCS, respectively, in comparison to the positive (20 % FCS gradient) and the negative (no chemoattractant) controls. For this purpose, the distances travelled by the cells throughout the recording time were investigated by computing the total distance travelled (Figure 31C), the maximum distance travelled (Figure 31D), as well as the track displacement which measures the distance between the first and the last tracked position (Figure 31E). The analysis of these parameters showed that EGFP$^+$ *pCR3.1-hCD4/pEGFP-N1*-co-transfected ddHaCaT cells significantly move to the applied gradients (Figure 31C – E). In particular, all three distance measurements were significantly higher when 20% FCS, TNFα or TNFα in experimental medium containing 2 % cFCS was applied to one reservoir in comparison to the negative control (Figure 31C – E). In addition, the total distance travelled by TNFα-treated cells was even significantly higher than those of 20 % FCS-treated cells (Figure 31C). However, the track displacement, which measures the absolute distance travelled towards the gradient, was significantly lower in TNFα-treated cells compared to 20 % FCS- and to TNFα-treated cells cultured in 2 % cFCS containing experimental medium (Figure 31E). Further analysis demonstrated that only 20 % FCS- and TNFα-treated cells cultured in 2 % cFCS containing experimental medium, but not TNFα-treated cells, showed significantly higher confinement ratio values compared to the negative control (Figure 31F). Since this parameter is an indicator for the “efficiency” of the cell movement away from its starting point these data suggest that only cells treated with 20 % FCS and TNFα in experimental medium containing 2 % cFCS move toward the gradients with a constant orientation. Finally, the mean straight line speed and the linearity of forward progression were analyzed (Figure 31G, H). The first mentioned value represents the mean speed of a cell that moves at a constant speed along a straight line from the first to the last spot of the track (Figure 31A).

The linearity of forward progression is calculated as the ratio of the mean straight line speed and the track mean speed. Thus, if the track is linear and if the time interval between two spots is always the same, its value is equal to the confinement ratio value (Figure 31A). As shown in Figure 31G the mean straight line speed was significantly higher in $EGFP^+$ cells moving towards the 20 % FCS- and the TNFα-gradient in 2 % cFCS containing experimental medium, whereas the TNFα-gradient in experimental medium without cFCS did not induce significant changes in mean straight line speed compared to the negative control. Moreover, the results of the linearity of forward progression analyses were similar to the confinement ratio values, showing that the $EGFP^+$ ddHaCaT cells moved in a linear track towards the gradient of 20 % FCS (positive control) and TNFα in experimental medium with 2 % cFCS, but not in the TNFα-only gradient (Figure 31H).
Altogether, these data demonstrate that $EGFP^+$ and thus to large parts (app. 70 %, see Figure 29) CD4-expressing ddHaCaT cells move straight forward toward the 20 % FCS gradient. In a similar fashion, the cells cultured in experimental medium containing 2 % cFCS also travelled to the TNFα gradient, but due to the very high track displacement values (Figure 31E) in a more circuitous route. In contrast, the TNFα-gradient induced a high cellular motility comparable to that of the positive control (Figure 31C, D) but without a comparable constant orientation (Figure 31F) or a comparable constant straight line speed (Figure 31G, H). This shows that although the cells move significantly more when a TNFα-gradient is added, this movement is not as straight as the movement of cells to the positive control or to the TNFα in experimental medium with 2 % cFCS.

4. Discussion

4.1. Generation of dedifferentiated, stable keratinocyte cell lines

Several protocols for the isolation and cultivation of human primary keratinocytes have been established in the past (Ścieżyńska et al. 2019). However, it is well-known that human primary keratinocytes have a limited lifespan and low division rates under *in vitro* culture conditions (Gragnani et al. 2007). Interestingly, the same protocol for isolation of primary human keratinocytes has been found to result in successful (McHeik et al. 2010) or failed experiments (Orazizadeh et al. 2015). In addition, the isolation and growth conditions for primary isolated human keratinocyte stem cells are very complex requiring special feeder layers, as well as a large number of supplementary growth factors, such as hydrocortisone, human epidermal growth factor, bovine pituitary extract and others (Papini et al. 2003). Another limitation is that the induction of differentiation in primary keratinocytes leads to their terminal differentiation and rapid cell death, leaving only several days to perform experiments (Johansen 2017; Pincelli and Marconi 2010). Because of these special requirements and limitations for culture of primary, isolated human keratinocytes, we chose stable keratinocyte cell lines to establish basal cell-like cells with a relatively easy access to high cell numbers along with simple culture requirements. The human HaCaT (Ha = human, Ca = calcium, T = temperature – origin and initial culture conditions) cells represent a spontaneously immortalized keratinocyte cell line, which was developed through long-term culture of normal, adult skin keratinocytes. In contrast to primary human keratinocytes, HaCaT cells can be grown in conventional media and maintained in culture for long time periods (> 140 passages) (Boukamp et al. 1988). Moreover, even though it is known that these cells possess mutations in both alleles of the p53 gene (Lehman et al. 1993) typical for UV-radiation-induced mutations (Brash et al. 1991), HaCaT cells, in contrast to virally transformed keratinocytes, maintain a constant balance of the genetic material and are non-tumorigenic (Boukamp et al. 1997). The cell line was initially established in a modified, minimum essential growth medium containing 15 % heat-inactivated FCS and other supplements such as antibiotics, vitamins and amino acids (Boukamp et al. 1988). Using these culture conditions, HaCaT cells proliferate (Boukamp et al. 1988) and have a highly conserved differentiation capacity, leading to epidermal organization (Schoop et al. 1999). Moreover, they can form an epidermis when transplanted into athymic (nude) mice (Breitkreutz et al. 1998). All these features and the large body of HaCaT-related literature make this cell line a good experimental model to study human keratinocyte cell differentiation and dedifferentiation. Parallel to HaCaT, the murine, immortalized non-tumorigenic keratinocyte C5N cell line was used in this work as well. The C5N cells have been shown to grow with wild type keratinocyte, epithelial morphology, with a cuboidal shape and a cobblestone growth pattern, do not harbor any mutations in the *H-ras* gene or *p53* and express keratins (Zoumpourlis et al. 2003).

In vivo, basal keratinocytes of the skin are subjected to low [Ca^{2+}] concentrations in contrast to differentiated keratinocytes in the upper layers of the epidermis, which are maintained by a vertical gradient of increasing [Ca^{2+}] concentrations (Menon

and Eliam 1985). *In vitro*, changes from low to high [Ca^{2+}] concentration cause terminal differentiation of the basal cell-like keratinocytes (Hennings H. et al. 1980). However, HaCaT, as well as C5N cells (as shown in this work) can revert from differentiated to a basal cell-like shape upon lowering the growth media [Ca^{2+}] concentration down to 0.03 mM (Wilson 2013). Because of these characteristics, HaCaT cells are most often used as an *in vitro* model for studying differentiation processes, as well as for analyzing keratinocyte function. However, the conditions for differentiation and dedifferentiation of the keratinocytes in culture in terms of [Ca^{2+}] concentrations and other nourishing substances vary in the literature (Hennings H. et al. 1980; Micallef et al. 2009; Wilson 2013). To address this paradigm systematically, different [Ca^{2+}] concentrations were used to generate ddHaCaT and ddC5N cells. We adopted a protocol from Deyrieux and Wilson (2007) and Deyrieux et al. (2007), according to which we maintained HaCaT and C5N cells for a period of three weeks in defined [Ca^{2+}] level-containing media. The cells were passaged at 60-70 % confluence, as it is known that they respond to higher cell density environment (Wilson 2013) which can act as a differentiation stimulus (Colombo et al. 2017). Deyrieux and Wilson (2007) reported that 3 weeks after switching HaCaT cells from conventional medium (CTRL) to low [Ca^{2+}] level medium (0.03 mM $CaCl_2$), the cell shape and morphology changed to that of basal keratinocytes. The same observations were made in our experiments, wherein HaCaT cells changed their morphology to a more basal cell-like morphology when cultured in media with low [Ca^{2+}] concentration (Figure 10). In particular, cells cultured under low [Ca^{2+}] conditions were spindle shaped and loosely packed, while cells cultured in CTRL medium exhibited a more cuboidal shape and were more tightly arranged. The same findings were observed for C5N cells (Figure 11). As resembled by the number of plates and passage number after finishing the experiment C5N and HaCaT cells did not proliferate and grow well in the A2 medium containing 2 % cFCS. Due to this observation experiments based on the A2 media were discontinued and further analyses were conducted by culturing the cells in A1 medium containing 10 % cFCS.

As explained in the introduction section, different epidermal layers express different keratins in a differentiation-dependent manner (see Figure 2). Thus, in addition to the morphological changes of ddHaCaT and ddC5N cells, we furthermore analyzed the dedifferentiation process by immunocytochemical stainings visualizing the keratin expression pattern. In particular, in the skin, proliferative active cells of the basal cell layer express high levels of K5 and K14, whereas the expression of these keratins is down-regulated during the differentiation process in suprabasal layers (Fuchs and Green 1980; Moll et al. 1982). Our immunofluorescence analyses verified the findings that ddHaCaT cells express higher levels of the basal cell marker K5 compared to HaCaT cells. Beyond that, these analyses also demonstrated that the cultured ddHaCaT cells show a low expression of K10, which is typically expressed in keratinocytes of the spinous cell layer. Analysis of the Ki67 expression profile (Figure 12D) furthermore revealed that low [Ca^{2+}] levels in the culture medium had no effect on the proliferative activity of the ddHaCaT cells although the

expression of this proliferation marker protein is regulated within differentiation processes in the skin (Ando et al. 1990; Heenen et al. 1998). However, primary human keratinocytes and HaCaT cells have been shown to oppositely react to culture in low [Ca^{2+}] level media (Micallef et al. 2009; Walker et al. 2006). In particular, primary keratinocytes proliferate more when cultured in media with low [Ca^{2+}] concentrations (0.09 mM $CaCl_2$) than with high [Ca^{2+}] concentrations (1.2 mM $CaCl_2$), whereas HaCaT cells proliferate less when cultured in media containing low [Ca^{2+}] concentrations compared to high [Ca^{2+}]-containing medium (Micallef et al. 2009). Walker *et al.* (2006) reported the same findings for primary keratinocytes and HaCaT cells cultured in media with low [Ca^{2+}] concentrations (0.09 mM $CaCl_2$) and high [Ca^{2+}] concentrations (2 mM $CaCl_2$). Similar results were also obtained by our BrdU-incorporation analyses (see below) which more precisely measure the proliferative activity of cells than immunofluorescence anti-p63 or anti-Ki67 antibody staining that rather reflect the general proliferative activity than the real quantification of proliferative active cells. Similar to HaCaT cells, our results showed that also the culture of C5N cells in low [Ca^{2+}]-containing medium increase the expression of the basal cell marker K5 (Figure 13).

In addition and in line with previous studies by Micallef *et al.* (2009), Walker *et al.* (2006) and Deyrieux and Wilson (2007), ddHaCaT cell differentiation was confirmed by immunofluorescence staining, which showed a reduction in basal cell marker K5 expression in cells cultured in high [Ca^{2+}] concentration (2.8 mM $CaCl_2$). Further qRT-PCR analyses validated the finding that ddHaCaT and ddC5N cells represent a more basal cell-like phenotype than the control cells and that they differentiate upon culture in high [Ca^{2+}] level medium. Unexpectedly, the mRNA *K5* expression level was significantly lower in ddHaCaT cells compared to HaCaT CTRL cells. In the skin K5 is expressed in mitotically active basal layer cells and its expression is downregulated with the onset of the differentiation process (see section 1.2.2). Alam *et al.* (2011) suggested that K5 plays a role in supporting the cell proliferation potential in the basal cell layer of stratified epithelia. Thus, hypothetically HaCaT cells grown in CTRL medium express high K5 levels in order to keep their proliferation potential and to maintain their long life which has been shown to last for up to 300 passages (Schürer et al. 1993). Moreover, high K5 expression level may also be associated with a generally lower passage number of HaCaT cells than ddHaCaT cells, since the latter were established by passaging for 12 to 15 times of the original HaCaT cells in A1 medium.

The culture of ddHaCaT cells in high [Ca^{2+}] level medium significantly reduced the *K5* and *K15* expression, while their *K1*, *K10* and *Involucrin* expression levels significantly increased. Similarly, ddC5N cells express significantly decreased *K5* and significantly increased *Involucrin* levels when cultured in high [Ca^{2+}]-containing medium compared to the cells maintained in CTRL or low [Ca^{2+}]-containing medium, respectively. A further validation of the results that the culture of HaCaT cells in low [Ca^{2+}] level medium induces cellular dedifferentiation and a subsequent switch to high [Ca^{2+}]-containing medium results in differentiation process was conducted by a microscopy-based quantification of the K5 and K10 protein expression.

As stated above, Micallef *et al.* (2009) and Walker et al. (2006) showed that the proliferative activity of HaCaT cells is correlated to the [Ca^{2+}] concentrations of the culture medium. Thus, the proliferation of HaCaT cells increases when cultured in media containing high [Ca^{2+}] levels compared to low [Ca^{2+}]-containing medium (Micallef et al. 2009; Walker et al. 2006). This is in contrast to primary human keratinocytes which proliferate more when cultured in medium with low [Ca^{2+}] levels, whereas exposure to high [Ca^{2+}] concentrations causes increased differentiation and reduced proliferation of these cells (Huang et al. 2006; Matsui et al. 1992). Moreover, physiological [Ca^{2+}] levels (1 to 1.5 mM) causes an increase of intracellular [Ca^{2+}] concentrations in primary human keratinocytes that result in phosphorylation and nuclear translocation of S100C/A11 and finally in a reduced cellular proliferation (Sakaguchi et al. 2003). Contrary to this, for the induction of a reduced proliferation rate in HaCaT cells, extracellular [Ca^{2+}] concentration of 5 to 10 mM are required (Sakaguchi et al. 2003). Thus, it was hypothesized that during their spontaneous transformation and immortalization, HaCaT cells changed their response to extracellular [Ca^{2+}] levels and thus developed an insensitivity to [Ca^{2+}]-induced inhibition of proliferation (Sakaguchi et al. 2003). Unfortunately, for C5N cells similar information is not available due to very limited data sets. Thus, the data presented in this thesis are the first results ever reported in this regard and can only be discussed in reference to available data for the human HaCaT cell line. However, since our immunohistological anti-p63 and anti-Ki67 analyses were not sufficient to verify these findings, also the proliferative activity of ddHaCaT and ddC5N cultured in low and high [Ca^{2+}]-containing media in comparison to HaCaT and C5N cells was analyzed via BrdU-incorporation assays. Remarkably, this approach showed that the culture of ddHaCaT and ddC5N cells in high [Ca^{2+}]-containing medium reduced the proliferative activity compared to the maintenance of the cells in low [Ca^{2+}]-containing medium. These data do not recapitulate the findings of Micallef *et al*. (2009) and Walker *et al.* (2006). However, this discrepancy may be due to the fact that ddHaCaT and ddC5N cells were cultured in medium containing 2.8 mM $CaCl_2$ in our experiment, compared to 1.2 mM $CaCl_2$ in the study from Micallef *et al*. (2009) or 2 mM $CaCl_2$ in the study from Walker *et al.* (2006). Moreover, and in contrast to study of Micallef *et al.* (2009) and Walker *et al.* (2006), we analyzed the proliferation rate of short term-cultured cells (e.g. 70 and 94 h), whereas Micallef *et al.* (2009) monitored the proliferative activity of cells cultured for 13 days and Walker *et al.* (2006) of cells cultured for 12 days.

However, our data demonstrate that the newly established ddHaCaT cell line proliferates and grows stably in low [Ca^{2+}]-containing medium, possesses a basal cell-like phenotype and differentiates upon short-term culture in high [Ca^{2+}]-containing medium. Beyond that, also a murine counterpart to ddHaCaT cells was established, which however was discarded after finishing the experiments. Nevertheless, ddHaCaT cells may be an advantageous tool for basic research concerning keratinocyte differentiation and proliferation, which are crucial for epidermal barrier maintenance (Wikramanayake et al. 2014) and whose disturbance can lead to var-

ious skin pathologies. For example, psoriasis, as a chronic inflammatory skin disease with a presumed hereditary condition (O'Rielly and Rahman 2015) is characterized by keratinocyte hyperproliferation. It also involves a complex immune system activation cascade and infiltration by immune cells into the dermis and epidermis (Armstrong and Read 2020; Ogawa et al. 2018). Keratinocytes have been verified as psoriasis triggers and executors that control the development of that disease (Benhadou et al. 2019; Ni and Lai 2020). Furthermore, interaction and interplay of the keratinocytes and the immune system are crucial for psoriasis. Thereby, the immune system involvement is very complex (Lee MR and Cooper 2006; Nickoloff et al. 2007) and involves interactions of the innate and adaptive immunity (Schön 2019).

The balance between the proliferation and differentiation of epidermal keratinocytes is significantly controlled by the Wnt signaling pathway and is thus important in during development, normal homeostasis and disease of the skin (Reya and Clevers 2005; Teo and Kahn 2010). In fact, several studies demonstrated that altered Wnt signaling in psoriatic skin with a substantially role of Wnt5a (Dou et al. 2017; Gudjonsson et al. 2010; Reischl et al. 2007). Moreover, Wnt5a/β-catenin signaling induces the [Ca^{2+}] gradient-mediated differentiation of primary keratinocytes (Popp et al. 2014) and knockdown of Wnt5a suppresses proliferation and initiates apoptosis in HaCaT cells and primary keratinocytes (Zhang et al. 2015). However, an overexpression of Wnt5a in the murine epidermis does not result in psoriasis development (Zhu X et al. 2014). Despite various different approaches to date, no good psoriatic mouse model is available (Schön et al. 2021). Thus, analyses of HaCaT-like cell lines may help to understand the complex and the still not elucidated role of Wnt5a in keratinocyte proliferation and differentiation.

4.2. Generation of an inducible *in vitro CD4*-expression system

For the generation of a keratinocyte cell line with inducible *CD4*-overexpression, we chose a commercially-available, tetracycline-regulated expression system (TetON) to stably transfect HaCaT cells. In general, TetON systems are powerful tools for the protein function studies, since they provide for the possibility to control the respective protein at the gene expression level. This feature is of special importance in case of *CD4* overexpression, since the CD4 protein most likely is involved in differentiation processes of basal cell-like cells of the skin and thus it's continuous expression (e.g. under the control of a CMV promoter) may lead to end-differentiation and cells death, which in turn would make it impossible to maintain *CD4*-overexpressing keratinocytes *in vitro* (Dale et al. 1997; Presland et al. 2001).

As already stated, the Tet-ON Advanced System is based on Tc regulated transcriptional transactivators (Gossen and Bujard 1992), but is characterized by some major improvements to the original system. Thus, the Tet-ON Advanced protein harbors amino acid substitutions that enhance its Dox-sensitivity to a minimum of 10-fold compared to the originally developed system (Urlinger et al. 2000). Furthermore, inserted mutations in the activation domains of the VP16 protein reduce its cross-reactivity and cytotoxicity (Baron et al. 1997). Indeed, several studies analyzing the

advantages of the Tet-On Advanced System over other expression systems reported that beside the expertly tight regulation of the system, there are no pleotropic effects (Harkin et al. 1999), a high inducibility, fast response time to Dox, low non-toxic Dox levels (Gossen et al. 1993; Yarranton 1992) and high GOI expression levels (Yin and Schimke 1995). In addition, the Tet-ON Advanced System, as all Tet-On systems do, has the advantage that in comparison to Tet-Off systems the cells are not exposed to Dox for extended periods (e.g. throughout the selection process and in the non-inducing process) since GOI expression is induced upon Dox treatment (Das et al. 2016).

For the establishment of ddHaCaT cells harboring the Tet-ON Advanced System for inducible CD4-overexpression the strategy shown in Figure 23 was chosen. However, the transfection efficiency of the ddHaCaT cells with the *pTet-DualON* plasmid fell short of expectations since it only yielded 10-20 % ZsGreen1^{+} cells after transfection, even when using more gentle transfection protocols, such as magnet-assisted transfection. Since we furthermore observed that ddHaCaT cells show very low survival rates and transfection efficiency than the HaCaT cells (Deyrieux and Wilson 2007) (also from our data) we focused on the generation of stably transfected HaCaT cells by adjusting the transfection conditions for these cells and planned to dedifferentiate the final cell line. In fact, the HaCaT Tet-ON Advanced cells were successfully created during this work, although Wang *et al.* (2015) reported that HaCaT cells are generally difficult to transfect, especially when using large plasmids. Unfortunately, all three different isolation protocols for picking ZsGreen^{+} HaCaT cells failed to establish a homogeneous HaCaT Tet-ON Advanced cell line without contamination of HaCaT only harboring the antibiotic selection marker. Several techniques were unsuccessfuly applied to isolate individual colonies from a mixture of ZsGreen^{+} and ZsGreen^{neg} cells, indicating that cells harboring the *pTet-DualON* plasmid and a linear antibiotic resistance marker and cells that only harbor the linear antibiotic resistance marker are generated by the Tet-On® Advanced Inducible Gene Expression System from Clontech. Due to lack of time, clonal HaCaT cells harboring the Tet-ON Advanced System were not established . However, the transfection efficiency most likely does not represent the limiting factor for this result since ZsGreen^{+} HaCaT colonies were successfully generated in this work. More likely, the usage of the linear antibiotic selection marker may be the critical point since ZsGreen^{neg} cells that were resistant to the antibiotic selection overgrew ZsGreen^{+} HaCaT cells. Therefore, as part of future work, Tet-ON Advanced plasmids containing antibiotic resistant cassettes (e.g. the pTet-DualON vector containing the antibiotic selection marker) should be generated and used for a new attempt to establish a Tet-On Advanced System for Dox-inducible CD4-overexpression in HaCaT cell.

4.3. Analyses of the putative function of CD4 in ddHaCaT cells

4.3.1. MHCII treatment decreases cAMP levels and the proliferation rate of CD4-expressing ddHaCaT cells

The intracellular signaling molecule and second messenger cAMP is released in response to exposure to extracellular signaling molecules (Kodis et al. 2012). cAMP

is largely produced by cellular adenylyl cyclase (AC) and signals further by binding to specific effectors like protein kinase A (PKA), exchange protein activated by cAMP (EPAC) 1 and cyclic nucleotide-gated ion channels (Biel and Michalakis 2009; Fu et al. 2014; Vitali et al. 2015). The release of cAMP triggers an intracellular signal transduction cascade inducing physiological changes at the cellular level such as proliferation and differentiation (Kodis et al. 2012; Lepski et al. 2013; Stork and Schmitt 2002). Furthermore, it has been shown that prolonged elevation of intracellular cAMP levels have inhibitory effects on immune cells of the innate and adaptive immune system like neutrophils (Shishikura et al. 2016), macrophages (Aronoff et al. 2005), B cells (Minguet et al. 2005), and T cells (Vang AG et al. 2013). Additionally, cAMP is also involved in immune cell functionality and homeostasis (Conche et al. 2009; Roper et al. 2002; Schnurr et al. 2005). Together the various effects elicited by cAMP most likely result from numerous factors such as the cell type, the cAMP level, the expression of different cAMP regulators and effectors, as well as the cAMP compartmentalization.

As explained in section 1.3.1 and shown in Figure 4A, in T lymphocytes, TCR/CD3 ligation to MHCII molecules induces a transient elevation of cAMP levels, which is probably triggered by segregation of stimulatory and inhibitory G proteins in the lipid rafts (Oh and Schnitzer 2001). The outcome, as well as the effects of this temporary rise in cAMP are mostly mediated by PKA (Conche et al. 2009) and is required for the T cell activation. After T cell activation, cAMP levels rise rapidly after only 1 minute, are maintained at high levels for 20 minutes and return to normal levels 60 minutes after T cell activation (Baroja et al. 1999; Conche et al. 2009). Opposite to T cell activation initiated with the transient rise in cAMP levels, a lasting cAMP level elevation induces suppression of the T cell activation (Vang T et al. 2001), T cell proliferation, progression and chemotaxis (Johnson et al. 1988; Tasken and Stokka 2006). Thus, a strict control of the cAMP levels is essential for T cell activation. Moreover, after binding to the MHCII molecules the production of the cAMP is generated by AC, while the degradation is controlled by PDEs which inhibit further cAMP signaling by transforming cAMP to 5´-AMP (Houslay and Adams 2003). Furthermore, the CD4 receptor in Th cells, acting as a co-receptor to the TCR/CD3 complex is actively participating in thymic development and antigen recognition in the periphery (Janeway 1992). The CD4 receptor presence enhances T cell sensitivity to antigens (Janeway et al. 1997; Madrenas et al. 1997; Marrack et al. 1983) and reduces the number of antigenic peptides on APCs required for sustained TCR signaling (Li QJ et al. 2004). Thus, $CD4^+$ T cell activation can be enhanced by coupled engagement of TCR/CD3 and CD4 receptor which further regulates the cAMP levels through differential activation of PDEs (Kammer et al. 1988). Moreover, it has been reported that the low concentrations of cAMP are able to enhance immune cell responses (Koh et al. 1995), as well as its role in the differentiation of the $CD4^+$ T cells subsets and the immune system response mediated by these cells (Datta et al. 2010; Li X et al. 2012). Zhou and König (2003) have investigated the T cell stimulation through CD4 signaling independent of T cell receptor-mediated signals. The study showed that TCR-independent dimerization of CD4 molecules or ligation of

CD4 with MHCII molecules in T cells cause increased intracellular Ca^{2+} and decreased intracellular cAMP levels. The decreased cAMP levels are obtained through the inhibition of the AC activity and activation of the PDE1 and 4, known to degrade cAMP to AMP (Bjørgo et al. 2011; Bjørgo et al. 2010). This TCR/CD3-independent CD4 signaling, its regulation of the intracellular calcium and cAMP levels and the fact that there are also numerous different immune cells that express CD4 but are TCR and/or CD3 negative (e.g. monocytes, macrophages and natural killer cells, dendritic cells, Langerhans cells, neutrophils, basophils and mast cells, eosinophils, megakaryocytes, neuronal cells), indicates that a TCR/CD3-independent CD4 function exists in these cells. Indeed, Zhen et al. (2014) demonstrated the possibility of a TCR/CD3-independent CD4 signaling and showed that CD4-MHCII ligation in TCR/$CD3^{neg}$ monocytes induces their differentiation to macrophages. However, the precise mechanisms of a TCR/CD3-independent CD4 signaling are not known completely. Moreover, the discovery of $CD4^+$ epidermal cells that do not express CD3 nor other immune markers (for details see section 1.3) suggests that CD4 signaling in these cells most likely also occurs in a TCR/CD3-independent manner. Therefore, we hypothesized that similarly to the $CD4^+$ monocytes the MHCII ligation to CD4-expressing basal cell-like keratinocytes (ddHaCaT cells) may also cause increased Ca^{2+} mobilization and decreased cAMP concentration leading to an increased proliferation or differentiation rate (for details see Figure 4B).

Our results showed that the intracellular cAMP levels in ddHaCaT cells stimulated with MHCII molecules for different time periods (for details see section 3.3.1) remained similar to each other irresectable of the transfected plasmid (Figure 25). However, 180 minutes after MHCII stimulation $CD4^+$ ddHaCaT cells showed significant less cAMP levels in comparison to the other ddHaCaT cells indicating that – similar to the findings from Zhen et al. (2014) – the MHCII/CD4-ligation leads to reduced cAMP levels in CD4-expressing basal cell-like keratinocytes. Since, a TCR/CD3-independent CD4 signaling in monocytes most probably is induced by decreased cAMP and increased Ca^{2+} mobilization (see above), our data strongly hints towards a similar regulative network in basal cell-like keratinocytes in which decreased cAMP levels may lead to proliferation and/or differentiation. However, experiments for proofing the hypothesis that TCR/CD3-independent CD4 signaling also in basal cell-like keratinocytes lead to changed intracellular Ca^{2+} levels and to Ca^{2+} mobilization should be analysed in the future.

Besides, the data of this thesis also showed that MHCII does not affect the proliferation rate of ddHaCaT and HaCaT cells in one experiment, whereas in a second experiment MHCII treatment of ddHaCaT, CD4-overexpressing as well as control cells (pulsed and *pCR3.1*-transfected ddHaCaT) results in increased proliferation rate after 24 h, followed by a decrease after 48 h (Figure 26). This increased proliferation rate caused by the MHCII treatment was observed in all analyzed cells of the second experiment, regardless of the CD4-expression. However, because of the possibility of low transfection efficiency the influence of CD4-MHCII interaction cannot be completely excluded. Nevertheless, we can conclude that ddHaCaT cells responded to MHCII treatment with enhanced proliferation rate (after 24 h), followed

by a decrease after 48 h, which may be due to an increased differentiation rate. The obtained results are in correlation with the already explained effect of MHCII-CD4 binding in $CD4^+$ T cells and monocytes (see above), which results in increased proliferation and enhanced differentiation of these cells (Luckheeram et al. 2012; Zhen et al. 2014). Thus, the development of an inducible *in vitro CD4*-expression system in ddHaCaT cells is crucial for further analyses and understanding of the impact of the MHCII-CD4 interaction on the proliferation rate in CD4-expressing ddHaCaT cells. Further experiments should include an evaluation and comparison of the *CD4*-expression levels in ddHaCaT cells cultured in A1 medium containing low [Ca^{2+}] concentration (0.03 mM $CaCl_2$), A1 medium containing high [Ca^{2+}] concentrations (2.8 mM $CaCl_2$) and CTRL medium. Furthermore, MHCII-treated ddHaCaT cells should be analyzed for expression of differentiation markers like K1/K10, as well as the basal cell markers like K5 and K14 (Eckert et al. 1997b) via immunofluorescence and qRT-PCR analyses.

4.3.2. The influence of IL-1α and TNFα on basal cell-like keratinocytes *in vitro*

Wound healing is one of the most complex processes in the human body and involves the interplay between immune and non-immune cells as well as a variety of cytokines and growth factors (Barrientos et al. 2008; Robson et al. 2001). Additionally directed cell migration towards an extracellular chemical gradient is crucial in wound repair (Grinnell 1992; Haugh 2006). Thereby epidermal keratinocytes move significantly slower and with more diffusive trajectories than fast-moving cells (e.g. leukocytes), that have a tendency to move relatively straightforward in the chemoattractant direction (Bear and Haugh 2014; Friedl and Bröcker 2000; Friedl and Wolf 2010). Immediately, after epidermal injury phagocytes and neutrophils are engaged to the wounded place by chemokine gradients (Singer and Clark 1999), which signifies the inflammatory phase. Next, the proliferative and remodeling phase, are specified by proliferation and migration of slow-moving cells (Singer and Clark 1999). During the proliferative phase, the platelet-derived growth factor (PDGF) from the coagulating platelets recruits the fibroblasts, which together with other proliferating cells are responsible for granulation tissue formation (Deuel et al. 1991; Seppä et al. 1982). In the remodeling or re-epithelialization phase, there is a migration of the basal keratinocytes from the wound margins over the newly formed tissue and with this they are closing the gap and restoring the skin barrier integrity (Pastar et al. 2014). Basal keratinocyte migration is triggered after few hours following the injury by numerous wound-initiated signals, as well as the mechanical stimuli such as the free edges of the wound margin (Klarlund and Block 2011), different tissue factors (Kirfel et al. 2003), as well as multiple growth factors (Martin and Nunan 2015; Seeger and Paller 2015).

Within the process of wound healing both IL-1α and TNFα play significant roles (Larouche et al. 2018; Ritsu et al. 2017). In mice, IL-1α is responsible for increased proliferation of the epidermal stem cells upon wound healing (Lee P et al. 2017). However, it also plays an important role in skin homoeostasis (section 1.2.3.3) and abundant quantities of IL-1α seem to be associated with psoriasis (Albanesi et al.

2018; Rendon and Schäkel 2019). Nevertheless, the results of this thesis show that IL-1α does not impact the proliferation rate of ddHaCaT or HaCaT cells within 24 h and also did not increase the expression of *CD4* as shown for microglia (Yu et al. 1998). In contrast, the *CD4*-expression of ddHaCaT cells decreases upon 24 h IL-1α treatment (Figure 28). Albeit, these experiments should be repeated. The results suggest that IL-1α may induce an increased differentiation of the ddHaCaT cells since the expression of S100A7, which is as a marker of keratinocyte differentiation (Martinsson et al. 2005), strongly increases upon IL-1α-treatment (this thesis) (Yano et al. 2008). Thus, if IL-1α indeed causes differentiation of ddHaCaT cells, a down-regulated *CD4*-expression seems to be plausible at the beginning of differentiation (e.g. at 24 h IL-1α-treatment) and to eventually rise again at an advanced differentiation step (e.g. at > 24 h IL-1α-treatment). In addition, repeated qRT-PCR-analyses and *CD4*-mRNA expression should be also measured via RNAscope. Moreover, gene expression analyses of differentiation markers (e.g. K1/K10) would help to reveal a possible relationship between differentiation processes and *CD4*-expression.

Immediately after disruption of the permeability barrier TNFα increases strongly in the murine and human epidermis (Grellner et al. 2000; Wood et al. 1992) which peaks after one day and decreases to the basal level 48 h after wounding (Ritsu et al. 2017). Interestingly, constant high TNFα levels inhibit the differentiation of calcium differentiated keratinocytes and thus delaying the skin barrier repair (Jensen JM et al. 1999; Kim et al. 2011), indicating that TNFα is crucial during early wound healing. The fact, that TNFα is furthermore known to be one of the key pro-inflammatory mediators in psoriasis skin lesions (Kristensen et al. 1993) further substantiates this conclusion. However, during the inflammatory phase of wound healing, TNFα upregulation is important for modulating the migratory phenotype, motility and attachment of the basal keratinocytes (Banno et al. 2004; Werner and Grose 2003). Thus, TNFα induces the migration of epidermal stem/progenitor cell (Albanesi et al. 2018; Benhadou et al. 2019; Bocheńska et al. 2017; Larouche et al. 2018; Rendon and Schäkel 2019; Wang Y et al. 2017).

These facts were the basis for the hypothesis that TNFα may also induce the migration of CD4-expressing basal cell-like keratinocytes (shown in Figure 5). Directed migration of slow moving cells, like keratinocytes, towards a gradient of FCS using the *µ-slide* chamber for long-term chemotaxis is reported in the literature (Zantl and Horn 2011; Zengel et al. 2011). Indeed, our results verified the previously described findings that TNFα induces a directed movement of keratinocytes, in particular of ddHaCaT cells. We demonstrate that *CD4*-expressing ddHaCaT cells are moving straight forward toward a 20 % FCS (positive control) as well as to TNFα gradient (when in 2 % cFCS-containing medium; see section 3.3.3.2). However, the route of $CD4^+$ ddHaCaT cells towards TNFα gradient in 2 % cFCS-containing medium was more circuitous compared to those of cells moving to the 20 % FCS gradient, while cells in cFCS-depleted medium moved without constant speed and straight line.

Obviously, the differential behavior of ddHaCaT cells with respect to the TNFα gradient can be explained by the presence of cFCS which is essential and necessary for cells survival (see above, section 4.1). However, these results show that although the TNFα-gradient induced a high cellular motility comparable to that of the positive control, this movement is not as straight as the movement of cells to the positive control or to the TNFα in experimental medium with 2 % cFCS.

5. Summary

To study the role of the Hedgehog-Patched (Hh/Ptch) signaling pathway in T-cells, the two-step DMBA/TPA carcinogenesis protocol have been applied to mice with an homozygous *Ptch* depletion in CD4-expressing cell (*Ptch*$^{flox/flox}$*CD4Cre*$^{+/-}$). This approach revealed that beside the typically DMBA/TPA-induced papilloma and squamous cell carcinoma also basal cell carcinoma developed in *Ptch*$^{flox/flox}$*CD4Cre*$^{+/-}$ mice (Uhmann Anja et al. 2014). These basal cell carcinoma derive from CD4^{+} cells of the murine skin that are characterized by their expression of the keratinocyte marker CD49f and the stem cell markers CD34 and Sca1. The progeny of these CD4^{+} epidermal stem cell-like cells grow permanently and increasingly with age and upon wound healing in adult mice in all epidermal layers and as multipotent hair follicle stem cells (Brandes 2021). Beside the murine skin, the existence of CD4^{+} epidermal cells was also confirmed in human skin in which the cells are characterized by their expression of the keratinocyte marker CD49f and the epidermal stem cell markers CD29 and K15 (Brandes 2021; Brandes et al. 2020; Scheile 2020). However, the function of the CD4 protein in epidermal stem cell-like keratinocytes is currently unknown and therefore the main aim of this dissertation was to analyze the CD4 protein function in stem cell-like keratinocytes.

Thus, a dedifferentiated, keratinocyte cell line (ddHaCaT) was established, which proliferates and grows stably in low [Ca^{2+}] levels medium, possesses a basal cell-like phenotype and differentiate upon short-term culture in high [Ca^{2+}] level-containing medium. Unfortunately, the generation of an inducible *in vitro CD4*-expression system in ddHaCaT failed. Thus, the putative function of CD4 in keratinocytes was investigated by transiently overexpress *CD4* in ddHaCaT cells, followed by treatment with major histocompatibility complex class II protein (MHCII), interleukin 1alpha (IL-1α), or tumor necrosis factor alpha (TNFα) and analyzing the putative role of TCR/CD3-independent CD4-mediated signaling (e.g. measurement of proliferation rate, differentiation status, intracellular cAMP levels and the cellular migration after MHCII or TNFα treatment) or *CD4* expression stimuli (e.g. qRT-PCR analyses after IL-1α treatment).

The results of these experiments demonstrate that (1) MHCII treatment of *CD4*-expressing ddHaCaT cells results in decreased proliferation and reduced cAMP levels compared to the respective controls, (2) IL-1α treatment does not impact the proliferation rate of ddHaCaT and of *CD4*-expressing ddHaCaT cells and, contrary to our expectations, decreased the *CD4* mRNA expression of ddHaCaT cells and (3) *CD4*-expressing ddHaCaT actively migrate to a TNFα gradient when cultured in 2 % cFCS-containing medium. Together the data strongly hint towards a functional role of the CD4 protein in basal cell-like keratinocytes. Moreover, the data provide evidence, that CD4 functions through a TCR/CD3-independent signaling in basal cell-like keratinocytes similar as shown for monocytes and induces differentiation of basal cell-like keratinocytes.

Nevertheless, future studies, with special focus on experiments using a stably transfected *CD4*-expressing ddHaCaT cells, are needed to confirm the finding of this

work and gain further insights into the functional role of CD4 in keratinocytes. However, the cryopreserved dedifferentiated, keratinocyte cell lines can be used as basis for further studies of keratinocyte differentiation and proliferation that are crucial for the epidermal barrier maintenance, as well as disturbance of these processes that can lead to various skin diseases (e.g. psoriasis).

6. References

Abraham J, Mathew S (2019): Merkel Cells: A Collective Review of Current Concepts. Int J Appl Basic Med Res 9, 9-13

Abramovits W, JJ RB, Valdecantos WC (2013): Role of interleukin 1 in atopic dermatitis. Dermatol Clin 31, 437-444

Adacehi K, Halprin KM, Takeda J, Nemoto O, Aoyagi T, Hzuka H, Yoshikawa K, Levine V (1982): Epidermal surface receptors which link pharmacological mediators to the adenylate cyclase system. Br J Dermatol 107, 111-118

Ahmad F, Gao G, Wang LM, Landstrom TR, Degerman E, Pierce JH, Manganiello VC (1999): IL-3 and IL-4 activate cyclic nucleotide phosphodiesterases 3 (PDE3) and 4 (PDE4) by different mechanisms in FDCP2 myeloid cells. J Immunol 162, 4864-4875

Alam H, Sehgal L, Kundu ST, Dalal SN, Vaidya MM (2011): Novel function of keratins 5 and 14 in proliferation and differentiation of stratified epithelial cells. Mol Biol Cell 22, 4068-4078

Albanesi C, Madonna S, Gisondi P, Girolomoni G (2018): The interplay between keratinocytes and immune cells in the pathogenesis of psoriasis. Front Immunol 9, 1549

Allen TD, Potten CS (1974): Fine-structural identification and organization of the epidermal proliferative unit. J Cell Sci 15, 291-319

Ando M, Kawashima T, Kobayashi H, Ohkawara A (1990): Immunohistological detection of proliferating cells in normal and psoriatic epidermis using Ki-67 monoclonal antibody. J Dermatol Sci 1, 441-446

Armstrong AW, Read C (2020): Pathophysiology, clinical presentation, and treatment of psoriasis: a review. JAMA 323, 1945-1960

Aronoff DM, Canetti C, Serezani CH, Luo M, Peters-Golden M (2005): Cutting edge: macrophage inhibition by cyclic AMP (cAMP): differential roles of protein kinase A and exchange protein directly activated by cAMP-1. J Immunol 174, 595-599

Bagati A, Koch Z, Bofinger D, Goli H, Weiss LS, Dau R, Thomas M, Zucker SN (2015): A modified in vitro invasion assay to determine the potential role of hormones, cytokines and/or growth factors in mediating cancer cell invasion. J Vis Exp, e51480

Banno T, Gazel A, Blumenberg M (2004): Effects of tumor necrosis factor-α (TNFα) in epidermal keratinocytes revealed using global transcriptional profiling. J Biol Chem 279, 32633-32642

Baroja ML, Cieslinski LB, Torphy TJ, Wange RL, Madrenas J (1999): Specific CD3ε association of a phosphodiesterase 4B isoform determines its selective tyrosine phosphorylation after CD3 ligation. J Immunol 162, 2016-2023

Baron U, Bujard H (2000): Tet repressor-based system for regulated gene expression in eukaryotic cells: principles and advances. Methods Enzymol 327, 401-421

Baron U, Gossen M, Bujard H (1997): Tetracycline-controlled transcription in eukaryotes: novel transactivators with graded transactivation potential. Nucleic Acids Res 25, 2723-2729

Barrandon Y, Green H (1987): Three clonal types of keratinocyte with different capacities for multiplication. Proc Natl Acad Sci U S A 84, 2302-2306

Barrientos S, Stojadinovic O, Golinko MS, Brem H, Tomic-Canic M (2008): Growth factors and cytokines in wound healing. Wound Repair Regen 16, 585-601

Bear JE, Haugh JM (2014): Directed migration of mesenchymal cells: where signaling and the cytoskeleton meet. Curr Opin Cell Biol 30, 74-82

Behm B, Babilas P, Landthaler M, Schreml S (2012): Cytokines, chemokines and growth factors in wound healing. J Eur Acad Dermatol Venereol 26, 812-820

Behne MJ, Sanchez S, Barry NP, Kirschner N, Meyer W, Mauro TM, Moll I, Gratton E (2011): Major translocation of calcium upon epidermal barrier insult: imaging and quantification via FLIM/Fourier vector analysis. Arch Dermatol Res 303, 103-115

Ben-Sasson SZ, Hu-Li J, Quiel J, Cauchetaux S, Ratner M, Shapira I, Dinarello CA, Paul WE (2009): IL-1 acts directly on CD4 T cells to enhance their antigen-driven expansion and differentiation. Proc Natl Acad Sci U S A 106, 7119-7124

Bender AT, Beavo JA (2006): Cyclic nucleotide phosphodiesterases: molecular regulation to clinical use. Pharmacol Rev 58, 488-520

Benhadou F, Mintoff D, Del Marmol V (2019): Psoriasis: keratinocytes or immune cells–which is the trigger? Dermatology 235, 91-100

Benitah SA, Frye M (2012): Stem cells in ectodermal development. J Mol Med (Berl) 90, 783-790

Bernstein HB, Plasterer MC, Schiff SE, Kitchen CM, Kitchen S, Zack JA (2006): CD4 expression on activated NK cells: ligation of CD4 induces cytokine expression and cell migration. J Immunol 177, 3669-3676

Berridge MJ (1975): The interaction of cyclic nucleotides and calcium in the control of cellular activity. Adv Cyclic Nucleotide Res 6, 1-98

Berridge MJ (1993): Cell signalling. A tale of two messengers. Nature 365, 388-389

Biel M, Michalakis S (2009): Cyclic nucleotide-gated channels. Handb Exp Pharmacol, 111-136

Bikle DD, Xie Z, Tu CL (2012): Calcium regulation of keratinocyte differentiation. Expert Rev Endocrinol Metab 7, 461-472

Bikle DD, Ng D, Tu CL, Oda Y, Xie Z (2001): Calcium- and vitamin D-regulated keratinocyte differentiation. Mol Cell Endocrinol 177, 161-171

Biswas P, Mantelli B, Sica A, Malnati M, Panzeri C, Saccani A, Hasson H, Vecchi A, Saniabadi A, Lusso P (2003): Expression of CD4 on human peripheral blood neutrophils. Blood 101, 4452-4456

Bjørgo E, Moltu K, Taskén K: Phosphodiesterases as targets for modulating T-cell responses. In: Francis SH, Conti M, Houslay MD (Eds.): Phosphodiesterases as Drug Targets. Volume 204; Springer, Heidelberg 2011, 345-363

Bjørgo E, Solheim SA, Abrahamsen H, Baillie GS, Brown KM, Berge T, Okkenhaug K, Houslay MD, Taskén K (2010): Cross talk between phosphatidylinositol 3-kinase and cyclic AMP (cAMP)-protein kinase a signaling pathways at the level of a protein kinase B/β-arrestin/cAMP phosphodiesterase 4 complex. Mol Cell Biol 30, 1660-1672

Blanpain C, Fuchs E (2009): Epidermal homeostasis: a balancing act of stem cells in the skin. Nat Rev Mol Cell Biol 10, 207-217

Blanpain C, Horsley V, Fuchs E (2007): Epithelial stem cells: turning over new leaves. Cell 128, 445-458

Blanpain C, Lowry WE, Pasolli HA, Fuchs E (2006): Canonical notch signaling functions as a commitment switch in the epidermal lineage. Genes Dev 20, 3022-3035

Blanton RA, Kupper TS, McDougall JK, Dower S (1989): Regulation of interleukin 1 and its receptor in human keratinocytes. Proc Natl Acad Sci U S A 86, 1273-1277

Bocheńska K, Smolińska E, Moskot M, Jakóbkiewicz-Banecka J, Gabig-Cimińska M (2017): Models in the research process of psoriasis. Int J Mol Sci 18, 2514

Borodinsky LN, Spitzer NC (2006): Second messenger pas de deux: the coordinated dance between calcium and cAMP. Sci STKE 2006, pe22-pe22

Bose A, Teh M-T, Mackenzie IC, Waseem A (2013): Keratin k15 as a biomarker of epidermal stem cells. Int J Mol Sci 14, 19385-19398

Boukamp P, Petrussevska RT, Breitkreutz D, Hornung J, Markham A, Fusenig NE (1988): Normal keratinization in a spontaneously immortalized aneuploid human keratinocyte cell line. J Cell Biol 106, 761-771

Boukamp P, Popp S, Altmeyer S, Hulsen A, Fasching C, Cremer T, Fusenig NE (1997): Sustained nontumorigenic phenotype correlates with a largely stable

chromosome content during long-term culture of the human keratinocyte line HaCaT. Genes Chromosomes Cancer 19, 201-214

Brady R, Barclay A: The Structure of CD4. In: Littman DR (Eds.): The CD4 Molecule. Springer, Heidelberg 1996, 1-18

Brandes N: Characterisation of CD4+ stem cells of the skin and their role in skin homeostasis and tumourigenesis. Dissertation Goettingen 2021

Brandes N, Mitkovska SH, Botermann DS, Maurer W, Müllen A, Scheile H, Zabel S, Frommhold A, Heß I, Hahn H (2020): Spreading of Isolated Ptch Mutant Basal Cell Carcinoma Precursors Is Physiologically Suppressed and Counteracts Tumor Formation in Mice. Int J Mol Sci 21, 9295

Brash DE, Rudolph JA, Simon JA, Lin A, McKenna GJ, Baden HP, Halperin AJ, Ponten J (1991): A role for sunlight in skin cancer: UV-induced p53 mutations in squamous cell carcinoma. Proc Natl Acad Sci U S A 88, 10124-10128

Braun KM, Niemann C, Jensen UB, Sundberg JP, Silva-Vargas V, Watt FM (2003): Manipulation of stem cell proliferation and lineage commitment: visualisation of label-retaining cells in wholemounts of mouse epidermis. Development 130, 5241-5255

Breitkreutz D, Schoop VM, Mirancea N, Baur M, Stark H-J, Fusenig NE (1998): Epidermal differentiation and basement membrane formation by HaCaT cells in surface transplants. Eur J Cell Biol 75, 273-286

Brennan EP, Tang XH, Stewart-Akers AM, Gudas LJ, Badylak SF (2008): Chemoattractant activity of degradation products of fetal and adult skin extracellular matrix for keratinocyte progenitor cells. J Tissue Eng Regen Med 2, 491-498

Brion DE, Raynaud F, Plet A, Laurent P, Leduc B, Anderson W (1986): Deficiency of cyclic AMP-dependent protein kinases in human psoriasis. Proc Natl Acad Sci U S A 83, 5272-5276

Briscoe J, Therond PP (2013): The mechanisms of Hedgehog signalling and its roles in development and disease. Nat Rev Mol Cell Biol 14, 416-429

Bugrim A (1999): Regulation of Ca2+ release by cAMP-dependent protein kinase A mechanism for agonist-specific calcium signaling? Cell Calcium 25, 219-226

Burgering B, Pronk G, van Weeren PC, Chardin P, Bos JL (1993): cAMP antagonizes p21ras-directed activation of extracellular signal-regulated kinase 2 and phosphorylation of mSos nucleotide exchange factor. The EMBO Journal 12, 4211-4220

Byrne C, Tainsky M, Fuchs E (1994): Programming gene expression in developing epidermis. Development 120, 2369-2383

Cai Y, Xue F, Quan C, Qu M, Liu N, Zhang Y, Fleming C, Hu X, Zhang H-g, Weichselbaum R (2019): A critical role of the IL-1β–IL-1R signaling pathway in skin inflammation and psoriasis pathogenesis. J Invest Dermatol 139, 146-156

Carter WG, Kaur P, Gil SG, Gahr PJ, Wayner EA (1990): Distinct functions for integrins alpha 3 beta 1 in focal adhesions and alpha 6 beta 4/bullous pemphigoid antigen in a new stable anchoring contact (SAC) of keratinocytes: relation to hemidesmosomes. J Cell Biol 111, 3141-3154

Celli A, Crumrine D, Meyer JM, Mauro TM (2016): Endoplasmic Reticulum Calcium Regulates Epidermal Barrier Response and Desmosomal Structure. J Invest Dermatol 136, 1840-1847

Celli A, Sanchez S, Behne M, Hazlett T, Gratton E, Mauro T (2010): The Epidermal Ca2+ Gradient: Measurement Using the Phasor Representation of Fluorescent Lifetime Imaging. Biophys J 98, 911-921

Cerbini T, Luo Y, Rao MS, Zou J (2015): Transfection, selection, and colony-picking of human induced pluripotent stem cells TALEN-targeted with a GFP gene into the AAVS1 safe harbor. J Vis Exp, e52504

Charbonneau H, Kumar S, Novack JP, Blumenthal DK, Griffin PR, Shabanowitz J, Hunt DF, Beavo JA, Walsh KA (1991): Evidence for domain organization within the 61-kDa calmodulin-dependent cyclic nucleotide phosphodiesterase from bovine brain. Biochemistry 30, 7931-7940

Chedid M, Rubin JS, Csaky KG, Aaronson SA (1994): Regulation of keratinocyte growth factor gene expression by interleukin 1. J Biol Chem 269, 10753-10757

Chen J, Cheng X, Merched-Sauvage M, Caulin C, Roop DR, Koch PJ (2006): An unexpected role for keratin 10 end domains in susceptibility to skin cancer. J Cell Sci 119, 5067-5076

Chu DH: Development and Structure of Skin. In: Wolff K, Goldsmith LA, Katz SI, Gilchrest BA, Paller AS, Leffell DJ (Eds.): Fitzpatrick's Dermatology in General Medicine. McGraw-Hill, New York 2008, 57-91

Chuong C-M, Nickoloff B, Elias P, Goldsmith L, Macher E, Maderson P, Sundberg J, Tagami H, Plonka P, Thestrup-Pederson K (2002): What is the 'true' function of skin? Exp Dermatol 11, 159-187

Clayton E, Doupe DP, Klein AM, Winton DJ, Simons BD, Jones PH (2007): A single type of progenitor cell maintains normal epidermis. Nature 446, 185-189

Clayton K, Vallejo AF, Davies J, Sirvent S, Polak ME (2017): Langerhans Cells-Programmed by the Epidermis. Front Immunol 8, 1676

Clontech: Tet-On Advanced inducible Gene Expression Systems User manual. 102312. Edition; Clontech, Mountain View 2012

Colombo I, Sangiovanni E, Maggio R, Mattozzi C, Zava S, Corbett Y, Fumagalli M, Carlino C, Corsetto PA, Scaccabarozzi D (2017): HaCaT cells as a reliable in vitro differentiation model to dissect the inflammatory/repair response of human keratinocytes. Mediators Inflamm 2017

Compton CC, Gill JM, Bradford DA, Regauer S, Gallico GG, O'Connor NE (1989): Skin regenerated from cultured epithelial autografts on full-thickness burn wounds from 6 days to 5 years after grafting. A light, electron microscopic and immunohistochemical study. Lab Invest 60, 600-612

Conche C, Boulla G, Trautmann A, Randriamampita C (2009): T cell adhesion primes antigen receptor-induced calcium responses through a transient rise in adenosine 3′, 5′-cyclic monophosphate. Immunity 30, 33-43

Cook SJ, McCormick F (1993): Inhibition by cAMP of Ras-dependent activation of Raf. Science 262, 1069-1072

Corado J, Le Deist F, Griscelli C, Fischer A (1990): Inositol 1, 4, 5-trisphosphate- and arachidonic acid-induced calcium mobilization in T and B lymphocytes. Cell Immunol 126, 245-254

Corthay A (2009): How do regulatory T cells work? Scand J Immunol 70, 326-336

Cotsarelis G, Sun T-T, Lavker RM (1990): Label-retaining cells reside in the bulge area of pilosebaceous unit: implications for follicular stem cells, hair cycle, and skin carcinogenesis. Cell 61, 1329-1337

Dale BA, Presland RB, Lewis SP, Underwood RA, Fleckman P (1997): Transient expression of epidermal filaggrin in cultured cells causes collapse of intermediate filament networks with alteration of cell shape and nuclear integrity. J Invest Dermatol 108, 179-187

Das AT, Tenenbaum L, Berkhout B (2016): Tet-on systems for doxycycline-inducible gene expression. Curr Gene Ther 16, 156-167

Datta SK, Sabet M, Nguyen KP, Valdez PA, Gonzalez-Navajas JM, Islam S, Mihajlov I, Fierer J, Insel PA, Webster NJ, et al. (2010): Mucosal adjuvant activity of cholera toxin requires Th17 cells and protects against inhalation anthrax. Proc Natl Acad Sci U S A 107, 10638-10643

Delescluse C, Colburn NH, Duell EA, Voorhees JJ (1974): Cyclic AMP-elevating agents inhibit proliferation of keratinizing guinea pig epidermal cells. Differentiation 2, 343-350

Denda M, Fuziwara S, Inoue K (2004): Association of cyclic adenosine monophosphate with permeability barrier homeostasis of murine skin. J Invest Dermatol 122, 140-146

Deucher A, Efimova T, Eckert RL (2002): Calcium-dependent involucrin expression is inversely regulated by protein kinase C (PKC) α and PKCδ. J Biol Chem 277, 17032-17040

Deuel TF, Kawahara RS, Mustoe TA, Pierce GF (1991): Growth factors and wound healing: platelet-derived growth factor as a model cytokine. Annu Rev Med 42, 567-584

Deyrieux AF, Wilson VG (2007): In vitro culture conditions to study keratinocyte differentiation using the HaCaT cell line. Cytotechnology 54, 77-83

Deyrieux AF, Rosas-Acosta G, Ozbun MA, Wilson VG (2007): Sumoylation dynamics during keratinocyte differentiation. J Cell Sci 120, 125-136

DiGiovanni J (1992): Multistage carcinogenesis in mouse skin. Pharmacol Ther 54, 63-128

Dlugosz AA, Yuspa SH (1993): Coordinate changes in gene expression which mark the spinous to granular cell transition in epidermis are regulated by protein kinase C. J Cell Biol 120, 217-225

Dlugosz AA, Yuspa SH (1994): Protein kinase C regulates keratinocyte transglutaminase (TGK) gene expression in cultured primary mouse epidermal keratinocytes induced to terminally differentiate by calcium. J Invest Dermatol 102, 409-414

Dou J, Zhang L, Xie X, Ye L, Yang C, Wen L, Shen C, Zhu C, Zhao S, Zhu Z, et al. (2017): Integrative analyses reveal biological pathways and key genes in psoriasis. Br J Dermatol 177, 1349-1357

Doupé DP, Klein AM, Simons BD, Jones PH (2010): The ordered architecture of murine ear epidermis is maintained by progenitor cells with random fate. Dev Cell 18, 317-323

Driskell RR, Jahoda CA, Chuong CM, Watt FM, Horsley V (2014): Defining dermal adipose tissue. Exp Dermatol 23, 629-631

Eckert RL, Crish JF, Robinson NA (1997b): The epidermal keratinocyte as a model for the study of gene regulation and cell differentiation. Physiol Rev 77, 397-424

Eckert RL, Crish JF, Banks EB, Welter JF (1997a): The epidermis: Genes on - Genes off. J Invest Dermatol 109, 501-509

Eckert RL, Broome AM, Ruse M, Robinson N, Ryan D, Lee K (2004): S100 proteins in the epidermis. J Invest Dermatol 123, 23-33

Elias PM, Ahn S, Brown B, Crumrine D, Feingold KR (2002): Origin of the epidermal calcium gradient: regulation by barrier status and role of active vs passive mechanisms. J Invest Dermatol 119, 1269-1274

Elias PM, Gruber R, Crumrine D, Menon G, Williams ML, Wakefield JS, Holleran WM, Uchida Y (2014): Formation and functions of the corneocyte lipid envelope (CLE). Biochim Biophys Acta 1841, 314-318

Eller MS, Yaar M, Ostrom K, Harkness DD, Gilchrest BA (1995): A role for interleukin-1 in epidermal differentiation: regulation by expression of functional versus decoy receptors. J Cell Sci 108, 2741-2746

Eming SA, Krieg T, Davidson JM (2007): Inflammation in wound repair: molecular and cellular mechanisms. J Invest Dermatol 127, 514-525

Essayan DM (2001): Cyclic nucleotide phosphodiesterases. J Allergy Clin Immunol 108, 671-680

Feingold KR, Schmuth M, Elias PM (2007): The regulation of permeability barrier homeostasis. J Invest Dermatol 127, 1574-1576

Feldmeyer L, Werner S, French LE, Beer H-D (2010): Interleukin-1, inflammasomes and the skin. Eur J Cell Biol 89, 638-644

Feske S (2007): Calcium signalling in lymphocyte activation and disease. Nat Rev Immunol 7, 690-702

Fleckman P, Dale BA, Holbrook KA (1985): Profilaggrin, a high-molecular-weight precursor of filaggrin in human epidermis and cultured keratinocytes. J Invest Dermatol 85, 507-512

Francis SH, Blount MA, Corbin JD (2011): Mammalian cyclic nucleotide phosphodiesterases: molecular mechanisms and physiological functions. Physiol Rev 91, 651-690

Freeman SC, Sonthalia S: Histology, Keratohyalin Granules Edition; StatPearls Publishing, Treasure Island 2021

Friedl P, Bröcker EB (2000): The biology of cell locomotion within three-dimensional extracellular matrix. Cell Mol Life Sci 57, 41-64

Friedl P, Wolf K (2010): Plasticity of cell migration: a multiscale tuning model. J Cell Biol 188, 11-19

Frödin M, Peraldi P, Van Obberghen E (1994): Cyclic AMP activates the mitogen-activated protein kinase cascade in PC12 cells. J Biol Chem 269, 6207-6214

Fu Q, Kim S, Soto D, De Arcangelis V, DiPilato L, Liu S, Xu B, Shi Q, Zhang J, Xiang YK (2014): A long lasting β1 adrenergic receptor stimulation of cAMP/protein kinase A (PKA) signal in cardiac myocytes. J Biol Chem 289, 14771-14781

Fuchs E (1995): Keratins and the skin. Annu Rev Cell Dev Biol 11, 123-153

Fuchs E (2007): Scratching the surface of skin development. Nature 445, 834-842

Fuchs E, Green H (1980): Changes in keratin gene expression during terminal differentiation of the keratinocyte. Cell 19, 1033-1042

Fuchs E, Raghavan S (2002): Getting under the skin of epidermal morphogenesis. Nat Rev Genet 3, 199-209

Fujisaki H, Futaki S, Yamada M, Sekiguchi K, Hayashi T, Ikejima T, Hattori S (2018): Respective optimal calcium concentrations for proliferation on type I collagen fibrils in two keratinocyte line cells, HaCaT and FEPE1L-8. Regen Ther 8, 73-79

Fukuyama K, Epstein WL (1968): Synthesis of RNA and protein during epidermal cell differentiation in man. Arch Dermatol 98, 75-79

Fukuyama K, Nakamura T, Benstein IA (1965): Differentially localized incorporation of amino acids in relation to epidermal keratinization in the newborn rat. Anat Rec 152, 525-535

Garcin CL, Ansell DM (2017): The battle of the bulge: re-evaluating hair follicle stem cells in wound repair. Exp Dermatol 26, 101-104

Garrod D, Chidgey M (2008): Desmosome structure, composition and function. Biochim Biophys Acta 1778, 572-587

Gelfo V, Romaniello D, Mazzeschi M, Sgarzi M, Grilli G, Morselli A, Manzan B, Rihawi K, Lauriola M (2020): Roles of IL-1 in cancer: from tumor progression to resistance to targeted therapies. Int J Mol Sci 21, 6009

Ghazizadeh S, Taichman LB (2001): Multiple classes of stem cells in cutaneous epithelium: a lineage analysis of adult mouse skin. EMBO J 20, 1215-1222

Gossen M, Bujard H (1992): Tight control of gene expression in mammalian cells by tetracycline-responsive promoters. Proc Natl Acad Sci U S A 89, 5547-5551

Gossen M, Bonin AL, Bujard H (1993): Control of gene activity in higher eukaryotic cells by prokaryotic regulatory elements. Trends Biochem Sci 18, 471-475

Gossen M, Freundlieb S, Bender G, Muller G, Hillen W, Bujard H (1995): Transcriptional activation by tetracyclines in mammalian cells. Science 268, 1766-1769

Gragnani A, Sobral CS, Ferreira LM (2007): Thermolysin in human cultured keratinocyte isolation. Braz J Biol 67, 105-109

Graves LM, Lawrence JC, Jr. (1996): Insulin, growth factors, and cAMP: antagonism in the signal transduction pathways. Trends Endocrinol Metab 7, 43-50

Green H (1978): Cyclic AMP in relation to proliferation of the epidermal cell: a new view. Cell 15, 801-811

Grellner W, Georg T, Wilske J (2000): Quantitative analysis of proinflammatory cytokines (IL-1β, IL-6, TNF-α) in human skin wounds. Forensic Sci Int 113, 251-264

Grinnell F (1992): Wound repair, keratinocyte activation and integrin modulation. J Cell Sci 101 (Pt 1), 1-5

Gudjonsson JE, Johnston A, Stoll SW, Riblett MB, Xing X, Kochkodan JJ, Ding J, Nair RP, Aphale A, Voorhees JJ (2010): Evidence for altered Wnt signaling in psoriatic skin. J Invest Dermatol 130, 1849-1859

Halprin KM (1972): Epidermal “Turnover Time”—A Re-Examination. Br J Dermatol 86, 14-19

Halprin KM, Adachi K, Yoshikawa K, Levine V, Mui MM, Hsia S (1975): Cyclic AMP and psoriasis. J Invest Dermatol 65, 170-178

Harkin DP, Bean JM, Miklos D, Song Y-H, Truong VB, Englert C, Christians FC, Ellisen LW, Maheswaran S, Oliner JD (1999): Induction of GADD45 and JNK/SAPK-dependent apoptosis following inducible expression of BRCA1. Cell 97, 575-586

Haugh JM (2006): Deterministic model of dermal wound invasion incorporating receptor-mediated signal transduction and spatial gradient sensing. Biophys J 90, 2297-2308

Heenen M, Thiriar S, Noel JC, Galand P (1998): Ki-67 immunostaining of normal human epidermis: comparison with 3H-thymidine labelling and PCNA immunostaining. Dermatology 197, 123-126

Hennings H, Holbrook KA (1983): Calcium regulation of cell-cell contact and differentiation of epidermal cells in culture: an ultrastructural study. Exp Cell Res 143, 127-142

Hennings H, Michael D, Cheng C, Steinert P, Holbrook K, Yuspa SH (1980): Calcium regulation of growth and differentiation of mouse epidermal cells in culture. Cell 19, 245-254

Hertle MD, Adams JC, Watt FM (1991): Integrin expression during human epidermal development in vivo and in vitro. Development 112, 193-206

Hobbs RP, Amargo EV, Somasundaram A, Simpson CL, Prakriya M, Denning MF, Green KJ (2011): The calcium ATPase SERCA2 regulates desmoplakin dynamics and intercellular adhesive strength through modulation of PKCα signaling. FASEB J 25, 990-1001

Hohl D, Lichti U, Breitkreutz D, Steinert PM, Roop DR (1991a): Transcription of the human loricrin gene in vitro is induced by calcium and cell density and suppressed by retinoic acid. J Invest Dermatol 96, 414-418

Hohl D, Mehrel T, Lichti U, Turner ML, Roop DR, Steinert PM (1991b): Characterization of human loricrin. Structure and function of a new class of epidermal cell envelope proteins. J Biol Chem 266, 6626-6636

Hotchin NA, Kovach NL, Watt FM (1993): Functional down-regulation of alpha 5 beta 1 integrin in keratinocytes is reversible but commitment to terminal differentiation is not. J Cell Sci 106, 1131-1138

Houslay MD, Adams DR (2003): PDE4 cAMP phosphodiesterases: modular enzymes that orchestrate signalling cross-talk, desensitization and compartmentalization. Biochem J 370, 1-18

Hsu YC, Li L, Fuchs E (2014): Emerging interactions between skin stem cells and their niches. Nat Med 20, 847-856

Huang YC, Wang TW, Sun JS, Lin FH (2006): Effect of Calcium Ion Concentration on Keratinocyte Behaviors in the Defined Media. Biomed Eng (Singapore) 18, 37-41

Huff CA, Yuspa SH, Rosenthal D (1993): Identification of control elements 3'to the human keratin 1 gene that regulate cell type and differentiation-specific expression. J Biol Chem 268, 377-384

Iizuka H (1994): Epidermal turnover time. J Dermatol Sci 8, 215-217

Indra AK, Castaneda E, Antal MC, Jiang M, Messaddeq N, Meng X, Loehr CV, Gariglio P, Kato S, Wahli W (2007): Malignant transformation of DMBA/TPA-induced papillomas and nevi in the skin of mice selectively lacking retinoid-X-receptor α in epidermal keratinocytes. J Invest Dermatol 127, 1250-1260

Irvine DJ, Purbhoo MA, Krogsgaard M, Davis MM (2002): Direct observation of ligand recognition by T cells. Nature 419, 845-849

Ito M, Liu Y, Yang Z, Nguyen J, Liang F, Morris RJ, Cotsarelis G (2005): Stem cells in the hair follicle bulge contribute to wound repair but not to homeostasis of the epidermis. Nat Med 11, 1351-1354

Janeway J, C. A. (1989): The role of CD4 in T-cell activation: accessory molecule or co-receptor? Immunol Today 10, 234-238

Janeway J, C. A. (1992): The T cell receptor as a multicomponent signalling machine: CD4/CD8 coreceptors and CD45 in T cell activation. Annu Rev Immunol 10, 645-674

Janeway J, C. A., Chervonsky AV, Sant'Angelo D (1997): T-cell receptors: Is the repertoire inherently MHC-specific? Curr Biol 7, R299-R300

Jensen JM, Schutze S, Forl M, Kronke M, Proksch E (1999): Roles for tumor necrosis factor receptor p55 and sphingomyelinase in repairing the cutaneous permeability barrier. J Clin Invest 104, 1761-1770

Jensen KB, Watt FM (2006): Single-cell expression profiling of human epidermal stem and transit-amplifying cells: Lrig1 is a regulator of stem cell quiescence. Proc Natl Acad Sci U S A 103, 11958-11963

Jensen KB, Collins CA, Nascimento E, Tan DW, Frye M, Itami S, Watt FM (2009): Lrig1 expression defines a distinct multipotent stem cell population in mammalian epidermis. Cell Stem Cell 4, 427-439

Johansen C (2017): Generation and Culturing of Primary Human Keratinocytes from Adult Skin. J Vis Exp, e56863

Johnson KW, Davis BH, Smith KA (1988): Camp Antagonizes Interleukin 2-Promoted T-Cell Cycle Progression at a Discrete Point in Early G1. Proc Natl Acad Sci U S A 85, 6072-6076

Jones PH, Harper S, Watt FM (1995): Stem cell patterning and fate in human epidermis. Cell 80, 83-93

Kamimura J, Lee D, Baden HP, Brissette J, Dotto GP (1997): Primary mouse keratinocyte cultures contain hair follicle progenitor cells with multiple differentiation potential. J Invest Dermatol 109, 534-540

Kammer GM, Boehm CA, Rudolph SA, Schultz LA (1988): Mobility of the human T lymphocyte surface molecules CD3, CD4, and CD8: regulation by a cAMP-dependent pathway. Proc Natl Acad Sci U S A 85, 792-796

Kanitakis J (2002): Anatomy, histology and immunohistochemistry of normal human skin. Eur J Dermatol 12, 390-401

Kaur P (2006): Interfollicular epidermal stem cells: identification, challenges, potential. J Invest Dermatol 126, 1450-1458

Kezic S, Jakasa I: Filaggrin and skin barrier function. In: Agner T (Eds.): Skin Barrier Function. Volume 49; Karger, Copenhagen 2016, 1-7

Khannpnavar B, Mehta V, Qi C, Korkhov V (2020): Structure and function of adenylyl cyclases, key enzymes in cellular signaling. Curr Opin Struct Biol 63, 34-41

Khavkin J, Ellis DA (2011): Aging skin: histology, physiology, and pathology. Facial Plast Surg Clin North Am 19, 229-234

Killeen N, Davis CB, Chu K, Crooks MC, Sawada S, Scarborough JD, Boyd KA, Stuart SG, Xu H, Littman DR (1993): CD4 function in thymocyte differentiation and T cell activation. Philos Trans R Soc Lond B Biol Sci 342, 25-34

Kim BE, Howell MD, Guttman E, Gilleaudeau PM, Cardinale IR, Boguniewicz M, Krueger JG, Leung DY (2011): TNF-α downregulates filaggrin and loricrin through c-Jun N-terminal kinase: role for TNF-α antagonists to improve skin barrier. J Invest Dermatol 131, 1272-1279

Kinch MS, Strominger JL, Doyle C (1993): Cell adhesion mediated by CD4 and MHC class II proteins requires active cellular processes. J Immunol 151, 4552-4561

Kirfel G, Rigort A, Borm B, Schulte C, Herzog V (2003): Structural and compositional analysis of the keratinocyte migration track. Cell Motil Cytoskeleton 55, 1-13

Klarlund JK, Block ER (2011): Free edges in epithelia as cues for motility. Cell Adh Migr 5, 106-110

Kodis EJ, Smindak RJ, Kefauver JM, Heffner DL, Aschenbach KL, Brennan ER, Chan K, Gamage KK, Lambeth PS, Lawler JR, et al.: First Messengers. eLS. 2012, 1-7

Koh WS, Yang KH, Kaminski NE (1995): Cyclic-Amp Is an Essential Factor in Immune-Responses. Biochem Biophys Res Commun 206, 703-709

Kolarsick PA, Kolarsick MA, Goodwin C (2011): Anatomy and physiology of the skin. J Dermatol Nurses Assoc 3, 203-213

König R, Zhou W (2004): Signal transduction in T helper cells: CD4 coreceptors exert complex regulatory effects on T cell activation and function. Curr Issues Mol Biol 6, 1-16

Koster MI (2010): p63 in skin development and ectodermal dysplasias. J Invest Dermatol 130, 2352-2358

Koster MI, Roop DR (2007): Mechanisms regulating epithelial stratification. Annu Rev Cell Dev Biol 23, 93-113

Kouri YH, Borkowsky W, Nardi M, Karpatkin S, Basch RS (1993): Human Megakaryocytes Have a Cd4 Molecule Capable of Binding Human Immunodeficiency Virus-1. Blood 81, 2664-2670

Krebsbach PH, Villa-Diaz LG (2017): The role of integrin α6 (CD49f) in stem cells: more than a conserved biomarker. Stem Cells Dev 26, 1090-1099

Krijgsman D, Hokland M, Kuppen PJ (2018): The role of natural killer T cells in cancer—a phenotypical and functional approach. Front Immunol 9, 367

Kristensen M, Chu C, Eedy D, Feldmann M, Brennan F, Breathnach S (1993): Localization of tumour necrosis factor-alpha (TNF-α) and its receptors in normal and psoriatic skin: epidermal cells express the 55-kD but not the 75-kD TNF receptor. Clin Exp Immunol 94, 354-362

Krummel MF, Sjaastad MD, Wülfing C, Davis MM (2000): Differential clustering of CD4 and CD3ζ during T cell recognition. Science 289, 1349-1352

Kumar S, Millis AJ, Baglioni C (1992): Expression of interleukin 1-inducible genes and production of interleukin 1 by aging human fibroblasts. Proc Natl Acad Sci U S A 89, 4683-4687

Kupper TS, Lee F, Birchall N, Clark S, Dower S (1988): Interleukin 1 binds to specific receptors on human keratinocytes and induces granulocyte macrophage colony-stimulating factor mRNA and protein. A potential autocrine role for interleukin 1 in epidermis. J Clin Invest 82, 1787-1792

Kupper TS, Ballard DW, Chua AO, McGuire JS, Flood PM, Horowitz MC, Langdon R, Lightfoot L, Gubler U (1986): Human keratinocytes contain mRNA indistinguishable from monocyte interleukin 1 alpha and beta mRNA. Keratinocyte

epidermal cell-derived thymocyte-activating factor is identical to interleukin 1. J Exp Med 164, 2095-2100

Kurasawa M, Maeda T, Oba A, Yamamoto T, Sasaki H (2011): Tight junction regulates epidermal calcium ion gradient and differentiation. Biochem Biophys Res Commun 406, 506-511

Kuroki T, Ito T, Hosomi J, Munakata K, Uchida T, Nagai Y (1982): Cyclic AMP as a mitotic signal for epidermal keratinocytes, but not for dermal fibroblasts. Cell Struct Funct 7, 295-305

Kwong PD, Wyatt R, Robinson J, Sweet RW, Sodroski J, Hendrickson WA (1998): Structure of an HIV gp120 envelope glycoprotein in complex with the CD4 receptor and a neutralizing human antibody. Nature 393, 648-659

Landén NX, Li D, Stahle M (2016): Transition from inflammation to proliferation: a critical step during wound healing. Cell Mol Life Sci 73, 3861-3885

Larouche J, Sheoran S, Maruyama K, Martino MM (2018): Immune regulation of skin wound healing: mechanisms and novel therapeutic targets. Adv Wound Care 7, 209-231

Lavker RM, Matoltsy AG (1970): Formation of horny cells: the fate of cell organelles and differentiation products in ruminal epithelium. J Cell Biol 44, 501-512

Laxminarayana D, Kammer GM (1996): Activation of type I protein kinase A during receptor-mediated human T lymphocyte activation. J Immunol 156, 497-506

Lechler T, Fuchs E (2005): Asymmetric cell divisions promote stratification and differentiation of mammalian skin. Nature 437, 275-280

Lee B, Sharron M, Montaner LJ, Weissman D, Doms RW (1999): Quantification of CD4, CCR5, and CXCR4 levels on lymphocyte subsets, dendritic cells, and differentially conditioned monocyte-derived macrophages. Proc Natl Acad Sci U S A 96, 5215-5220

Lee MR, Cooper AJ (2006): Immunopathogenesis of psoriasis. Australas J Dermatol 47, 151-159

Lee P, Gund R, Dutta A, Pincha N, Rana I, Ghosh S, Witherden D, Kandyba E, MacLeod A, Kobielak K (2017): Stimulation of hair follicle stem cell proliferation through an IL-1 dependent activation of γδT-cells. Elife 6, e28875

Lehman TA, Modali R, Boukamp P, Stanek J, Bennett WP, Welsh JA, Metcalf RA, Stampfer MR, Fusenig N, Rogan EM (1993): p53 mutations in human immortalized epithelial cell lines. Carcinogenesis 14, 833-839

León X, Bothe C, García J, Parreño M, Alcolea S, Quer M, Vila L, Camacho M (2015): Expression of IL-1α correlates with distant metastasis in patients with head and neck squamous cell carcinoma. Oncotarget 6, 37398

Lepski G, Jannes CE, Nikkhah G, Bischofberger J (2013): cAMP promotes the differentiation of neural progenitor cells in vitro via modulation of voltage-gated calcium channels. Front Cell Neurosci 7, 155

Levy V, Lindon C, Harfe BD, Morgan BA (2005): Distinct stem cell populations regenerate the follicle and interfollicular epidermis. Dev Cell 9, 855-861

Lewis RS (2001): Calcium signaling mechanisms in T lymphocytes. Annu Rev Immunol 19, 497-521

Li A, Simmons PJ, Kaur P (1998): Identification and isolation of candidate human keratinocyte stem cells based on cell surface phenotype. Proc Natl Acad Sci U S A 95, 3902-3907

Li QJ, Dinner AR, Qi SY, Irvine DJ, Huppa JB, Davis MM, Chakraborty AK (2004): CD4 enhances T cell sensitivity to antigen by coordinating Lck accumulation at the immunological synapse. Nat Immunol 5, 791-799

Li X, Murray F, Koide N, Goldstone J, Dann SM, Chen J, Bertin S, Fu G, Weinstein LS, Chen M, et al. (2012): Divergent requirement for Galphas and cAMP in the differentiation and inflammatory profile of distinct mouse Th subsets. J Clin Invest 122, 963-973

Li X, Upadhyay AK, Bullock AJ, Dicolandrea T, Xu J, Binder RL, Robinson MK, Finlay DR, Mills KJ, Bascom CC, et al. (2013): Skin Stem Cell Hypotheses and Long Term Clone Survival - Explored Using Agent-based Modelling. Sci Rep 3, 1-9

Li Y, Li LX, Wadley R, Reddel SW, Qi JC, Archis C, Collins A, Clark E, Cooley M, Kouts S, et al. (2001): Mast cells/basophils in the peripheral blood of allergic individuals who are HIV-1 susceptible due to their surface expression of CD4 and the chemokine receptors CCR3, CCR5, and CXCR4. Blood 97, 3484-3490

Littman DR (1987): The structure of the CD4 and CD8 genes. Annu Rev Immunol 5, 561-584

Liu Y, Cruikshank WW, O'Reilly P, Center DM, Kornfeld H, O'Loughlin T (1999): Identification of a CD4 domain required for interleukin-16 binding and lymphocyte activation. J Biol Chem 274, 23387-23395

Lloyd C, Yu QC, Cheng J, Turksen K, Degenstein L, Hutton E, Fuchs E (1995): The basal keratin network of stratified squamous epithelia: defining K15 function in the absence of K14. J Cell Biol 129, 1329-1344

Loughney K, Martins TJ, Harris EA, Sadhu K, Hicks JB, Sonnenburg WK, Beavo JA, Ferguson K (1996): Isolation and characterization of cDNAs corresponding to two human calcium, calmodulin-regulated, 3′, 5′-cyclic nucleotide phosphodiesterases. J Biol Chem 271, 796-806

Lucey DR, Dorsky DI, Nicholson-Weller A, Weller PF (1989): Human eosinophils express CD4 protein and bind human immunodeficiency virus 1 gp120. J Exp Med 169, 327-332

Luckheeram RV, Zhou R, Verma AD, Xia B (2012): CD4+ T cells: differentiation and functions. Clin Dev Immunol 2012

Lynch G, Slaytor E, Elliott F, Saurajen A, Turville S, Sloane A, Cameron P, Cunningham A, Halliday G (2003): CD4 is expressed by epidermal Langerhans' cells predominantly as covalent dimers. Exp Dermatol 12, 700-711

Mackenzie IC, Bickenbach JR (1985): Label-retaining keratinocytes and Langerhans cells in mouse epithelia. Cell Tissue Res 242, 551-556

MacKenzie SJ, Yarwood SJ, Peden AH, Bolger GB, Vernon RG, Houslay MD (1998): Stimulation of p70S6 kinase via a growth hormone-controlled phosphatidylinositol 3-kinase pathway leads to the activation of a PDE4A cyclic AMP-specific phosphodiesterase in 3T3-F442A preadipocytes. Proc Natl Acad Sci U S A 95, 3549-3554

Madrenas J, Chau LA, Smith J, Bluestone JA, Germain RN (1997): The efficiency of CD4 recruitment to ligand-engaged TCR controls the agonist/partial agonist properties of peptide–MHC molecule ligands. J Exp Med 185, 219-230

Mammone T, Marenus K, Maes D, Lockshin RA (1998): The induction of terminal differentiation markers by the cAMP pathway in human HaCaT keratinocytes. Skin Pharmacol Physiol 11, 152-160

Markova NG, Marekov LN, Chipev CC, Gan SQ, Idler WW, Steinert PM (1993): Profilaggrin Is a Major Epidermal Calcium-Binding Protein. Molecular and Cellular Biology 13, 613-625

Marrack P, Endres R, Shimonkevitz R, Zlotnik A, Dialynas D, Fitch F, Kappler J (1983): The major histocompatibility complex-restricted antigen receptor on T cells. II. Role of the L3T4 product. J Exp Med 158, 1077-1091

Martin P, Nunan R (2015): Cellular and molecular mechanisms of repair in acute and chronic wound healing. Br J Dermatol 173, 370-378

Martinsson H, Yhr M, Enerback C (2005): Expression patterns of S100A7 (psoriasin) and S100A9 (calgranulin-B) in keratinocyte differentiation. Exp Dermatol 14, 161-168

Mascré G, Dekoninck S, Drogat B, Youssef KK, Brohée S, Sotiropoulou PA, Simons BD, Blanpain C (2012): Distinct contribution of stem and progenitor cells to epidermal maintenance. Nature 489, 257-262

Mast BA, Schultz GS (1996): Interactions of cytokines, growth factors, and proteases in acute and chronic wounds. Wound Repair Regen 4, 411-420

Matsui MS, Chew SL, DeLeo VA (1992): Protein kinase C in normal human epidermal keratinocytes during proliferation and calcium-induced differentiation. J Invest Dermatol 99, 565-571

Matz MV, Fradkov AF, Labas YA, Savitsky AP, Zaraisky AG, Markelov ML, Lukyanov SA (1999): Fluorescent proteins from nonbioluminescent Anthozoa species. Nat Biotechnol 17, 969-973

McGrath J, Eady R, Pope F: Anatomy and organization of human skin. In: Burns T, Breathnach S, Cox N, Griffiths C (Eds.): Rook's Textbook of Dermatology. Volume 1; Blackwell Science, Oxford 2004, 3.1 - 3.15

McHeik J, Barrault C, Bernard F, Levard G (2010): Quantitative and qualitative study in keratinocytes from foreskin in children: Perspective application in paediatric burns. Burns 36, 1277-1282

McMillan JR, Akiyama M, Shimizu H (2003): Epidermal basement membrane zone components: ultrastructural distribution and molecular interactions. J Dermatol Sci 31, 169-177

Menon GK, Eliam PM (1985): Ultrastructural localization by ioncapture cytochemistry. J Invest Dermatol 84, 508-512

Menon GK, Elias PM, Feingold KR (1994): Integrity of the Permeability Barrier Is Crucial for Maintenance of the Epidermal Calcium Gradient. Br J Dermatol 130, 139-147

Micallef L, Belaubre F, Pinon A, Jayat-Vignoles C, Delage C, Charveron M, Simon A (2009): Effects of extracellular calcium on the growth-differentiation switch in immortalized keratinocyte HaCaT cells compared with normal human keratinocytes. Exp Dermatol 18, 143-151

Michel KD, Uhmann A, Dressel R, van den Brandt J, Hahn H, Reichardt HM (2013): The Hedgehog Receptor Patched1 in T Cells Is Dispensable for Adaptive Immunity in Mice. PLoS One 8

Minguet S, Huber M, Rosenkranz L, Schamel WW, Reth M, Brummer T (2005): Adenosine and cAMP are potent inhibitors of the NF-κB pathway downstream of immunoreceptors. Eur J Immunol 35, 31-41

Moll R, Moll I, Wiest W (1982): Changes in the pattern of cytokeratin polypeptides in epidermis and hair follicles during skin development in human fetuses. Differentiation 23, 170-178

Morris RJ, Fischer SM, Slaga TJ (1985): Evidence that the centrally and peripherally located cells in the murine epidermal proliferative unit are two distinct cell populations. J Invest Dermatol 84, 277-281

Murphy JE, Robert C, Kupper TS (2000): Interleukin-1 and cutaneous inflammation: A crucial link between innate and acquired immunity. J Invest Dermatol 114, 602-608

Ng DC, Su M-J, Kim R, Bikle DD (1996): Regulation of involucrin gene expression by calcium in normal human keratinocytes. Front Biosci 1, a16-24

Ni X, Lai Y (2020): Keratinocyte: A trigger or an executor of psoriasis? J Leukoc Biol 108, 485-491

Nickoloff BJ, Qin J-Z, Nestle FO (2007): Immunopathogenesis of psoriasis. Clin Rev Allergy Immunol 33, 45-56

Niessen CM (2007): Tight junctions/adherens junctions: basic structure and function. J Invest Dermatol 127, 2525-2532

O'Rielly DD, Rahman P (2015): Genetic, Epigenetic and Pharmacogenetic Aspects of Psoriasis and Psoriatic Arthritis. Rheum Dis Clin North Am 41, 623-642

Ogawa E, Sato Y, Minagawa A, Okuyama R (2018): Pathogenesis of psoriasis and development of treatment. J Dermatol 45, 264-272

Oh P, Schnitzer JE (2001): Segregation of heterotrimeric G proteins in cell surface microdomains: Gq binds caveolin to concentrate in caveolae, whereas Gi and Gs target lipid rafts by default. Mol Biol Cell 12, 685-698

Okada N, Kitano Y, Ichihara K (1982): Effects of cholera toxin on proliferation of cultured human keratinocytes in relation to intracellular cyclic AMP levels. J Invest Dermatol 79, 42-47

Omori K, Kotera J (2007): Overview of PDEs and their regulation. Circ Res 100, 309-327

Omri B, Crisanti P, Alliot F, Marty MC, Rutin J, Levallois C, Privat A, Pessac B (1994): CD4 expression in neurons of the central nervous system. Int Immunol 6, 377-385

Orazizadeh M, Hashemitabar M, Bahramzadeh S, Dehbashi FN, Saremy S (2015): Comparison of the enzymatic and explant methods for the culture of keratinocytes isolated from human foreskin. Biomed Rep 3, 304-308

Oshima H, Rochat A, Kedzia C, Kobayashi K, Barrandon Y (2001): Morphogenesis and renewal of hair follicles from adult multipotent stem cells. Cell 104, 233-245

Papini S, Cecchetti D, Campani D, Fitzgerald W, Grivel JC, Chen S, Margolis L, Revoltella RP (2003): Isolation and clonal analysis of human epidermal keratinocyte stem cells in long-term culture. Stem Cells 21, 481-494

Paramio JM, Casanova ML, Segrelles C, Mittnacht S, Lane EB, Jorcano JL (1999): Modulation of cell proliferation by cytokeratins K10 and K16. Mol Cell Biol 19, 3086-3094

Partridge M, Chantry D, Turner M, Feldman M (1991): Production of interleukin-1 and interleukin-6 by human keratinocytes and squamous cell carcinoma cell lines. J Invest Dermatol 96, 771-776

Pastar I, Stojadinovic O, Yin NC, Ramirez H, Nusbaum AG, Sawaya A, Patel SB, Khalid L, Isseroff RR, Tomic-Canic M (2014): Epithelialization in Wound Healing: A Comprehensive Review. Adv Wound Care (New Rochelle) 3, 445-464

Pillai S, Bikle DD, Hincenbergs M, Elias PM (1988): Biochemical and morphological characterization of growth and differentiation of normal human neonatal keratinocytes in a serum-free medium. J Cell Physiol 134, 229-237

Pillai S, Bikle DD, Mancianti ML, Cline P, Hincenbergs M (1990): Calcium regulation of growth and differentiation of normal human keratinocytes: modulation of differentiation competence by stages of growth and extracellular calcium. J Cell Physiol 143, 294-302

Pincelli C, Marconi A (2010): Keratinocyte stem cells: friends and foes. J Cell Physiol 225, 310-315

Popp T, Steinritz D, Breit A, Deppe J, Egea V, Schmidt A, Gudermann T, Weber C, Ries C (2014): Wnt5a/β-catenin signaling drives calcium-induced differentiation of human primary keratinocytes. J Invest Dermatol 134, 2183-2191

Postlethwaite AE, Raghow R, Stricklin GP, Poppleton H, Seyer JM, Kang AH (1988): Modulation of fibroblast functions by interleukin 1: increased steady-state accumulation of type I procollagen messenger RNAs and stimulation of other functions but not chemotaxis by human recombinant interleukin 1 alpha and beta. J Cell Biol 106, 311-318

Potten CS (1981): Cell replacement in epidermis (keratopoiesis) via discrete units of proliferation. Int Rev Cytol 69, 271-318

Potten CS, Hendry JH (1973): Letter: Clonogenic cells and stem cells in epidermis. Int J Radiat Biol Relat Stud Phys Chem Med 24, 537-540

Potten CS, Morris RJ (1988): Epithelial stem cells in vivo. J Cell Sci Suppl 10, 45-62

Potten CS, Saffhill R, Maibach HI (1987): Measurement of the Transit-Time for Cells through the Epidermis and Stratum-Corneum of the Mouse and Guinea-Pig. Cell Tissue Kinet 20, 461-472

Potter H (2003): Transfection by Electroporation. Curr Protoc Mol Biol 62

Presland RB, Kuechle MK, Lewis SP, Fleckman P, Dale BA (2001): Regulated expression of human filaggrin in keratinocytes results in cytoskeletal disruption, loss of cell–cell adhesion, and cell cycle arrest. Exp Cell Res 270, 199-213

Rahemtulla A, Fung-Leung W, Schilham M, Kündig T, Sambhara S, Narendran A, Arabian A, Wakeham A, Paige C, Zinkernagel R (1991): Normal development and function of CD8+ cells but markedly decreased helper cell activity in mice lacking CD4. Nature 353, 180-184

Raja SK, Garcia MS, Isseroff RR (2007): Wound re-epithelialization: modulating keratinocyte migration in wound healing. Front Biosci 12, 2849-2868

Reinke JM, Sorg H (2012): Wound repair and regeneration. Eur Surg Res 49, 35-43

Reischl J, Schwenke S, Beekman JM, Mrowietz U, Stürzebecher S, Heubach JF (2007): Increased expression of Wnt5a in psoriatic plaques. J Invest Dermatol 127, 163-169

Rendon A, Schäkel K (2019): Psoriasis pathogenesis and treatment. Int J Mol Sci 20, 1475

Reya T, Clevers H (2005): Wnt signalling in stem cells and cancer. Nature 434, 843-850

Rice RH, Green H (1979): Presence in human epidermal cells of a soluble protein precursor of the cross-linked envelope: activation of the cross-linking by calcium ions. Cell 18, 681-694

Richmond J, Tuzova M, Cruikshank W, Center D (2014): Regulation of cellular processes by interleukin-16 in homeostasis and cancer. J Cell Physiol 229, 139-147

Ristow HJ (1987): A Major Factor Contributing to Epidermal Proliferation in Inflammatory Skin Diseases Appears to Be Interleukin-1 or a Related Protein. Proc Natl Acad Sci U S A 84, 1940-1944

Ritsu M, Kawakami K, Kanno E, Tanno H, Ishii K, Imai Y, Maruyama R, Tachi M (2017): Critical role of tumor necrosis factor-α in the early process of wound healing in skin. J Dermatol Dermatol Surg 21, 14-19

Robson MC, Steed DL, Franz MG (2001): Wound healing: biologic features and approaches to maximize healing trajectories. Curr Probl Surg 38, 72-140

Roop D (1995): Defects in the barrier. Science 267, 474-476

Roper RL, Graf B, Phipps RP (2002): Prostaglandin E2 and cAMP promote B lymphocyte class switching to IgG1. Immunol Lett 84, 191-198

Rosińczuk J, Taradaj J, Dymarek R, Sopel M (2016): Mechanoregulation of wound healing and skin homeostasis. Biomed Res Int, 461-477

Rothnagel JA, Greenhalgh DA, Gagne TA, Longley MA, Roop DR (1993): Identification of a calcium-inducible, epidermal-specific regulatory element in the 3'-flanking region of the human keratin 1 gene. J Invest Dermatol 101, 506-513

Sakaguchi M, Miyazaki M, Takaishi M, Sakaguchi Y, Makino E, Kataoka N, Yamada H, Namba M, Huh NH (2003): S100C/A11 is a key mediator of Ca2+-induced growth inhibition of human epidermal keratinocytes. J Cell Biol 163, 825-835

Sandilands A, Sutherland C, Irvine AD, McLean WI (2009): Filaggrin in the frontline: role in skin barrier function and disease. J Cell Sci 122, 1285-1294

Santarlasci V, Cosmi L, Maggi L, Liotta F, Annunziato F (2013): IL-1 and T helper immune responses. Front Immunol 4, 182

Sauder DN, Dinarello CA, Morhenn VB (1984): Langerhans cell production of interleukin-1. J Invest Dermatol 82, 605-607

Sauder DN, Stanulis-Praeger BM, Gilchrest BA (1988): Autocrine growth stimulation of human keratinocytes by epidermal cell-derived thymocyte-activating factor: implications for skin aging. Arch Dermatol Res 280, 71-76

Scheile H: CD4+ epidermale Zellen: Nachweis und Charakterisierung in humaner und muriner Epidermis. Med. Diss. Göttingen 2020

Schindelin J, Arganda-Carreras I, Frise E, Kaynig V, Longair M, Pietzsch T, Preibisch S, Rueden C, Saalfeld S, Schmid B (2012): Fiji: an open-source platform for biological-image analysis. Nat Methods 9, 676-682

Schnurr M, Toy T, Shin A, Wagner M, Cebon J, Maraskovsky E (2005): Extracellular nucleotide signaling by P2 receptors inhibits IL-12 and enhances IL-23 expression in human dendritic cells: a novel role for the cAMP pathway. Blood 105, 1582-1589

Schön MP (2019): Adaptive and innate immunity in psoriasis and other inflammatory disorders. Front Immunol 10, 1764

Schön MP, Manzke V, Erpenbeck L (2021): Animal models of psoriasis-highlights and drawbacks. J Allergy Clin Immunol 147, 439-455

Schoop VM, Fusenig NE, Mirancea N (1999): Epidermal organization and differentiation of HaCaT keratinocytes in organotypic coculture with human dermal fibroblasts. J Invest Dermatol 112, 343-353

Schürer N, Köhne A, Schliep V, Barlag K, Goerz G (1993): Lipid composition and synthesis of HaCaT cells, an immortalized human keratinocyte line, in comparison with normal human adult keratinocytes. Exp Dermatol 2, 179-185

Ścieżyńska A, Nogowska A, Sikorska M, Konys J, Karpińska A, Komorowski M, Ołdak M, Malejczyk J (2019): Isolation and culture of human primary keratinocytes—a methods review. Exp Dermatol 28, 107-112

Seeger MA, Paller AS (2015): The roles of growth factors in keratinocyte migration. Adv Wound Care 4, 213-224

Senoo M (2013): Epidermal stem cells in homeostasis and wound repair of the skin. Adv Wound Care 2, 273-282

Senoo M, Pinto F, Crum CP, McKeon F (2007): p63 Is essential for the proliferative potential of stem cells in stratified epithelia. Cell 129, 523-536

Seo EY, Namkung JH, Lee KM, Lee WH, Im M, Kee SH, Park GT, Yang JM, Seo YJ, Park JK (2005): Analysis of calcium-inducible genes in keratinocytes using suppression subtractive hybridization and cDNA microarray. Genomics 86, 528-538

Seppä H, Grotendorst G, Seppä S, Schiffmann E, Martin GR (1982): Platelet-derived growth factor in chemotactic for fibroblasts. J Cell Biol 92, 584-588

Serezani CH, Ballinger MN, Aronoff DM, Peters-Golden M (2008): Cyclic AMP: master regulator of innate immune cell function. Am J Respir Cell Mol Biol 39, 127-132

Shishikura K, Horiuchi T, Sakata N, Trinh DA, Shirakawa R, Kimura T, Asada Y, Horiuchi H (2016): Prostaglandin E2 inhibits neutrophil extracellular trap formation through production of cyclic AMP. Br J Pharmacol 173, 319-331

Singer AJ, Clark RA (1999): Cutaneous wound healing. N Engl J Med 341, 738-746

Skoda AM, Simovic D, Karin V, Kardum V, Vranic S, Serman L (2018): The role of the Hedgehog signaling pathway in cancer: A comprehensive review. Bosn J Basic Med Sci 18, 8-20

Smart I (1970): Variation in the plane of cell cleavage during the process of stratification in the mouse epidermis. Br J Dermatol 82, 276-282

Smeden Jv: A breached barrier: analysis of stratum corneum lipids and their role in eczematous patients. Dissertation Leiden 2013

Sotiropoulou PA, Blanpain C (2012): Development and homeostasis of the skin epidermis. Cold Spring Harb Perspect Biol 4, a008383

Stark HJ, Boehnke K, Mirancea N, Willhauck MJ, Pavesio A, Fusenig NE, Boukamp P (2006): Epidermal homeostasis in long-term scaffold-enforced skin equivalents. J Investig Dermatol Symp Proc 11, 93-105

Steven AC, Steinert PM (1994): Protein composition of cornified cell envelopes of epidermal keratinocytes. J Cell Sci 107, 693-700

Stork PJ, Schmitt JM (2002): Crosstalk between cAMP and MAP kinase signaling in the regulation of cell proliferation. Trends Cell Biol 12, 258-266

Strukov YG, Belmont AS (2008): Development of Mammalian Cell Lines with lac Operator-Tagged Chromosomes. CSH Protoc 2008, pdb prot4903

Takahashi H, Honma M, Miyauchi Y, Nakamura S, Ishida-Yamamoto A, Iizuka H (2004): Cyclic AMP differentially regulates cell proliferation of normal human keratinocytes through ERK activation depending on the expression pattern of B-Raf. Arch Dermatol Res 296, 74-82

Tani H, Morris RJ, Kaur P (2000): Enrichment for murine keratinocyte stem cells based on cell surface phenotype. Proc Natl Acad Sci U S A 97, 10960-10965

Tasken K, Stokka A (2006): The molecular machinery for cAMP-dependent immunomodulation in T-cells. Biochem Soc Trans 34, 476-479

Taylor G, Lehrer MS, Jensen PJ, Sun T-T, Lavker RM (2000): Involvement of follicular stem cells in forming not only the follicle but also the epidermis. Cell 102, 451-461

Teo JL, Kahn M (2010): The Wnt signaling pathway in cellular proliferation and differentiation: A tale of two coactivators. Adv Drug Deliv Rev 62, 1149-1155

Tinevez J-Y, Perry N, Schindelin J, Hoopes GM, Reynolds GD, Laplantine E, Bednarek SY, Shorte SL, Eliceiri KW (2017): TrackMate: An open and extensible platform for single-particle tracking. Methods 115, 80-90

Triel C, Vestergaard ME, Bolund L, Jensen TG, Jensen UB (2004): Side population cells in human and mouse epidermis lack stem cell characteristics. Exp Cell Res 295, 79-90

Triezenberg SJ, Kingsbury RC, McKnight SL (1988): Functional dissection of VP16, the trans-activator of herpes simplex virus immediate early gene expression. Genes Dev 2, 718-729

Trollinger DR, Rivkah Isseroff R, Nuccitelli R (2002): Calcium channel blockers inhibit galvanotaxis in human keratinocytes. J Cell Physiol 193, 1-9

Truong AB, Kretz M, Ridky TW, Kimmel R, Khavari PA (2006): p63 regulates proliferation and differentiation of developmentally mature keratinocytes. Genes Dev 20, 3185-3197

Tsatmali M, Ancans J, Thody AJ (2002): Melanocyte function and its control by melanocortin peptides. J Histochem Cytochem 50, 125-133

Uhmann A, Heß I, Frommhold A, König S, Zabel S, Nitzki F, Dittmann K, Lühder F, Christiansen H, Reifenberger J (2014): DMBA/TPA Treatment Is Necessary for BCC Formation from Patched Deficient Epidermal Cells in Ptchflox/floxCD4Cre+/− Mice. J Invest Dermatol 134, 2620-2629

Uhmann A, van den Brandt J, Dittmann K, Hess I, Dressel R, Binder C, Luhder F, Christiansen H, Fassnacht M, Bhandoola A, et al. (2011): T cell development critically depends on prethymic stromal patched expression. J Immunol 186, 3383-3391

Uhmann A, Dittmann K, Nitzki F, Dressel R, Koleva M, Frommhold A, Zibat A, Binder C, Adham I, Nitsche M, et al. (2007): The Hedgehog receptor Patched controls lymphoid lineage commitment. Blood 110, 1814-1823

Urlinger S, Baron U, Thellmann M, Hasan MT, Bujard H, Hillen W (2000): Exploring the sequence space for tetracycline-dependent transcriptional activators: novel mutations yield expanded range and sensitivity. Proc Natl Acad Sci U S A 97, 7963-7968

Vang AG, Housley W, Dong H, Basole C, Ben-Sasson SZ, Kream BE, Epstein PM, Clark RB, Brocke S (2013): Regulatory T-cells and cAMP suppress effector T-cells independently of PKA-CREM/ICER: a potential role for Epac. Biochem J 456, 463-473

Vang T, Torgersen KM, Sundvold V, Saxena M, Levy FO, Skalhegg BS, Hansson V, Mustelin T, Tasken K (2001): Activation of the COOH-terminal Src kinase (Csk) by cAMP-dependent protein kinase inhibits signaling through the T cell receptor. J Exp Med 193, 497-507

Vitali E, Cambiaghi V, Spada A, Tresoldi A, Zerbi A, Peverelli E, Carnaghi C, Mantovani G, Lania A (2015): cAMP effects in neuroendocrine tumors: The role of Epac and PKA in cell proliferation and adhesion. Exp Cell Res 339, 241-251

Walker D, Sun T, Macneil S, Smallwood R (2006): Modeling the effect of exogenous calcium on keratinocyte and HaCat cell proliferation and differentiation using an agent-based computational paradigm. Tissue Eng 12, 2301-2309

Wan H, Stone MG, Simpson C, Reynolds LE, Marshall JF, Hart IR, Hodivala-Dilke KM, Eady RA (2003): Desmosomal proteins, including desmoglein 3, serve as novel negative markers for epidermal stem cell-containing population of keratinocytes. J Cell Sci 116, 4239-4248

Wang X, Chen H, Tian R, Zhang Y, Drutskaya MS, Wang C, Ge J, Fan Z, Kong D, Wang X (2017): Macrophages induce AKT/β-catenin-dependent Lgr5+ stem cell activation and hair follicle regeneration through TNF. Nat Commun 8, 1-14

Wang Y, Xu J, Zhang X, Wang C, Huang Y, Dai K, Zhang X (2017): TNF-alpha-induced LRG1 promotes angiogenesis and mesenchymal stem cell migration in the subchondral bone during osteoarthritis. Cell Death Dis 8, e2715

Wang YS, Peng D, Wang LM, Dong Z, He B (2015): Screening of HaCaT clones for CCL20 gene knockout and preliminary exploration of gene-targeting vector transfection approaches in this cell line. Med Sci Monit Basic Res 21, 21

Watt FM (1998): Epidermal stem cells: markers, patterning and the control of stem cell fate. Philos Trans R Soc Lond B Biol Sci 353, 831-837

Watt FM, Celso CL, Silva-Vargas V (2006): Epidermal stem cells: an update. Curr Opin Genet Dev 16, 518-524

Wehbi VL, Taskén K (2016): Molecular mechanisms for cAMP-mediated immunoregulation in T cells–role of anchored protein kinase a signaling units. Front Immunol 7, 222

Weissman IL, Anderson DJ, Gage F (2001): Stem and progenitor cells: origins, phenotypes, lineage commitments, and transdifferentiations. Annu Rev Cell Dev Biol 17, 387-403

Werner S, Grose R (2003): Regulation of wound healing by growth factors and cytokines. Physiol Rev 83, 835-870

White R, Mason D, Williams A, Galfre G, Milstein C (1978): T-lymphocyte heterogeneity in the rat: separation of functional subpopulations using a monoclonal antibody. J Exp Med 148, 664-673

Wikramanayake TC, Stojadinovic O, Tomic-Canic M (2014): Epidermal differentiation in barrier maintenance and wound healing. Adv Wound Care 3, 272-280

Williams AF, Galfrè G, Milstein C (1977): Analysis of cell surfaces by xenogeneic myeloma-hybrid antibodies: differentiation antigens of rat lymphocytes. Cell 12, 663-673

Wilson VG: Growth and differentiation of HaCaT keratinocytes. In: Turksen K (Eds.): Epidermal cells (Methods in Molecular Biology). Springer, New York 2013, 33-41

Withers DJ, Bloom SR, Rozengurt E (1995): Dissociation of cAMP-stimulated mitogenesis from activation of the mitogen-activated protein kinase cascade in Swiss 3T3 cells. J Biol Chem 270, 21411-21419

Withers HR (1967): Recovery and repopulation in vivo by mouse skin epithelial cells during fractionated irradiation. Radiat Res 32, 227-239

Wood LC, Jackson SM, Elias PM, Grunfeld C, Feingold KR (1992): Cutaneous barrier perturbation stimulates cytokine production in the epidermis of mice. J Clin Invest 90, 482-487

Wu H, Kwong PD, Hendrickson WA (1997): Dimeric association and segmental variability in the structure of human CD4. Nature 387, 527-530

Wu N, Rollin J, Masse I, Lamartine J, Gidrol X (2012): p63 regulates human keratinocyte proliferation via MYC-regulated gene network and differentiation commitment through cell adhesion-related gene network. J Biol Chem 287, 5627-5638

Wülfing C, Rabinowitz JD, Beeson C, Sjaastad MD, McConnell HM, Davis MM (1997): Kinetics and extent of T cell activation as measured with the calcium signal. J Exp Med 185, 1815-1825

Yamanishi K, Kishimoto S, Yasuno H (1989): Cyclic AMP as a negative regulator of DNA synthesis in FRSK cells, a fetal rat epidermal cell line. J Dermatol 16, 2-6

Yang A, Schweitzer R, Sun D, Kaghad M, Walker N, Bronson RT, Tabin C, Sharpe A, Caput D, Crum C (1999): p63 is essential for regenerative proliferation in limb, craniofacial and epithelial development. Nature 398, 714-718

Yano S, Banno T, Walsh R, Blumenberg M (2008): Transcriptional responses of human epidermal keratinocytes to cytokine interleukin-1. J Cell Physiol 214, 1-13

Yao E, Chuang PT (2015): Hedgehog signaling: From basic research to clinical applications. J Formos Med Assoc 114, 569-576

Yarranton GT (1992): Inducible vectors for expression in mammalian cells. Curr Opin Biotechnol 3, 506-511

Yin DX, Schimke RT (1995): BCL-2 expression delays drug-induced apoptosis but does not increase clonogenic survival after drug treatment in HeLa cells. Cancer Res 55, 4922-4928

Yousef H, Alhajj M, Sharma S: Anatomy, Skin (Integument), Epidermis Edition; StatPearls Publishing, Treasure Island 2021

Yu N, Zhang X, Magistretti PJ, Bloom FE (1998): IL-1-alpha and TNF-alpha differentially regulate CD4 and Mac-1 expression in mouse microglia. Neuroimmunomodulation 5, 42-52

Yuspa SH, Kilkenny AE, Steinert PM, Roop DR (1989): Expression of murine epidermal differentiation markers is tightly regulated by restricted extracellular calcium concentrations in vitro. J Cell Biol 109, 1207-1217

Zaidi Z, Lanigan SW: Dermatology in clinical practice. 1. Edition; Springer, London 2010

Zantl R, Horn E: Chemotaxis of slow migrating mammalian cells analysed by video microscopy. Cell Migration. Springer 2011, 191-203

Zengel P, Nguyen-Hoang A, Schildhammer C, Zantl R, Kahl V, Horn E (2011): µ-Slide Chemotaxis: a new chamber for long-term chemotaxis studies. BMC Cell Biol 12, 1-14

Zhang Y, Tu C, Zhang D, Zheng Y, Peng Z, Feng Y, Xiao S, Li Z (2015): Wnt/β-catenin and Wnt5a/Ca2+ pathways regulate proliferation and apoptosis of keratinocytes in psoriasis lesions. Cell Physiol Biochem 36, 1890-1902

Zhen A, Krutzik SR, Levin BR, Kasparian S, Zack JA, Kitchen SG (2014): CD4 ligation on human blood monocytes triggers macrophage differentiation and enhances HIV infection. J Virol 88, 9934-9946

Zhou W, König R (2003): T cell receptor-independent CD4 signalling: CD4–MHC class II interactions regulate intracellular calcium and cyclic AMP. Cell Signal 15, 751-762

Zhu J, Paul WE (2010): Peripheral CD4+ T-cell differentiation regulated by networks of cytokines and transcription factors. Immunol Rev 238, 247-262

Zhu X, Wu Y, Huang S, Chen Y, Tao Y, Wang Y, He S, Shen S, Wu J, Guo X, et al. (2014): Overexpression of Wnt5a in mouse epidermis causes no psoriasis phenotype but an impairment of hair follicle anagen development. Exp Dermatol 23, 926-928

Zoumpourlis V, Solakidi S, Papathoma A, Papaevangeliou D (2003): Alterations in signal transduction pathways implicated in tumour progression during multistage mouse skin carcinogenesis. Carcinogenesis 24, 1159-1165

Acknowledgements

I could not have undertaken this journey and finished this project without the support of the following people:
It is a genuine pleasure to express my deepest gratitude to my mentor and primary supervisor, PD Dr. rer. nat, Anja Uhmann, who guided me throughout this project. I would like to thank you for the opportunity to work with you on this project, your patience, lab work instructions, the friendly discussions, the encouragement, the constructive criticism and the help in writing this thesis. Through your leadership and knowledge, I gained research experience and became a better researcher. Words cannot express my gratitude for your always having time to listen, help and encourage me, which alltogether paved the way for the great results shown in this dissertation.
I would like to extend my sincere thanks to Prof. Dr. med. Heidi Hahn for the support, the discussions of results and their interpretation and the constructive tips and ideas for improving my work.
I wish to show my appreciation to Prof. Dr. Michael Schön for accepting to be my second supervisor. I am thankful for the support, the discussions during the thesis committee presentations and the improvement suggestions that offered me a deeper insight into this project.
In addition, many thanks to the people from the department who have accompanied me on this journey. Thank you Julia Bauer for all laboratory instructions and for always taking time to kindly help me in performing and learning various methods. Furthermore, I would like to thank Dominik Botermann for the friendly discussions and being available whenever I had a problem or a question. I am especially grateful to Nadine Brandes: it was a real pleasure to work with you together. I am grateful for your support, your ideas and your help. I wish to also acknowledge the help provided by the technical and support staff in the department. My thanks are extended to the technicians Anke Frommhold and Ina Heß, without which daily smooth working would have been impossible.